Fast Hydrothermal Liquefaction: Processing Conditions, Product Characterization, and Kinetic Modeling

by

Julia L. Faeth

A dissertation submitted in partial fulfillment
of the requirements for the degree of
Doctor of Philosophy
(Chemical Engineering)
in The University of Michigan
2015

Doctoral Committee:

Professor Emeritus Phillip E. Savage, Chair
Professor Emeritus John R. Barker
Professor H. Scott Fogler
Professor Henry Yee-Neen Wang

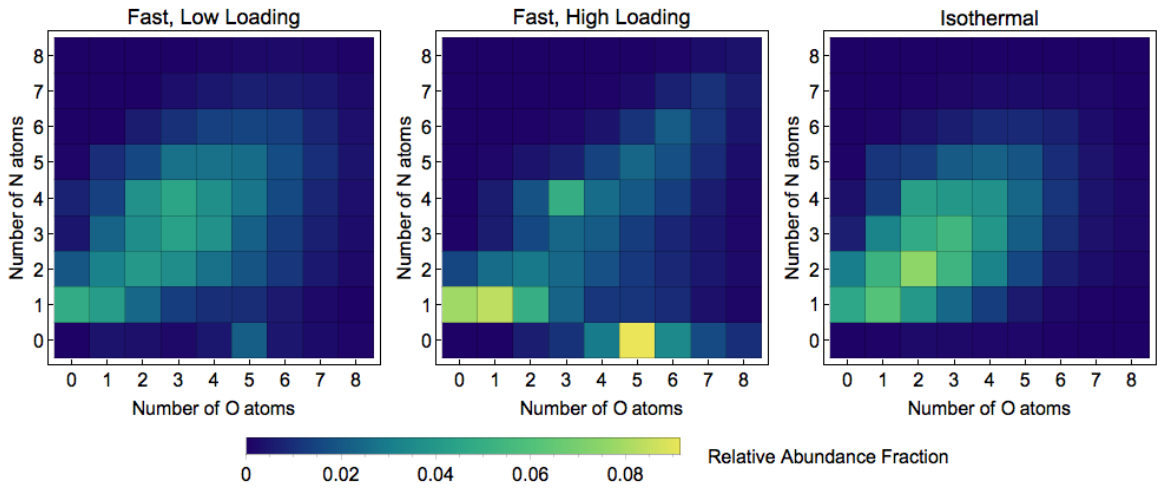

Heteroatom density plots of biocrude from hydrothermal liquefaction of *Nannochloropsis* sp. microalgal biomass

For my family.

Their unconditional love and support made this dissertation possible.

ACKNOWLEDGEMENTS

I would like to thank my advisor, Phillip Savage, for his support and guidance throughout my time as a graduate student at the University of Michigan. He always supplied me with high quality feedback on my work, and I have learned a great deal about research and technical writing from him. His advice enabled me to be more successful in graduate school than I ever imagined possible. I would also like to thank H. Scott Fogler, Henry Wang, and John Barker, the members of my dissertation committee, for their input on my dissertation. H. Scott Fogler also served as my mentor for my first collegiate teaching experience. I learned so much from him (and our students!) about teaching engineering courses, and I also learned more about myself and my presentation style.

I am forever grateful to my parents. They have always supported me in every decision that shaped my career in engineering. When I was upset, they listened. When I was excited about an award or successful experiment, they celebrated with me. They often made surprise visits to Ann Arbor and joined me in sampling the local cuisine. I am especially thankful for a visit my mother made during final exams in my first year that helped me work through a massive worrying session. Without my parents, pursuing my Ph.D. would have been significantly more difficult.

I thank my husband Jason for his patience, love, and support during all the highs and lows of my graduate school experience. Jason knew the time I spent in graduate school would be a difficult several years for our relationship. Nevertheless, Jason was there for me through even the worst of my disappointments and failures.

I thank my sister for understanding what graduate school can be like and for listening to my graduate school struggles, even while dealing with her own. I thank my Grandma and Grandpa Miller for their love, support, scholarships, and money for educational and recreational activities they provided throughout undergraduate and graduate school. I also thank my Grandma Faeth for keeping me in her thoughts and prayers.

I thank the past and present members of the Savage Group who helped shape my graduate school experience at the University of Michigan: Shujauddin Changi, Chad Huelsman, Bobby Levine, Peter Valdez, Jacob Dickinson, Thomas Yeh, Allison Franck, Na (Tiffany) Mo, David Hietala, Jennifer Jocz, Yingda Lu, Zheng Li, Yang Guo, Le (Claire) Yang, Donghai Xu, Ligang Luo, Nattapol (Mink) Arunattanamook, Teri Gule, and Sha (Lisa) Li. I learned a great deal from each of them over the years, and their various questions and comments about my research helped me solidify my understanding of the hydrothermal liquefaction process.

I especially thank Peter Valdez for training me in the experimental methods that formed the foundation of my research. He made the laboratory a safe and organized place to work during his term as the Chemical Hygiene Officer, a role he eventually passed down to me. He taught me how to use and maintain equipment in the lab and was a huge help to me as I prepared for my qualifying and preliminary examinations. We were co-authors on publications, presentations, and a patent application. Peter selflessly helped me, and many others, with anything and everything that came up in our research group, and I greatly appreciate his support.

Special thanks to David Hietala for being the "Mathemagician" and a generally tech-savvy member of our research group during the last two years. Coding is not one of my strengths, but I have improved greatly (at least in Mathematica and LaTeX) with his assistance. We also collaborated to produce a kinetic model encompassing fast and isothermal hydrothermal liquefaction, where his knowledge of MATLAB® made

development of this model possible. David also graciously agreed to help proofread my dissertation, and his comments were extremely helpful as I prepared to submit my dissertation.

I thank Thomas Yeh for his experimental expertise and mechanical know-how. I also thank him for many interesting lunchtime conversations. Thomas introduced me to Dungeons & Dragons, a role-playing game that filled many evenings with amusement and silliness. Thanks also to Lilian Hsiao, Chad Huelsman, Matt Morabito, Luke Griffith, Ryan Franck, and Jenn Jocz for serving as my traveling companions in our imaginary journeys!

I thank Na (Tiffany) Mo for being a great friend. We started graduate school at the same time, and we shared many learning experiences during our time together. I especially enjoyed celebrating our birthdays each year! I thank Jacob Dickinson for his thought-provoking questions during research group meetings. Jake helped me learn to think more critically about my work and the work of others. Thanks also to Allison Franck and Jenn Jocz for happy conversations in the group office!

I thank Charles Monroe for his superb teaching in the graduate-level transport and advanced mathematics classes. He also served on my qualifying, preliminary, and data meeting committees and provided extremely valuable insight and advice for my dissertation.

I thank Nick Garza, VJ Tocco, Hao Chen, Ryan Hockstad, and Catherine Griffith for their assistance with experimental data collection for this dissertation. Their work and attention to detail were great assets, and they helped collect a large portion of the data presented in this dissertation. I thank Mike Nelson for his knowledge of bacteria, yeast, and the aqueous-phase products of hydrothermal liquefaction. I also thank Jacqueline Jarvis and Amy McKenna for their expertise in ultra-high resolution mass spectrometry.

I thank Susan Montgomery for her support and guidance, and for listening when

I needed someone with whom to talk. Thanks to Kelly Raickovich, Susan Hamlin, Shelley Fellers, Pam Bogdanski, Jennifer Downey, Sandy Swisher, Laurel Neff, and Christine Moellering for their administrative support and assistance. Kelly always kept her grad student "kids" well fed, for which I am especially grateful.

I thank my MSalsa co-instructors for the time spent together taking my mind off research through dancing. I am grateful for the many friends I made at the University of Michigan, the University of Dayton, and elsewhere. Though too numerous to list individually, they have all shaped my life in some way and supported me in my endeavors.

I thank the National Science Foundation (Grant EFRI-0937992), the Rackham Graduate School, and the College of Engineering for financial support. I also acknowledge that much of the material herein is based on work supported by the National Science Foundation Graduate Student Research Fellowship under Grant DGE 1256260.

TABLE OF CONTENTS

LIST OF FIGURES

Figure

LIST OF TABLES

Table

LIST OF APPENDICES

Appendix

LIST OF ABBREVIATIONS

Btu British thermal units

EROI energy return on investment

ESI electrospray ionization

DBE double bond equivalent

DCM dichloromethane

FT-ICR MS Fourier Transform Ion Cyclotron Resonance Mass Spectrometry

GC gas chromatograph

GC-MS gas chromatograph with mass spectrometry

HHV higher heating value

HHVs higher heating values

HTL hydrothermal liquefaction

LCA life cycle assessment

ppm parts per million

rcf relative centrifugal force

rms root-mean-square

rpm rotations per min

SEM scanning electron microscopy

STEM science, technology, engineering and math

TCD thermal conductivity detector

ABSTRACT

This dissertation describes the study of processing conditions for the hydrothermal liquefaction (HTL) of microalgae, which resulted in the development and subsequent examination of fast HTL, a variation of the HTL process that produces similar biocrude yields in a fraction of the time necessary for isothermal HTL. Application of the fast HTL process to bacteria and yeast biomass (in addition to other algae species) successfully produced biocrude, establishing fast HTL as a robust biomass-conversion process. Experiments probing different reaction conditions and biomass loadings indicate that heating rate, temperature, time, and the fraction of the reactor volume occupied by liquid water have a significant effect on product formation from fast HTL, while slurry solid content does not. Fast HTL of microalgal slurries in reactors with different loaded volume fractions yields biocrude and aqueous-phase products of significantly different composition, as identified via elemental analysis and molecular characterization using Fourier Transform Ion Cyclotron Resonance Mass Spectrometry (FT-ICR MS). Biocrude products of less desirable composition were obtained in greater quantities than those with more desirable composition, indicating the existence of trade-offs between product yield and quality for different HTL reaction conditions.

The aforementioned results warranted a more comprehensive study of both fast and isothermal HTL reaction conditions, especially at low conversion of algal biomass. Systematic evaluation of fast and isothermal HTL reaction conditions at both low and high liquid water-occupied volumes informed the formulation of a modified HTL reaction network, including a novel pathway for physical disruption of algal cells. This

network enabled calculation of pathway kinetic parameters using MATLAB®. These kinetic parameters are physically realistic and enable calculation of product yields that accurately match those observed experimentally. This model captures observed trends for all products from HTL at both low and high algal cell conversion, including the effects of heating rate.

CHAPTER I

Introduction

1.1 Motivation

The scientific consensus of anthropogenic global climate change was endorsed in 97.1 % of peer-reviewed papers presenting a position on global climate change and published between 1991 - 2001 [1]. One major anthropogenic source of carbon dioxide (CO_2) and other environmentally disruptive emissions contributing to global climate change is the combustion of transportation fuels. In 2014, 24.8 quadrillion British thermal units (Btu) of petroleum-based liquid fuels were consumed in the United States transportation sector [2]. These transportation-related emissions, in addition to other natural and anthropogenic sources, contribute to the increasing concentration of CO_2 in Earth's atmosphere. In fact, the global atmospheric concentration of CO_2 increased from less than 320 parts per million (ppm) to more than 400 ppm over the past 50 years [3]. Greenhouse gases, such as CO_2, limit the release of radiant heat from Earth, leading to an increase in average global temperature, commonly referred to as global warming or global climate change.

Fuels from biomass could be produced to mitigate the impact of transportation fuel combustion. All living organisms require energy from photosynthesis (the process of converting energy from the sun to chemical energy), either directly or indirectly, by consuming other organisms. This driving force allows CO_2 from the atmosphere

to become fixed into biomass. The combustion of fuels derived from biomass would effectively recycle atmospheric CO_2, in contrast with fossil fuels which were previously stored underground and release additional CO_2 into the atmosphere upon combustion.

One particularly promising biomass feedstock for biofuel production is microalgae. Microalgae are generally more efficient at photosynthesis than terrestrial plants [4]. Some algae species can thrive in conditions ill-suited for terrestrial plants, positioning algae as a much more versatile biomass feedstock [5]. Additionally, many algae species grow quite rapidly and can accumulate up to half their dry weight in high-energy lipids [5]; although, algal cultures rarely exceed densities of 5 g/L [6, 7]. At such low culture concentrations, algae cells inherently have a much higher moisture content than do terrestrial plants.

The dilute, aquatic nature of microalgae necessitates some form of concentration, including flocculation, filtration, or centrifugation, prior to processing [8]. Irrespective of harvesting technique, the resulting slurry still retains a great deal of water. Many biofuel production processes, such as pyrolysis, for example, require a dry feedstock thereby introducing the need for additional drying. Drying biomass is very energy-intensive and reduces the overall energy return on investment (EROI). Maximizing EROI is of paramount importance for the development of a biofuel that could truly reduce CO_2 emissions relative to petroleum-derived fuels.

1.2 Hydrothermal Liquefaction

To reduce drying-related energy expenditures, biomass can be processed in high-temperature, high-pressure water (sub- or supercritical water), via a technique called hydrothermal liquefaction (HTL). HTL relies on the properties of liquid water at high temperatures and pressures to facilitate reactions of organic compounds (including microalgae) to produce bio-crude oil, an oily, water-insoluble, energy-dense substance resembling petroleum crude, henceforth referred to as "biocrude". Some of the prop-

erties of high-temperature water that enable this transformation include increased solubility of organic compounds, an increased ion product, and a decreased dielectric constant [9]. Additionally, the entire cell (or the entire leaf, stalk, etc., in the case of terrestrial biomass) can be processed without the extraction of lipids or other substances using potentially hazardous solvents. This approach captures more of the chemical energy, avoids generating another waste stream (the extracted biomass), and minimizes environmental hazards.

Several different algae species have been processed using HTL, including both microalgae and macroalgae. Microalgae species treated using HTL include *Botryococcus braunii* [10–12], *Chlorella* sp. [13–15], *Chlorella pyrenoidosa* [16–19], *Chlorella vulgaris* [20–22], *Dunaliella tertiolecta* [12, 20, 23, 24], *Nannochloropsis gaditana* [15, 20], *Nannochloropsis salina* [25, 26], *Nannochloropsis* sp. [14, 27–36], *Phaeodactylum tricornutum* [20, 37], *Scenedesmus* sp. [36, 38], *Spirulina* sp. [13, 21, 38–41], *Spirulina platensis* [25, 42–44], mixtures of several species [45, 46], and other single-species monocultures [24, 47–49]. Some of the macroalgae species investigated using HTL include *Enteromorpha prolifera* [44, 50], *Laminaria saccharina* [51, 52], and several others [53–57].

Regardless of the algae species treated via HTL, the products of HTL are water-soluble products (henceforth referred to as "aqueous-phase" products), solids (including ash and un-reacted algal biomass), gases, and biocrude. In theory, this biocrude product could be processed in a similar, or possibly even identical, way to petroleum crude oils. Biocrudes can have similar energy density to petroleum crude oils [10, 24, 27, 38, 42, 47], although they typically have a higher heteroatom (e.g. nitrogen, oxygen, etc.) content [19, 33, 40, 42]. Table 1.1 includes a summary of the microalgae HTL literature at the time research for this dissertation began (recent literature is discussed within the chapters of this dissertation, where relevant). The optimal reaction conditions varied between sources, though many point to a range

of reaction temperatures from 300 - 350 ℃ and a reaction time of approximately 1 hr [17, 21, 27–29, 42, 43, 45, 58–60]. For studies investigating the use of catalyst, only data from non-catalytic runs were included, and only studies investigating the reaction of whole cells, not cell components, were included in Table 1.1.

As Table 1.1 indicates, nearly all of the microalgal HTL literature focused on reaction times on the order of tens of minutes (at the time the research for this dissertation began). Of the sources indicating reaction times less than 10 minutes [16, 23, 42, 47, 53, 63], the time to heat the reactor to the desired set-point temperature was not included in the definition of the reaction time. The heating times reported by Garcia Alba et al. [47], Li et al. [53], and Yu et al. [16, 63] were long enough to result in total reaction times on the order of tens of minutes, consistent with other isothermal HTL literature. Jena, Das, and Kastner [42] and Minowa et al. [23] did not report heating times, but the reactor volumes and heat transfer methods indicate the heating times were likely long enough to result in total reaction times on the order of tens of minutes as well.

1.3 Summary of Research Activities

HTL of microalgal biomass is the subject of a growing body of literature, but there are still significant gaps in understanding. Few of the HTL studies include the examination of reactions at short timescales, and moreover, the studies that do approach short timescales show promising results, indicating that examining even shorter reaction times may be beneficial [31, 47]. Results from other biomass conversion processes like pyrolysis indicate that reaction times (or residence times, for continuously flowing systems) on the order of seconds are sufficient, and possibly beneficial, for the production of energy-dense liquid products [65]. Furthermore, the high molecular weight of many compounds present in the products from HTL and the complexity of these products limits characterization by gas chromatograph (GC) to

Table 1.1: Summary of microalgal HTL studies

Author(s), Year	Temperature (°C)	Reaction Time (min)	Maximum Biocrude Yield (wt % dry basis)	Biomass
Barnard, 2009 [61]	260 - 340	15 - 45	16	Microalgae (*Microcystis aeruginosa*, *Cyclotella meneghinia*, and *Nitzschia pusilla*)
Biller, Riley, & Ross, 2011 [58]	350	60	36 (DAF)	Microalgae (*Chlorella vulgaris* and *Nannochloropsis occulata*)
Biller & Ross, 2011 [21]	350	60	40 (DAF)	Microalgae (*Chlorella vulgaris*, *Nannochloropsis occulata*, *Porphyridium cruentum*), Cyanobacteria (*Spirulina*)
Biller et al., 2012 [59]	300 - 350	60	47	Microalgae (*Chlorella vulgaris* and *Scenedesmus dimorphus*) and Cyanobacteria (*Spirulina platensis* and *Chlorogloeopsis fritschii*)
Brown et al., 2010 [27]	200 - 500	60	43	Microalgae (*Nannochloropsis* sp.)
Dote et al., 1994 [10]	200 - 340	60	57 - 64	Microalgae (*Botryococcus braunii*)
Duan & Savage, 2011 [28]	350	60	35	Microalgae (*Nannochloropsis* sp.)
Duan et al., 2013 [17]	350	60	44	Microalgae (*Chlorella pyrenoidosa*)
Garcia Alba et al., 2012 [47]	175 - 450	5 - 60	49	Microalgae (*Desmodesmus* sp.)
Inoue et al., 1994 [11]	200 - 340	Not reported	54	Microalgae (*Botryococcus braunii*)
Jena & Das, 2011 [43]	350	60	41	Cyanobacteria (*Spirulina platensis*)
Jena, Das, & Kastner, 2011 [42]	200 - 380	0 - 120	40	Cyanobacteria (*Spirulina platensis*)
Jena et al., 2011 [60]	350	60	40	Cyanobacteria (*Spirulina platensis*)
Minowa et al., 1995 [23]	250 - 340	5 - 60	44	Microalgae (*Dunaliella tertiolecta*)
Roberts et al., 2013 [45]	350	60	45	Microalgae polyculture (multiple species)
Toor et al., 2013 [25]	220 - 375	90 - 180	46	Microalgae (*Nannochloropsis salina*) and Cyanobacteria (*Spirulina*)
Valdez, Dickinson, & Savage, 2011 [29]	350	60	40	Microalgae (*Nannochloropsis* sp.)
Valdez et al. 2012, [31]	250 - 400	10 - 90	50	Microalgae (*Nannochloropsis* sp.)
Vardon et al., 2011 [40]	300	30	33	Cyanobacteria (*Spirulina*)
Vardon et al., 2012 [38]	300	30	45	Microalgae (*Scenedesmus*) and Cyanobacteria (*Spirulina*)
Yang et al., 2004 [62]	300 - 340	30 - 60	29	Microalgae (*Microcystis viridis*)
Yu, et al., 2011 [63]	100 - 300	0 - 120	39	Microalgae (*Chlorella pyrenoidosa*)
Yu, et al., 2011 [16]	200 - 300	0 - 120	39	Microalgae (*Chlorella pyrenoidosa*)
Zou, et al., 2010 [64]	300 - 380	10 - 90	37	Microalgae (*Dunaliella tertiolecta*)
Note: DAF indicates dry ash-free basis				

a small fraction of the compounds present in a sample [29]; many of the compounds in the biocrude have yet to be characterized in greater detail than elemental analysis. In addition to more detailed characterization of HTL products, predicting product yields at different processing conditions is necessary for the optimization and industrial implementation of HTL. Previous attempts to model HTL do not include short reaction times or processing conditions that lead to low conversion of algal biomass and thus fail to predict product yields at short reaction times.

The following chapters describe our examination of some of these gaps, with each chapter addressing a specific objective. Chapter II addresses the investigation of short reaction times for HTL, which led to the development of fast HTL [33]. We then examine the application of both fast and isothermal HTL to bacteria and yeast biomass in Chapter III [66]. Chapter IV provides a more detailed examination of the effects of reactor loading and other processing conditions on biocrude yields over short timescales [67]. Chapter V describes the comprehensive examination of HTL reaction temperatures, times, heating rates, and reactor loadings for the purpose of generating a data set for kinetic modeling [68]. Chapter VI addresses the lack of detailed characterization of products from fast and isothermal HTL using Fourier Transform Ion Cyclotron Resonance Mass Spectrometry (FT-ICR MS) [69]. Chapter VII describes the development of a unified kinetic model to calculate product yields from both fast and isothermal HTL, including the effects of heating rate [68]. Chapter VIII contains the conclusions of all work in this dissertation and recommendations for future research.

CHAPTER II

Development of Fast Hydrothermal Liquefaction

This chapter discusses the HTL of green marine alga *Nannochloropsis* sp. at batch reaction times of 1, 3, 5, and 60 min and set-point temperatures of 300 - 600 ℃. These experiments comprise the broadest range of reaction conditions examined for HTL of microalgae at the time the contents of this chapter were published [33]. We found that biocrude yields from HTL after 1 min in a sand bath with a high set-point temperature were comparable to or higher than those from HTL at longer batch reaction times and lower sand-bath set-point temperatures, even at comparable quench temperatures. We term this variation on the HTL process "fast" HTL since the reaction times necessary to produce biocrude are significantly shorter than those previously reported for HTL of microalgae. The maximum biocrude yield from HTL of *Nannochloropsis* sp. at the reaction conditions examined in this chapter was 51.6 ± 6.2 wt % on a dry basis after 1 min in a 500 ℃ sand bath.

For a reaction time of 1 min, light biocrude (e.g., hexane-soluble biocrude) makes up a decreasing fraction of the total biocrude as the set-point temperature increases. The biocrudes produced by fast HTL contain similar amounts of carbon (by wt %) and exhibit higher heating values (HHVs) similar to biocrudes from isothermal HTL, which involves a reaction time of at least 10 min. These results indicate that biocrudes of similar quality may be produced in comparable or higher yields and in a fraction

of the time previously thought necessary. For a specified throughput, reducing the reaction time decreases the required reactor volume and, hence, the capital costs for a continuous HTL process. We also show that the reaction ordinate is a useful parameter for interpreting results from algae HTL performed at different temperatures and reaction times.

2.1 Introduction

Reports of microalgal HTL in the literature typically describe slow heating to a specified reaction temperature and/or reaction times of at least 10 min [21, 27, 29, 40, 42, 53, 62, 70], but some recent results suggest that shorter reaction times may be sufficient [31, 47, 71]. For example, Knežević et al. found that the yield of acetone- and water-soluble organics (referred to as oil by the authors) from HTL of woody biomass reached a maximum at reaction times 3 - 5 min and then decreased with further increases in reaction time [71]. This reaction time includes the 140 s required to heat the reaction mixture to the set-point temperature of 350 ℃.

We also draw inspiration from the fast pyrolysis processes used for making bio-oils from dried, millimeter-sized ligno-cellulosic biomass particles. Fast pyrolysis processes rely on very fast heating rates (from 10^2 ℃/min [72] to 10^2 ℃/s [73]) and reaction times (or residence times, for continuous systems) on the order of 1 s [65]. These operating conditions minimize undesirable secondary reactions, resulting in higher yields of liquid and vapor products, compared to slow pyrolysis [65].

To the best of our knowledge, HTL of microalgae at short reaction times (a few min) and fast heating rates had not yet been explored at the time of this study. This work focuses on what we term "fast HTL". We report results from experiments at total reaction times as short as 1 min and average heating rates as high as 233 ± 4 ℃/min (standard error). We also compare the yield and elemental composition of biocrude products from fast HTL to those from isothermal HTL of the same algae.

2.2 Materials and Methods

Nannochloropsis sp. algae was purchased from Reed Mariculture, Inc. as a preservative-free slurry with roughly 32.5 wt % solids content and used as received. The ash (inorganic, non-combustible material) content of dried *Nannochloropsis* sp. was 6.25 ± 0.13 wt % (standard error), which is lower than the ash content of the preservative-containing Reed Mariculture *Nannochloropsis* sp. used in some of our laboratory's earlier work [27]. All chemicals were purchased and are identical to those described by Valdez et al. [31], specifically Optima grade (> 95 %) dichloromethane (DCM) and n-hexane from Fisher Scientific, and 99.998 % pure N_2 from Metro Welding Supply Corp. Figure 2.1 depicts a reactor with a U.S. nickel for scale. Each reactor was constructed from a $^3/_8$ in. Swagelok® port connector and two caps, all 316 stainless steel. The internal volume of an assembled reactor was approximately 1.67 mL, smaller than the 4.1 mL internal volume reactors used by Valdez et al. [31].

Figure 2.1: 1.67 mL mini batch reactor with U.S. nickel for scale

Additional vessels were constructed using one port connector, one cap, and a bored-through reducing union (from $^3/_8$ to $^1/_8$ in.). Omega Engineering, Inc. $^1/_8$ in. diameter 18 in. stainless steel-clad K-type thermocouples were inserted in the $^1/_8$ in. end of the reducing union to construct a sealed reactor with temperature data acquisition capabilities. These vessels were filled only with air and served as "proxy reactors" to estimate the temperature inside the loaded reactors. Figure 2.2

depicts a proxy reactor. An Omega Engineering, Inc. HH309A datalogger recorded the temperature of proxy reactors during reactions. We calculated that the algae paste contributed ≤ 15 % of the total thermal mass of a loaded reactor; therefore, the proxy reactors provided a reasonable estimate of the thermal history of the reactors.

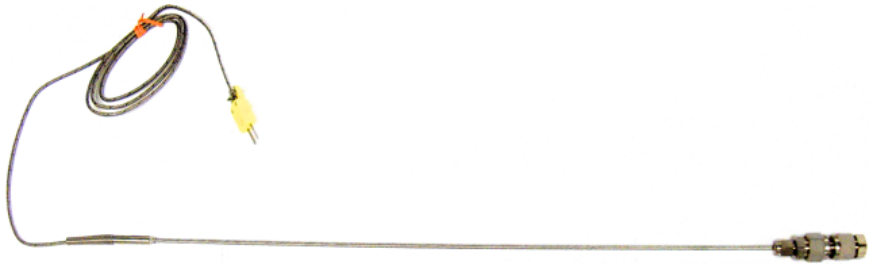

Figure 2.2: Proxy reactor with K-type 18 in. thermocouple

Reactors were loaded with 0.1 - 0.62 g of algae paste and 0.19 - 1.13 g of additional deionized water (see Table A.1 for loading details) according to the procedure outlined by Valdez et al. [31] and placed in a preheated isothermal Techne IFB-51 fluidized sand bath with a Eurotherm 3216 PID controller. In all cases, the reactors contained 15 wt % algae. Steam tables were used to determine the water density at each set-point temperature that would result in a pressure of roughly 400 bar at that temperature. Proxy reactors were inserted into the sand bath alongside loaded reactors, and both were removed at the completion of the desired reaction time (1, 3, 5, or 60 min) and immediately quenched in cold water for at least 5 min. Cooled reactors were allowed to equilibrate for roughly 60 min before product recovery.

The procedure for recovering the biocrude was identical to that described by Valdez et al. [31]. Specifically, this procedure involved opening the reactor, pouring the reactor contents into a conical glass centrifuge tube, rinsing the inside of the reactor with 9 mL of DCM (added in small aliquots), agitating the DCM inside the reactor, and collecting these rinsings in the same centrifuge tube. The contents of the conical centrifuge tube were mixed using a vortex mixer at 3000 rotations per min (rpm) for 1 min and then centrifuged in an Eppendorf 5810 centrifuge at 500

relative centrifugal force (rcf) for 1 min. Solid products collected at the interface between the aqueous (top) and organic (bottom) phases. We collected the organic phase product using a pipette and transferred this phase to another pre-weighed glass tube.

We then mixed the remaining contents of the original conical tube using a vortex mixer at the same conditions described previously and centrifuged the conical tube again at 1500 rcf for 3 min to remove suspended solids from the aqueous phase. The aqueous phase was transferred to a another pre-weighed glass tube using a glass pipette, leaving the residual solids in the original conical centrifuge tube. Following separation, the organic and solid phases were dried under N_2, and the mass of each dried product was recorded. The biocrude is defined as the material in the organic phase that remains after solvent removal. The biocrude yield was calculated by dividing the mass of biocrude by the mass of dry algae originally loaded into the reactor. Yields of biocrude are reported later in this chapter, whereas yields of solid products are reported in Table A.2 in the Appendices.

After the biocrude mass was recorded, 8 mL of hexane was added to the biocrude to recover the "light", hexane-soluble portion of the biocrude. The hexane and biocrude were mixed via vortex mixer for 60 min at 1000 rpm, then centrifuged for 3 min at 1500 rcf. The hexane-soluble products were transferred to another vial via glass pipette and dried, and the mass was recorded. The residual biocrude material that was not hexane soluble (but DCM soluble) was termed "heavy biocrude". All reactions were carried out in at least triplicate, and the uncertainty reported for the biocrude yield represents the standard error of the population. Unreacted algae, light biocrude, and heavy biocrude samples were sent to Atlantic Microlabs, Inc. for analysis of C, H, N, and S content (wt %). The O content (wt %) was calculated by difference (i.e. O = 100 − C − H − N − S − ash).

2.3 Results and Discussion

This section describes the results of fast HTL experiments at fluidized sand-bath set-point temperatures of 300 - 600 ℃. The analysis discussed here includes the temperature profiles, product yields, and elemental composition of the biocrudes obtained through fast HTL.

2.3.1 Product Yields

Figure 2.3 depicts the average temperature profiles of the reactors at set-point temperatures of 300, 400, 500, and 600 ℃. The text boxes overlaid on the profiles at 1, 3, and 5 min indicate the total biocrude yields (wt % on a dry basis) obtained at those reaction times. Confidence intervals represent the standard error of all replicates at that condition. Figure 2.3 shows that the biocrude yield increased with the batch holding time from 12 wt % at 1 min to 41 wt % at 5 min when the sand-bath set-point temperature was 300 ℃. In contrast, the biocrude yields reached maxima and then decreased at the other set-point temperatures shown. The maximum biocrude yield (52 wt % dry basis) was observed after 1 min at the 500 ℃ set-point temperature. For comparison, biocrude yields from traditional HTL of this alga have reached but not exceeded 50 wt % [31]. It is evident that high biocrude yields are accessible at very short reaction times via fast HTL.

Although the chemistry that produces the higher yields during fast HTL is not yet clear, there are multiple potential explanations. The rapid heating may better facilitate lysing of the algal cells, releasing cell contents into the hydrothermal environment for subsequent reaction. Alternatively, hydrolysis and other reactions may simply take place faster than originally thought. Another possible explanation is that undesirable side reactions that become more favorable at more severe conditions are largely avoided during fast HTL.

Figure 2.3 indicates that the temperature within the reactor is roughly 250 ℃ after

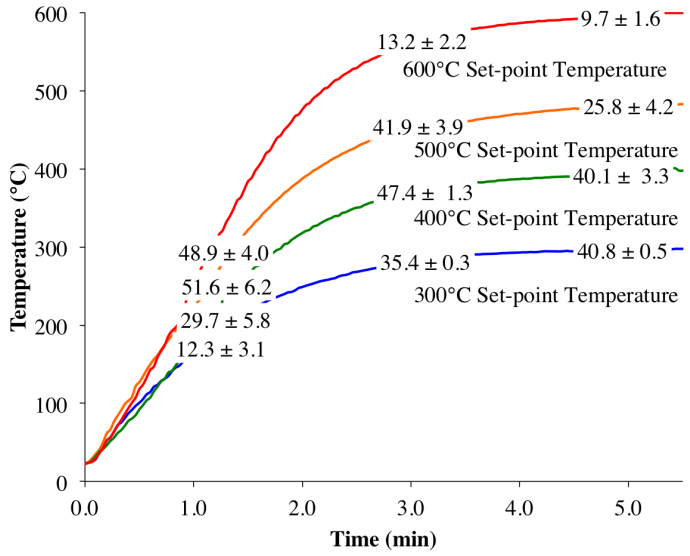

Figure 2.3: Temperature profiles with corresponding biocrude yields (wt % dry basis) for different set-point temperatures of 300, 400, 500, and 600 ℃

submersion in the 500 ℃ sand bath for 1 min. This condition led to the highest biocrude yield and is likely desirable for fast HTL. Because the reaction mixture only reached 250 ℃, a temperature similar to that used in isothermal HTL, we anticipate that fast HTL brings no new concerns regarding reactor corrosion or process energy requirements.

Table 2.1 provides a complete listing of the experimental conditions used for fast HTL and a more detailed summary of results. It gives the biocrude yield, the fraction of the total biocrude that was soluble in hexane (light biocrude fraction), the atomic composition of the biocrude, its higher heating value (HHV), and the percentage of biomass heating value recovered in the biocrude (energy recovery). Confidence intervals reflect standard error. Table 2.1 also gives the value of the reaction ordinate (R_0) for each run. This parameter will be explained fully in a subsequent section. Note that run A provides data for the unreacted, dried algae. Run B provides data from Valdez et al. [31] for the DCM solubles (e.g., "biocrude") extracted from unreacted dry algae. All other runs in Table 2.1 provide data for the biocrude obtained in the present work from HTL at the reaction conditions indicated.

Table 2.1: Summary of results and reaction conditions for fast HTL

Run	Set-point Temp. (°C)	Holding Time (min)	log(R_0)	Biocrude Yield (wt % dry basis)	% Light Biocrude (of Total BC)	C (wt %)	H (wt %)	N (wt %)	S (wt %)	O (wt %)	HHV (MJ/kg)	Energy Recovery (%)
A	25	0	N/A	N/A	N/A	52.35 ± 0.004	7.27 ± 0.014	8.88 ± 0.025	0.66 ± 0.021	24.60 ± 0.014	23.75 ± 0.020	N/A
B	25	0	N/A	9.2 ± 1.3	71.9 ± 4.7	71.9 ± 1.6	10.0 ± 0.2	2.5 ± 0.5	0.17 ± 0.05	14.8 ± 1.3	N/A	N/A
1	300	1	0.806	12.3 ± 3.1	86.8 ± 2.5	71.06	9.61	1.87	0.25	17.22	34.38	17.1 ± 4.3
2	300	3	4.93	35.4 ± 0.3	52.9 ± 0.6	70.43	9.49	4.74	0.59	14.75	34.52	49.4 ± 0.4
3	300	5	5.91	40.8 ± 0.5	45.5 ± 2.9	71.62	9.72	5.45	0.58	12.63	35.48	58.5 ± 0.7
4	350	1	0.675	21.6 ± 2.2	83.2 ± 9.5	70.98	10.05	2.00	0.30	16.67	34.94	30.5 ± 3.1
5	350	3	6.19	46.9 ± 1.6	46.3 ± 2.9	70.56	9.64	6.01	0.64	13.15	35.00	66.3 ± 2.3
6	350	5	7.45	47.5 ± 2.1	50.6 ± 2.6	72.62	9.43	5.84	0.63	11.48	35.66	68.4 ± 3
7	400	1	0.680	29.7 ± 5.8	64.4 ± 6.1	68.94	9.39	4.13	0.45	17.09	33.57	40.2 ± 7.9
8	400	3	7.67	47.4 ± 1.3	53.7 ± 3.6	73.00	9.35	6.10	0.69	10.85	35.79	68.6 ± 1.8
9	400	5	8.60	40.1 ± 3.3	61.1 ± 0.8	73.90	9.22	5.62	0.74	10.52	35.96	58.3 ± 4.8
10	450	1	1.98	48.4 ± 2.7	47.3 ± 3.1	68.68	9.03	5.53	0.66	16.10	33.28	65 ± 3.7
11	450	3	8.80	45 ± 2.5	59.2 ± 2	74.25	9.28	5.70	0.85	9.93	36.23	65.9 ± 3.7
12	450	5	10.1	39 ± 1.9	57.2 ± 1.3	74.40	9.20	5.80	0.89	9.72	36.23	57.1 ± 2.8
13	500	1	3.16	51.6 ± 6.2	37 ± 3.2	68.89	8.99	6.41	0.65	15.05	33.47	69.8 ± 8.4
14	500	3	10.5	41.9 ± 3.9	44.2 ± 8.2	73.36	8.48	6.75	1.18	10.23	35.06	59.3 ± 5.6
15	500	5	11.4	25.8 ± 4.2	42.7 ± 10	73.67	8.01	7.05	0.94	10.33	34.61	36.1 ± 5.8
16	550	1	3.71	47.9 ± 0.8	36.2 ± 3.7	69.70	8.93	6.84	0.74	13.79	33.86	65.6 ± 1.1
17	550	3	11.5	18.5 ± 3.1	14.9 ± 8.1	N/A	N/A	N/A	N/A	N/A	N/A	N/A
18	550	5	12.8	9.7 ± 1.1	8.1 ± 7	N/A	N/A	N/A	N/A	N/A	N/A	N/A
19	600	1	5.14	48.9 ± 4.0	40.4 ± 4.5	70.58	9.00	6.92	0.74	12.75	34.38	86.5 ± 7.9
20	600	3	13.1	13.2 ± 2.2	23.9 ± 9	N/A	N/A	N/A	N/A	N/A	N/A	N/A
21	600	5	14.4	9.7 ± 1.6	33.2 ± 15.7	N/A	N/A	N/A	N/A	N/A	N/A	N/A
N/A - not applicable or not available due to insufficient sample available for elemental analysis												

Table 2.2 provides similar information from experiments with the same alga using isothermal rather than fast HTL. Isothermal HTL reactors reached and maintained the set-point temperature for $\geq$ 10 min (including heat-up time), whereas in some cases, the fast HTL reactors never reached the set-point temperature of the sand bath. Runs 1 - 7 are new experiments performed in this work. Runs 8 - 25 provide data calculated from the results of Valdez et al. [31]. We omit the isothermal HTL results from Brown et al. [27] because the solids content of the reaction mixtures varied from 3 - 16 wt % rather than the constant 15 wt % in the present work. Variation in the solids content has been reported to influence biocrude yields for HTL of *Nannochloropsis* sp. [31].

The atomic compositions of the total biocrude were calculated from the compositions determined separately for the light and heavy fractions and the relative amounts of each. The HHV was estimated using the Boie formula (Equation 2.1 [74]) and the C, H, O, N, and S weight percentages in Tables 2.1 and 2.2.

$$\mathbf{HHV}(MJ/kg) = 35.160 \times \mathbf{C} + 116.225 \times \mathbf{H} - 11.09 \times \mathbf{O} + 6.28 \times \mathbf{N} + 10.465 \times \mathbf{S} \quad (2.1)$$

The calculated HHV was not validated with calorimetry because of insufficient sample mass. However, HHV calculation models based on elemental analysis have been considered to be sufficient for different types of biomass [75].

As indicated in Table 2.1, the *Nannochloropsis* sp. biomass had a HHV of 24.75 $\pm$ 0.016 MJ/kg on an ash-free basis. The HHV of all biocrudes produced by fast HTL range between 33 - 37 MJ/kg, which is consistent with the 34 - 38 MJ/kg HHV range in Table 2.2 for biocrudes from isothermal HTL of *Nannochloropsis* sp. Fast HTL can produce biocrudes of comparable energy content (based on HHV estimations) to those obtained from isothermal HTL.

Table 2.2: Summary of results and reaction conditions for isothermal HTL

Run	Set-point Temp. (°C)	Holding Time (min)	log(R_0)	Biocrude Yield (wt % dry basis)	% Light Biocrude (of Total BC)	C (wt %)	H (wt %)	N (wt %)	S (wt %)	O (wt %)	HHV (MJ/kg)	Energy Recovery (%)
1	300	60	7.53	44	52	N/A	N/A	N/A	N/A	N/A	N/A	N/A
2	350	60	8.90	37	75	N/A	N/A	N/A	N/A	N/A	N/A	N/A
3	400	60	10.6	32	60	N/A	N/A	N/A	N/A	N/A	N/A	N/A
4	450	60	12.0	16	45	N/A	N/A	N/A	N/A	N/A	N/A	N/A
5	500	60	13.5	7	6	N/A	N/A	N/A	N/A	N/A	N/A	N/A
6	550	60	15.1	0	0	N/A	N/A	N/A	N/A	N/A	N/A	N/A
7	600	10	15.5	7	56	N/A	N/A	N/A	N/A	N/A	N/A	N/A
8	250	20	5.7	33.5	48.5	70.82	9.51	5.34	0.59	13.14	34.89	49.31
9	250	30	5.9	34.4	47.7	70.03	9.29	5.75	0.64	13.70	34.32	49.85
10	250	60	6.2	41.8	43.3	71.80	9.52	6.13	0.58	11.38	35.49	62.61
11	250	90	6.4	33.3	38.2	71.42	9.19	6.78	0.70	11.31	35.04	49.19
12	300	10	6.9	49.8	41.9	71.19	9.19	6.21	0.64	12.17	34.82	73.15
13	300	20	7.2	50.2	42.2	70.18	9.21	5.94	0.61	13.46	34.33	72.71
14	300	40	7.5	47.5	45.1	74.18	9.66	5.96	0.59	9.02	36.74	73.74
15	300	60	7.7	39.9	48.8	74.53	9.79	5.28	0.52	9.28	36.94	62.26
16	300	90	7.8	39.7	49.8	73.26	9.37	6.32	0.62	9.83	36.02	60.39
17	350	10	8.4	42.3	42.4	71.40	9.12	6.08	0.60	12.19	34.79	61.71
18	350	20	8.7	39.9	45.5	73.05	9.28	6.23	0.62	10.22	35.79	59.45
19	350	40	9	42.4	50.1	74.58	9.49	5.65	0.49	9.19	36.64	66.50
20	350	60	9.1	40.6	58.4	74.81	9.62	5.43	0.52	9.02	36.88	63.14
21	350	90	9.3	42.5	56.3	75.57	9.60	5.36	0.43	8.44	37.17	65.75
22	400	10	9.8	38	59.4	74.86	9.41	5.91	0.63	8.60	36.74	58.98
23	400	20	10.1	37.9	67.5	74.725	9.63	6.01	0.73	8.31	36.99	59.25
24	400	30	10.3	33.6	65.1	76.07	9.45	5.54	0.71	7.63	37.31	52.95
25	400	40	10.4	32.5	66.71	76.29	9.34	5.37	0.71	7.69	37.24	51.03
N/A - not applicable or not available due to insufficient sample available for elemental analysis												

The energy recovery reported in Table 2.1 was calculated as the energy content (product of HHV and mass) in the biocrude relative to that in the initial algal biomass. An energy recovery of 100 % indicates that all of the chemical energy in the algal biomass has been transferred to the biocrude. The energy recovery for fast HTL varies from 17 to 87 % within the reaction conditions investigated. For reactions lasting 1 min, the energy recovery generally increases with increasing set-point temperature (see runs 1, 4, 7, 10, 13, 16, and 19), reaching a maximum of 87 $\pm$ 8 % at a set-point temperature of 600 ℃. Table 2.2 shows that the highest energy recovery achieved by isothermal HTL of this same alga was 74 %. The energy recovery was more typically 60 - 70 % for the different conditions examined. A majority of the energy recoveries displayed in Table 2.1 for fast HTL are also within this range, but all were acquired at shorter reaction times.

The data in Tables 2.1 and 2.2 provide a wealth of information about the biocrude formed from HTL of the same alga over a very wide range of conditions. Thus, they provide an opportunity to examine how the yield and properties of the biocrude vary with the severity of these reaction conditions. The data in Table 2.1 are from non-isothermal fast HTL experiments, whereas the data in Table 2.2 are from primarily isothermal HTL experiments. To facilitate a meaningful comparison of such results, we employ the reaction ordinate, R_0 [76], which has been used in the biomass processing (wood pulping) literature to combine the effects of both reaction time and temperature into a single parameter that serves as a metric for the severity of the reaction conditions. We note that the literature includes other similar parameters, such as the severity factor [77], prehydrolysis factor [78], and H factor [79].

The reaction ordinate increases with both time and temperature, and its value is unity at the reference temperature (often 100 ℃ [79]) and reference time (1 min in this work). The values of R_0 for each run in Table 2.1 and for runs 1 - 7 in Table 2.2 were calculated from the experimental temperature profile by numerically integrating

the expression in Equation 2.2, where t represents reaction time in minutes [77]. The reaction ordinate value has no physical meaning in isolation. It is strictly used to compare relative thermal treatment intensities using a single parameter.

$$R_0 = \int_0^t e^{\frac{T(t)-100^\circ\mathrm{C}}{14.75^\circ\mathrm{C}}}\, dt \tag{2.2}$$

The values of R_0 for runs 8 - 25 in Table 2.2 were calculated by assuming that the reactor was at the temperature indicated for the entire reaction time. That is, we assumed that the reactors heated instantaneously to the set-point temperature. Given the long reaction times in Table 2.2, this assumption has a negligible effect on the values of R_0. Table 2.2 shows that previous work on HTL of this particular alga has encompassed reaction conditions resulting in R_0 ranging from 10^5 to 10^{10}. Brown et al. [27] used conditions that lead to a R_0 range from 10^4 to 10^{14}, but we omit these results because the solids content of the reaction mixtures varied from 3 - 16 wt %, which is known to affect the biocrude yield [31]. The present work investigates HTL reaction conditions covering a range of R_0 values from 10^1 to 10^{16}. Thus, this report provides information about HTL at reaction conditions both more mild and more severe than those previously examined.

2.3.2 Trends in Fast Hydrothermal Liquefaction Product Yield and Composition with Reaction Ordinate

Figure 2.4 shows how the biocrude yields from fast and isothermal HTL vary with R_0. Biocrude yields at the lowest values of R_0 are 10 - 30 wt %, although the uncertainties in these data are large enough that we cannot be certain that the differences in yield are statistically significant. The lowest biocrude yield shown is comparable to the 9.5 wt % available via DCM extraction of the unreacted algae, as indicated in Table 2.1. This similarity suggests that very little hydrothermal

treatment has occurred at this very mild condition (heating at 300 ℃ for 1 min). As the severity of treatment increases, the biocrude yield increases to 50 wt % or more, but mean yields this high were not observed for any runs with $R_0 > 10^8$. The biocrude yield decreases steadily as the reaction ordinate exceeds 10^8, most likely the result of increased gasification reactions under such severe reaction conditions. The availability of high biocrude yields at values of R_0 between 10^2 and 10^5 indicates that there is no need to use the longer reaction times of isothermal HTL to achieve high yields.

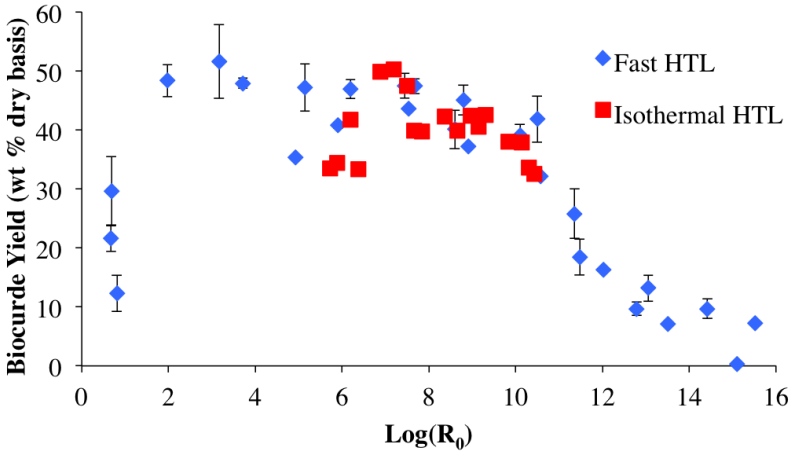

Figure 2.4: Biocrude yields (wt % dry basis) from fast and isothermal HTL with respect to reaction ordinate

The biocrude yields from isothermal HTL in Figure 2.4 show reasonable agreement with the data from this present investigation into fast HTL. This similarity in the yields at similar values of the reaction ordinate suggests that R_0 might be a useful parameter for judging the severity of HTL reaction conditions in both fast and isothermal HTL.

A final observation that we make from Figure 2.4 is that the biocrude yields obtained from fast HTL at the two conditions that give R_0 values of about 10^5 differ substantially. The higher yield of 49 ± 4 wt % was obtained by heating the reactor at 600 ℃ for 1 min, whereas the lower yield of 35 ± 0.3 wt % was obtained by heating

at 300 ℃ for 3 min. According to Figure 2.3, the final reactor temperatures were similar in both experiments. These results indicate that the reaction ordinate alone, although useful for making qualitative comparisons of the combined effects of time and temperature, might not be sufficient to fully characterize fast HTL. It appears that the heating rate during fast HTL may also be important. The three data points at R_0 values of around $10^{0.75}$ are also consistent with this view. Higher yields appeared when using higher set-point temperatures (faster heating rates), even though the values for the reaction ordinate were all similar. Of course, as was mentioned above, the larger uncertainties associated with these data prevent firm conclusions. Nevertheless, it does appear that the influence of heating rate during fast HTL deserves additional attention.

Figure 2.5 illustrates how the HHV of the biocrude varies with the reaction ordinate. Within the range of R_0 from 10^2 to 10^8, where biocrude yields of 40 wt % or more are reported in Tables 2.1 and 2.2, the HHV increases steadily from 33 to 36 - 37 MJ/kg. This increase in HHV with R_0, although lesser in relative magnitude than the decrease in biocrude yield with R_0, could compensate, at least in part, for the decrease in biocrude yield at higher values of the reaction ordinate. Figure 2.6 illustrates the realization of this expectation by showing that the energy recovery at large values of R_0 (e.g., 10^8) can be as high as it is at milder conditions (e.g., $R_0 = 10^2$).

As mentioned previously, the total biocrude was fractionated into light (hexane-soluble) and heavy (hexane-insoluble) components. The light fraction generally has a higher H/C ratio and lower O/C, N/C, and S/C ratios (Table A.3), which makes it a more desirable product than the heavy fraction. Figure 2.7 shows that the light biocrude yield (wt % dry basis) increases from about 10 wt % at R_0 values less than 10^1 to roughly 28 % at R_0 of approximately 10^9. The yield for R_0 values less than 10^1 is only slightly higher than the 6.5 wt % light biocrude yield available without HTL

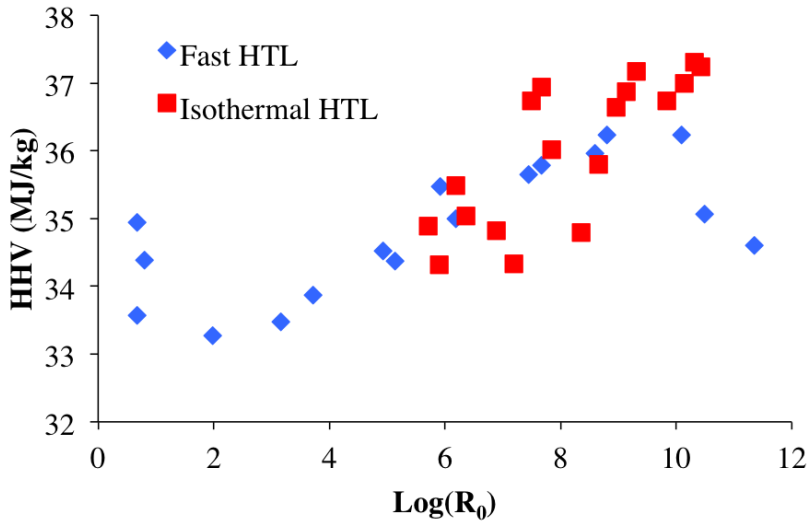

Figure 2.5: Variation of the biocrude HHV with reaction ordinate

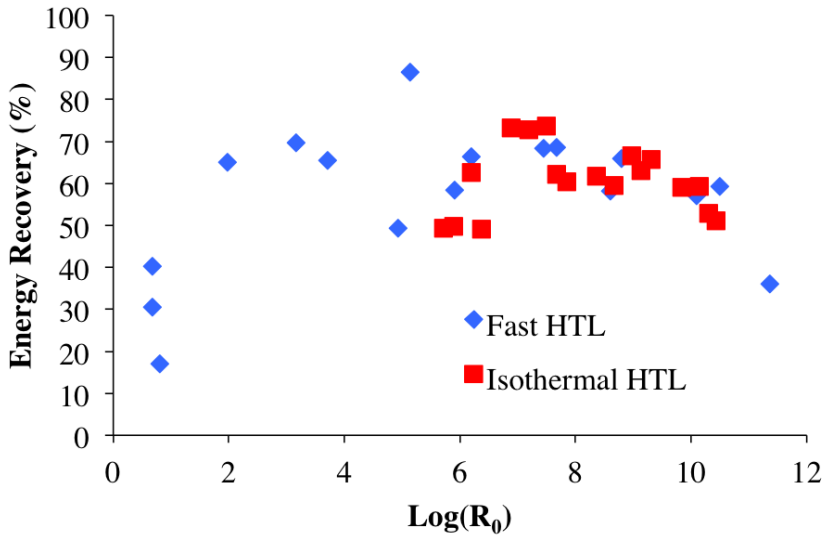

Figure 2.6: Variation of the energy recovery to the biocrude with reaction ordinate

via DCM extraction of raw algae. Large run-to-run variability is observed, possibly because of the difficulty of working with the small sample masses. At higher values of the reaction ordinate, however, the yield of light biocrude dramatically decreased, and it is < 5 wt % at $R_0 > 10^{12}$. This decrease in yield is most likely due to conversion of light biocrude into gaseous products, as discussed in relation to Figure 2.4. It is

also possible that some light biocrude may have undergone secondary reactions to form heavy biocrude (presumably higher molecular weight compounds), although the literature contains conflicting views about this point [31, 70].

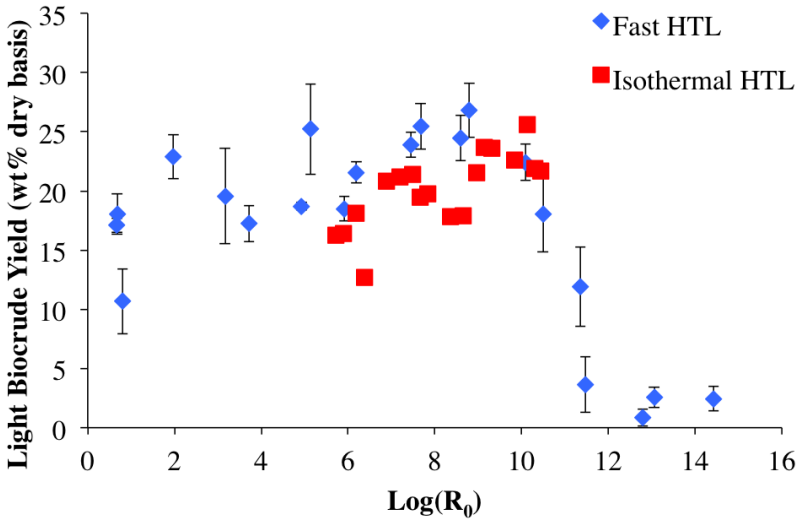

Figure 2.7: Variation of light biocrude yield with reaction ordinate

The yields of light and total biocrude are important metrics for assessing HTL, but the composition of the total biocrude is also important. Biocrudes with more H and C and less O, N, and S are more desirable as fuel precursors. Accordingly, we next examine the influence of the processing conditions, as characterized by the reaction ordinate, on the atomic composition of the total biocrude. Figure 2.8a shows that the H/C ratio of the total biocrude decreases gradually with the reaction ordinate up to a value of about 10^9, at which point the decline becomes more pronounced. These harsher reaction conditions probably promote reactions that lead to the production of aromatic compounds [27]. For comparison, the H/C ratio of petroleum crudes ranges from 1.4 - 1.9 [80].

Figure 2.8b shows that the O/C ratio of the biocrude is less than 0.2, even with very mild hydrothermal treatment. The O/C ratio of the initial algal biomass is 0.35. A similar sharp initial decline in the O/C ratio between the algae and the biocrude

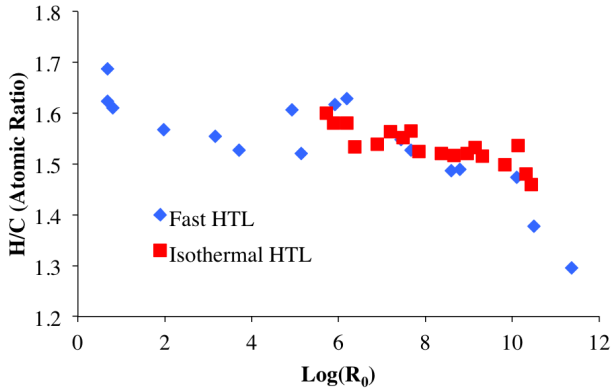

a H/C atomic ratio

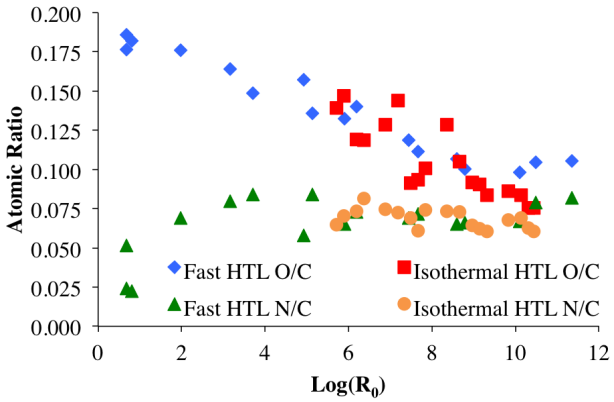

b O/C and N/C atomic ratios

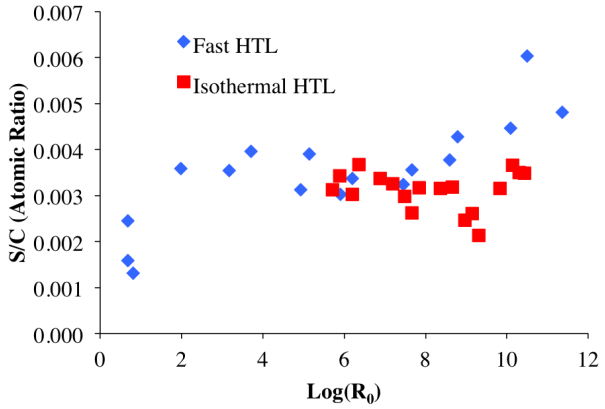

c S/C atomic ratio

Figure 2.8: Variation of biocrude atomic ratios with reaction ordinate (a - H/C, b - O/C and N/C, and c - S/C)

has been noted in previous studies with isothermal HTL [27]. The O/C ratio in Figure 2.8b decreases steadily to approximately 0.08 - 0.1 as the reaction ordinate increases. More severe reaction conditions drive more of the O atoms out of the biocrude, but

the O/C ratio still greatly exceeds the 0.0004 - 0.01 O/C ratio for petroleum crude oils [80]. This reduction in O content is the driving force behind the increase in HHV with R_0 in Figure 2.5. Figure 2.8b also shows how the N/C ratio varies with the reaction ordinate. This ratio is 0.14 for the initial algal biomass, but it is as low as 0.02 for the biocrude formed at mild conditions ($R_0 < 10^1$). The N/C ratio increases sharply with the reaction ordinate, however, and reaches a value of about 0.07 at $R_0 = 10^2$. It remains near this value even as reaction conditions become more severe. N/C ratios for petroleum crudes are 0.001 - 0.02 [80].

Figure 2.8c shows that the S/C ratio exhibits trends similar to the N/C ratio. The biocrudes formed at the mildest conditions have the lowest S/C ratios, and these fall below that of the original algal biomass (0.0047). For reference, the range of S/C ratios for petroleum crudes is 0.0002 - 0.03 [80]. The S/C ratio then quickly rises to a plateau at $R_0 = 10^2$. Unlike the N/C data, the S/C data indicate that this ratio can increase again at the most severe conditions investigated.

The similar trends in panels b and c of Figure 2.8 for the N/C and S/C ratios led us to plot these two ratios together. Figure 2.9 shows the correlation between the N/C and S/C ratios for both the light and heavy biocrudes. It appears that these atomic ratios may be correlated, and further replication may clarify the trend. Generally, low N/C and low S/C occur together, as do high N/C and high S/C. This correlation suggests a common origin and/or common reaction paths for the N and S atoms in the biocrude. The protein fraction in algae is generally where most of the N atoms reside, and the protein fraction can contain S atoms as well. As more molecules from the protein fraction become incorporated into the biocrude, both its S and N contents increase. These ratios were lowest at the mildest conditions examined, which suggests very little incorporation of protein-derived products in the biocrude at those mild conditions.

In addition to exploring how the composition of the total biocrude varied with the

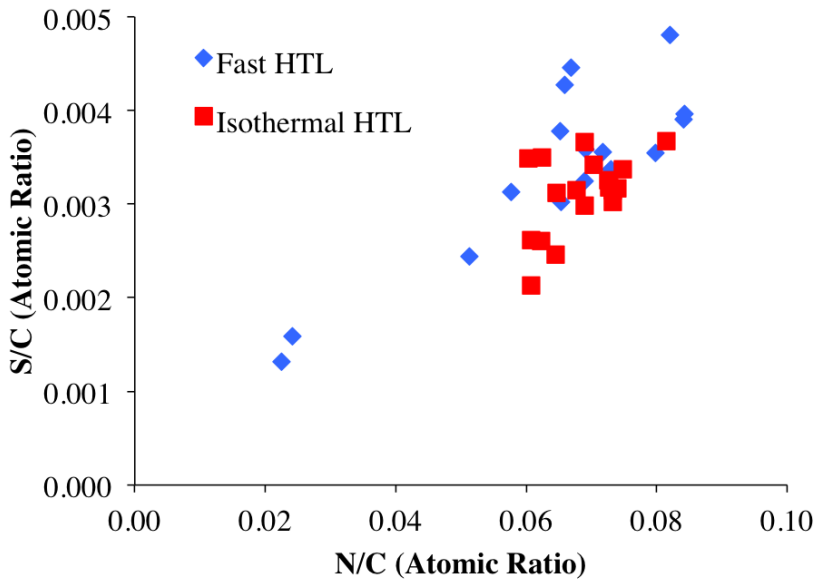

Figure 2.9: Comparison of atomic ratios (N/C and S/C)

reaction ordinate, we also examined this variation for the light and heavy biocrude. Figure 2.10 depicts the H/C and N/C atomic ratios for the light and heavy biocrude. Figure 2.10a shows that the H/C ratio for the light biocrude consistently exceeds the H/C ratio for the heavy biocrude produced at the corresponding R_0 value. A higher H/C atomic ratio is indicative of a higher energy content, making light biocrude preferable to heavy biocrude. Figure 2.10b reinforces the idea that light biocrude is preferable, because the N/C ratio for the heavy biocrude exceeds that of the light biocrude at all of the reaction conditions examined here. The difference between the N/C ratios for the light and heavy biocrude is greatest at the mildest reaction conditions, and as the reaction ordinate increases, the difference becomes much smaller. Low N/C atomic ratios are preferred, because a high N content leads to undesirable NO_X emissions upon combustion.

Overall, the data in Figures 2.4 - 2.8 and Figure 2.10 show consistent trends in several important biocrude quality metrics (e.g., yield, composition, and HHV) over the range of R_0 values explored in this work. Thus, the reaction ordinate or some

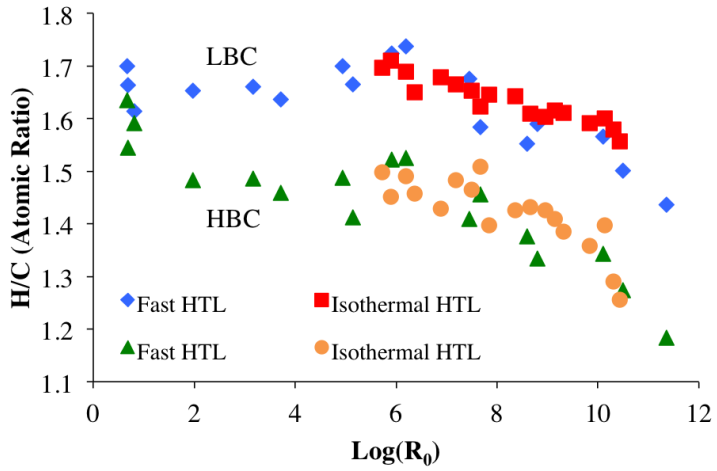

a H/C atomic ratio

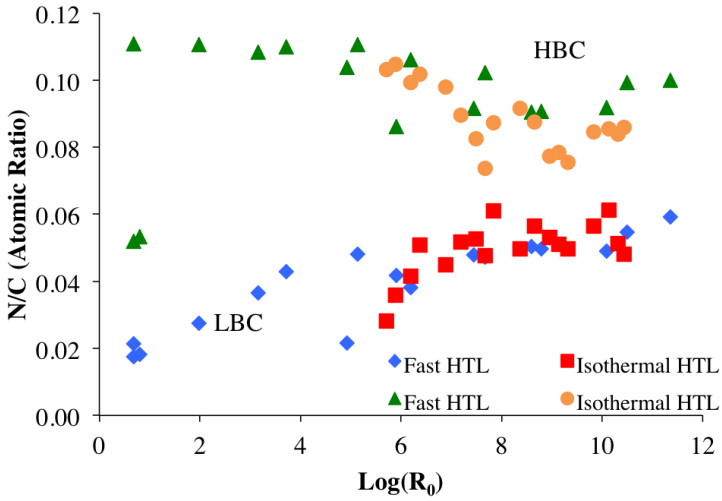

b N/C atomic ratio

Figure 2.10: Variation of light (LBC) and heavy biocrude (HBC) atomic ratios with reaction ordinate: (a - H/C and b - N/C

similar metric may be a useful way to consolidate the effects of time and temperature into one parameter for the HTL of microalgae. The consolidation of time and temperature is particularly useful when considering non-isothermal conditions, such as those used in this study of fast HTL.

2.4 Conclusions

A biocrude yield of 52 ± 6.2 wt % dry basis was obtained from HTL of *Nannochloropsis* sp. in a 500 ℃ sand bath after a reaction time of 1 min and set-point temperature of 500 ℃. This yield exceeds any reported previously for the HTL of this *Nannochloropsis* sp. [27, 31]. Up to 87 ± 8 % of the energy in the dry algae was retained in the biocrude produced at similar conditions (1 min in a 600 ℃ sand bath). HHVs for the biocrudes produced via fast HTL at 1, 3, and 5 min reaction times were 33 - 37 MJ/kg, consistent with the 34 - 38 MJ/kg range for isothermal HTL of *Nannochloropsis* sp. Further, light biocrude was preferable to heavy biocrude obtained using identical reaction conditions, based on atomic composition.

The total biocrude products from fast and isothermal HTL were similar in atomic composition and energy content. For both HTL process variations, H/C ratios decreased with increasing reaction ordinate (and severity). N/C ratios increased slightly then remained fairly consistent throughout the entire range of reaction conditions examined, though O/C ratios decreased with increasing reaction ordinate. S/C ratios were lowest at the least severe conditions, fairly consistent throughout moderate reaction ordinate values, and increased at the most severe reaction conditions. Overall, the biocrude products from HTL at nearly all reaction conditions exhibit H/C ratios similar to those of petroleum crude oils, but higher O/C, N/C and S/C ratios than those of petroleum crude oils. Compounds with high N/C ratios frequently also exhibited high S/C ratios, suggesting a common origin and/or common reaction path may be responsible for incorporation of N and S atoms in the compounds present in the biocrude products.

This work indicates that energy-dense biocrudes may be obtained in high yield in a matter of minutes by rapidly heating algae slurries to perform HTL. This new approach, which we term fast HTL, is a significant improvement over the tens of minutes traditionally used to perform HTL. Such a reduction in reaction time may translate

to a decreased reactor volume required for a specified throughput and, subsequently, reduced capital costs associated with a continuous HTL process.

This work also demonstrated the utility of the reaction ordinate as a means to combine the effects of time and temperature into one parameter for the HTL of algae. We find that the yield, composition, and heating value of biocrudes produced under different conditions can be correlated using the reaction ordinate. Additionally, results obtained by both fast and isothermal HTL exhibit the same trends with the reaction ordinate, which indicates that this parameter might be generally useful for uniting and comparing results from HTL experiments performed under different reaction conditions.

CHAPTER III

Application of Fast Hydrothermal Liquefaction to Microbial Biomass

In this chapter, we discuss the fast (rapid heating for 1 min) and isothermal (350 ℃ for 60 min) HTL reactions of *Escherichia coli*, *Pseudomonas putida*, *Bacillus subtilis*, and *Saccharomyces cerevisiae* monocultures. This work was the first known attempt to use bacteria and yeast monocultures as a feedstock for biocrude production from either fast or isothermal HTL at the time it was published [66], and was the result of collaboration between Peter Valdez, Michael Nelson, Nina Lin, Henry Wang, Phillip Savage, and the author of this dissertation.

Fast HTL of *P. putida* and *S. cerevisiae* produced the highest biocrude yields of 41 ± 4 and 39 ± 8 wt % (dry basis, standard error), respectively. Biocrudes generated via fast HTL were always richer in O and N and had a higher yield of hexane-insoluble products. Isothermal HTL of all microorganisms always produced an aqueous phase richer in ammonia than the aqueous phase from fast HTL. Up to 58 ± 12 % (standard error) of the chemical energy in the biomass could be recovered in the biocrude product fraction. These results demonstrate the feasibility of applying fast and isothermal HTL to produce high yields of biocrude from bacteria and yeast that are high in protein ($\leq$ 72 wt %, dry basis) and low in lipids ($<$ 3 wt %, dry basis). Such microorganisms could serve as a renewable feedstock for biofuels.

3.1 Introduction

Bacteria and yeasts are widely used in industrial biochemical processes that convert feedstock substrates into finished products, such as specialty chemicals [81], food products [82], and biofuels [83–86]. Although there is significant value in the aforementioned products, the microbial biomass itself is usually discarded as waste. Biochemical processes are also used in wastewater treatment, and they create a secondary sludge that is rich in microorganisms, which are often collected and discarded [87]. This microbial biomass can have HHVs comparable to that of microalgae, which has received tremendous attention as a feedstock for biofuels. HTL, a high-temperature and high-pressure process, can convert whole wet biomass into energy-dense biocrude, a product similar to petroleum crude [21, 27, 31, 40]. HTL of bacteria and yeasts may create an opportunity to produce a renewable biofuel from low-value materials and even wastes.

The HTL of microbial communities in sludge is not new. HTL of sludge from biologically treated cornstarch and pulp/paper waste resulted in biocrude yields of 15 - 30 and 42 - 65 wt %, respectively [88, 89]. HTL of anaerobically digested sludge from municipal sources has been less successful, producing biocrude yields of $\leq$ 10 wt % [40, 90].

Recent studies of HTL of microorganisms have focused on microalgae as a feedstock and produced biocrude yields as high as 52 wt % [21, 27, 31, 33, 40, 45, 47]. Although a large portion of the algal biomass is converted to biocrude, the aqueous-phase byproduct also contains some organic C and other nutrients, including N- and P-containing substrates. This aqueous-phase product can be used for cultivating additional biomass. However, using it to grow more algae can be difficult, as several studies have shown that the aqueous-phase product from HTL can be toxic and/or nutrient-limited [59, 60, 91, 92]. Moreover, recycling this water, which contains organic C, to an open pond for algae growth may substantially increase the

risk of contamination by invading heterotrophs. However, Nelson et al. recently demonstrated the feasibility of cultivating *Escherichia coli* and *Pseudomonas putida* monocultures using aqueous phase (from HTL of *Nannochloropsis* sp.) with minimal dilution and nutrient supplementation [93]. Adding a microbial cultivation step in an algae HTL biorefinery to consume the organic carbon in the aqueous phase from HTL of microalgae can enhance the ease of recycling aqueous-phase products to an open algae cultivation pond and provide additional biomass for HTL. To the best of our knowledge, HTL of microbial monocultures, such as bacteria and yeast, has not been examined.

We cultivated *Escherichia coli*, *Pseudomonas putida*, *Bacillus subtilis*, and *Saccharomyces cerevisiae* and subjected the biomass to hydrothermal treatment at fast (rapid heating for 1 min) and isothermal (350 ℃ for 60 min) HTL conditions. *E. coli* and *S. cerevisiae* are bacterial and yeast species, respectively, that are frequently used in industrial bioprocesses. We selected *P. putida* because it is known to metabolize a diverse array of substrates, which makes it a good candidate for growth on complex waste streams [94]. *B. subtilis*, a widely studied Gram-positive bacterium [95], was included to investigate the impact of its differing cellular composition (particularly in the peptidoglycan-abundant cell wall) on the products from HTL when compared to the other two Gram-negative bacteria (*E. coli* and *P. putida*). We report herein the results of how microorganism selection, growth media, cellular structure (Gram-positive versus Gram-negative), and reaction conditions affect the yield and composition of the different product fractions from HTL.

3.2 Materials and Methods

This section first describes the cultivation and analysis of the biomass feedstocks and then describes the procedures for fast and isothermal HTL and subsequent collection, separation, and analysis of the product fractions.

3.2.1 Biomass Cultivation and Harvesting

We cultivated all four microorganisms in various "rich" media containing high concentrations of complex biologically-derived materials, such as yeast extract and peptone, to maximize the biomass yield per volume of culture. For the rich media, we used LuriaBertani medium (10 g/L tryptone, 5 g/L yeast extract, and 10 g/L NaCl) for *P. putida*, terrific broth medium (12 g/L tryptone, 24 g/L yeast extract, 4 mL/L glycerol, 2.31 g/L KH_2PO_4), and 12.54 g/L K_2HPO_4 for *E. coli* and *B. subtilis*, and yeast peptone dextrose medium (10 g/L yeast extract, 20 g/L peptone, and 20 g/L dextrose) for *S. cerevisiae*. We also grew *E. coli* in a "minimal" medium, which contained only chemically defined substrates and nutrients. For the *E. coli* minimal medium, we used M9 medium (20 g/ L glucose, 1 g/L NH_4Cl, 6 g/L Na_2HPO_4, 3 g/L KH_2PO_4, 0.5 g/L NaCl, 1 mM Mg_2SO_4, and 0.1 mM $CaCl_2$). Both seed cultures and final cultures were grown in the same media. *E. coli* grown in terrific broth and M9 minimal medium will hereafter be referred to as *E. coli* TB and *E. coli* MM, respectively.

To grow the biomass feedstock, we first obtained cryogenically preserved (-80 ℃) stocks of *E. coli* K12 MG1655, *P. putida* KT2440, *B. subtilis* SB491, and *S. cerevisiae* S288C and cultivated a 20 mL seed culture of each organism in separate 50 mL test tubes. We incubated the seed cultures for 24 h at 30 ℃ and agitated them at 250 rpm in a New Brunswick Excella E24 incubator. We then added the seed cultures to fresh growth media at a ratio of 20 mL seed culture/2 L medium in 1.5 - 2.0 L cultures and grew them for 24 - 48 h in a New Brunswick I26 or Innova 4400 incubator agitated at 120 rpm. Incubation temperatures ranged from 30 - 37 ℃, and growth vessels were capped with a sterile filter to allow for O_2 transport.

We harvested cell cultures by centrifuging them in 1 L vessels at 5000 rcf for 15 min in a Beckman Coulter Avanti J-20XP or Thermo Scientific Sorvall Lynx 6000 centrifuge. To "wash" the biomass to remove potential substrates remaining from

the media, we discarded the supernatant media, resuspended the cell pellets in an equal volume of deionized water, and then reformed the pellet with centrifugation for 20 min. We then discarded the supernatant water, resuspended each cell pellet in 10 mL of water, transferred this slurry to 50 mL centrifuge tubes, and centrifuged it once more at 5000 - 12,000 rcf in an Allegra 21R or Eppendorf 5810R centrifuge. We discarded the supernatant water from these tubes and used the resulting cell pellets as the biomass feedstock for HTL. The collected biomass was always a slurry containing at least 12 wt % (dry basis) biomass solids.

3.2.2 Biomass Feedstock Analysis

We dried biomass samples in a 70 ℃ oven for 48 h to completely remove any remaining water. To determine the ash content, we transferred 50 mg of the dried biomass into a pre-weighed aluminum weigh boat. A Ney Vulcan 3-130 muffle furnace heated the sample to 250 ℃ from room temperature at a rate of 10 ℃/min. After a 30 min holding period, the temperature was increased at a rate of 20 ℃/min to 550 ℃ and then held for 30 h. After removing the samples from the furnace, we cooled them in a desiccator to room temperature and then recorded the mass of residual material, the ash. We sent dried samples of the different biomass slurries to Atlantic Microlabs, Inc. for analysis of C, H, N, and S contents. We calculated the O content as the difference between 100 wt % and the combined contents of C, H, N, S, and ash.

We developed a lipid analysis method by combining practices from Levine et al. [96] and Lewis et al. [97] and purchased chemicals of $>$ 99 % purity from Fisher Scientific. We transferred approximately 20 mg of dried biomass into a glass test tube and then added 2 mL of a 5 % (v/v) solution of acetyl chloride in methanol and a magnetic stir bar. We vigorously stirred the reaction mixture ($>$ 100 rpm) for 90 min at 100 ℃ using a magnetic stir plate and temperature-controlled heating

block. After the 90 min holding period, we quenched the reaction by adding 1 mL of room-temperature deionized water. After the solution cooled for 10 min, we added 4 mL of n-heptane and agitated each tube for 10 min on a vortexer at 1000 rpm. We centrifuged the mixture for 3 min at 1500 rcf to separate and then collect the heptane layer for gas chromatographic analysis.

For GC analysis, We injected 1 μL of sample, with a 2:1 split ratio, into an Agilent 7890 gas chromatograph equipped with an Agilent DB-FFAP column (30 m $\times$ 320 μm $\times$ 0.25 μm). We used helium as the carrier gas at a flow rate of 1 mL/min. The injector temperature was 250 ℃. The oven temperature was maintained at 60 ℃ until the injection and then increased to 200 ℃ at a rate of 20 ℃/min and then to 240 ℃ at a rate of 5 ℃/min. The final temperature was held for 3 min. We generated calibration curves using a RESTEK Marine Oil mixture of 20 fatty acid methyl esters as an external standard.

We estimated the protein content (wt %) of the biomass by multiplying its N content (wt %) by 6.25 [98, 99]. We calculated the carbohydrate content as the difference between 100 wt % and the sum of the lipid, protein, and ash contents.

3.2.3 Hydrothermal Liquefaction

We constructed Swagelok® reactors using $^3/_8$ in. port connectors fitted with a cap on one end and a $^3/_8$ to $^1/_8$ in. reducing union on the other end. The union allowed for the attachment of a 15,000 psi-rated High Pressure Equipment Co. valve with grafoil packing for sampling the gas products. The valve was attached to the reactor body via 8.5 in. of $^1/_8$ in. outer diameter tubing. The nominal volume added by the valve was 0.5 mL. The total volume of the reactor and valve is approximately 2.2 mL (depicted in Figure 3.1).

For isothermal HTL, we loaded 1.35 g of biomass slurry ($\geq$ 12 wt % solids) to each Swagelok® reactor. At this loading, water would fill 95 % of the reactor volume at the

reaction conditions. We sealed the reactors and placed them into a Techne fluidized sand bath preheated to 350 ℃. The reactors were submerged in the sand bath and agitated using a Burrell Wrist-Action shaker for 60 min [31]. For fast HTL reactions (performed with rapid heating), we loaded the reactor with 0.30 g of biomass slurry ($\geq$ 12 wt % solids). This water loading matched previous experiments in our laboratory for fast HTL [33]. After sealing the reactors, they were placed in a 600 ℃ sand bath for 1 min. As described in Chapter II, we used proxy reactors (previously depicted in Figure 2.2), fitted with a thermocouple to record the temperature and calculate the heating rate [33]. In both cases, after the desired holding time had elapsed, we removed the reactors from the sand bath and quenched them in a water bath.

Figure 3.1: Reactor with gas valve assembly

3.2.4 Recovery and Analysis of Product Fractions from Hydrothermal Liquefaction

After the reactors were quenched, we analyzed the gas phase using the method described by Brown et al. [27]. Specifically, we connected the high pressure valve of the reactor to a sampling valve attached to an Agilent Technologies model 6890N GC equipped with a thermal conductivity detector (TCD). A 15 ft. stainless steel column with $^{1}/_{8}$ in. inner diameter, packed with 60 - 80 mesh Carboxen 1000 (Supleco), separated each component in the gas phase sample. We used Ar as the carrier gas at a flow rate of 15 mL/min. The temperature of the column was initially held at 35 ℃ for 5 min, heated at a rate of 20 ℃/min until it reached 225 ℃, and held at this temperature for 15 min, giving a total run-time of 35 min. We generated a calibration curve using

gas standards purchased from Air Liquide Specialty Gases. The calibration curve relates the mole fraction, y_i, and the peak area for each component. The molar yield, n_i, of each component was subsequently calculated from the mole fractions of each compound detected in the gas chromatagraph using Equation 3.1. We used the ideal gas law to determine the moles of N_2 from air in the reactor, based on the volume of the headspace in each reactor when it was loaded and sealed.

$$n_i = \frac{y_i}{y_{N_2}} n_{N_2} \tag{3.1}$$

After gas analysis, the reactor was opened and the remaining products were collected according to the methods described in Chapter II and by Valdez et al. [31, 33]. We report the gravimetric yield of each product fraction as its mass divided by the mass of biomass loaded into the reactor on a dry basis (wt %). Solvent-free samples of the light and heavy biocrude were sent to Atlantic Microlab, Inc. for measurement of the weight percent of C, H, N, and S. The O content in the light and heavy biocrudes was calculated by difference. We report elemental distribution as the mass of an element in each of the product fractions per the total mass of that element in the biomass. We diluted the aqueous phase 1:600 with deionized water to measure NH_3 in the aqueous phase, which was carried out using methods described previously [31].

The hexane-soluble product, also referred to as the light biocrude, was analyzed with an Agilent 6890N gas chromatograph fitted with an Agilent 5973 mass spectrometer. We injected 1 μL into a 300 ℃ split injection port using a split ratio of 2:1 onto an Agilent HP-5 capillary column (50 m $\times$ 200 μm $\times$ 0.33 μm). The oven was set to 100 ℃, and the temperature increased to 300 ℃ at a rate of 5 ℃/min immediately after injection. The samples exited the column into an electron ionization mass spectrometer. We used matching software to tentatively identify molecular constituents

in the biocrude sample based on mass spectra. We calculated the HHV of the light and heavy biocrude products using the Boie formula (previously discussed in Chapter II, Equation 2.1 [74]) and the elemental composition data (wt % on a dry basis of C, H, N, S, and O).

We used the HHV and gravimetric yields of the biocrude product fractions to estimate the energy recovered in the biocrudes from the original biomass, calculated as described in Chapter II. We report the average of at least three replicate experiments, unless otherwise noted. When available, we report experimental variation as standard error.

3.2.5 Control Experiments

We added approximately 160 mg of dried biomass to a glass test tube, which is similar to the biomass loading in the reactor for isothermal HTL. We then added 9 mL of DCM and agitated the samples on a vortex mixer set at 1000 rpm for 1 h. After mixing, we added 1.2 mL of deionized water, which mimics the water loading in a reactor, and agitated the samples for another 1 h. We then followed the workup procedure described previously to collect and measure the yield of each of the product fractions, except for gas [31]. This control experiment provides the yields of each product fraction available from the biomass simply by wet extraction without HTL.

3.3 Results and Discussion

This section first reports the characteristics of the microorganisms that we cultivated and then the results of HTL. The latter section describes the yield, elemental composition, and selected molecular composition of the product fractions. We also report the HHV and energy recovery of the biocrudes and compare results among the various microorganisms and HTL process variations.

3.3.1 Feedstock Analysis

Table 3.1 shows the elemental and biochemical contents of each of the biomass feedstocks. There are but modest variations in the elemental compositions of C, H, N, and S. The C and N weight percents for *E. coli* are within 6 % relative difference of those reported previously [100, 101]. Although the two *E. coli* cultures were cultivated using different growth media, their C, H, N, and O contents were within 10 % of each other on a relative basis. *B. subtilis* and *P. putida* had the highest ash compositions of 13 and 11 wt %, respectively, whereas the other organisms had < 7 wt % ash content.

Table 3.1: Elemental and biochemical compositions (wt %) and HHV (MJ/kg) of the bacterial and yeast biomass

	C	H	N	S	O	Ash	Lipid	Protein	Carb	HHV
E. coli TB	46.54	6.69	13.7	0.67	25.58	6.82 ± 0.02	0.57 ± 0.36	86	7	22
E. coli MM	47.32	6.88	13.17	0.58	27.15	4.9 ± 0.1	2.6 ± 0.1	82	10	23
P. putida	46.58	7.08	13.23	0.55	21.48	11	2.7 ± 0.7	83	4	23
B. subtilis	42.65	6.56	11.45	0.43	25.91	13.0 ± 0.4	0.55 ± 0.03	72	15	21
S. cerevisiae	46.47	7.31	12.04	0.47	29.03	4.68 ± 0.01	2.7 ± 0.6	75	17	22

E. coli MM, *S. cerevisiae*, and *P. putida* had the highest lipid contents, but they were all ≤ 2.7 wt %. *E. coli* TB and *B. subtilis* contained < 0.6 wt % lipids. *E. coli* TB was cultivated in a nutrient-rich media; therefore, it is reasonable that the cells would accumulate less lipids than the *E. coli* MM, since other microorganisms are known to accumulate more lipids under nutrient-deficient conditions [102]. Likewise, Gram-positive organisms, such as *B. subtilis*, have fewer lipids possibly because of the lack of an outer membrane in the cell envelope compared to Gram-negative organisms. The carbohydrate content of each biomass sample varied between 4 and 17 wt %. All biomass samples were rich in protein (≥ 72 wt %). In comparison to the microalgae feedstocks typically subjected to HTL, the yeast and bacteria have a much lower lipid content and much higher protein (and N) content [103].

3.3.2 Yields of Product Fractions

As a control experiment, we exposed dried, unreacted biomass to fresh solvents at room temperature. After exposure to DCM and water, ≤ 4 wt % of the biomass partitioned to the organic phase as biocrude. The remaining biomass partitioned to the solid product fraction. Therefore, solvent extraction alone does not generate the high biocrude yields that are typical after HTL.

Figure 3.2 shows the yields (wt %, dry basis) of light and heavy biocrudes from each organism after both HTL conditions (yields are also included in Table B.1 for clarity). Isothermal HTL at 350 ℃ for 60 min is common practice [21, 27, 29, 42, 104]; therefore, the present results from the yeast and bacterial biomass can be compared to those from isothermal HTL of other feedstocks. We also used rapid heating or fast HTL, which can increase the biocrude yield [33]. The average maximum temperature observed in the proxy reactor during fast HTL was 276 ± 9 ℃, and the average heating rate of the reactors at fast HTL conditions was 217 ± 9 ℃/min, with the uncertainty representing standard error.

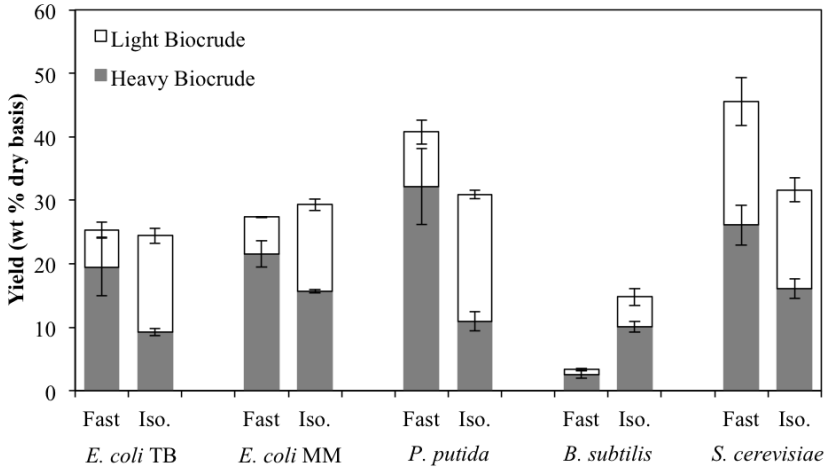

Figure 3.2: Yields of light and heavy biocrude (wt % dry basis) for fast and isothermal HTL of each biomass

B. subtilis showed the lowest total yield of biocrude for both fast (3 ± 1 wt %) and isothermal (15 ± 2 wt %) HTL. These low yields may be linked to the cellular

structure of *B. subtilis*. One such contributing factor may be the different molecular composition of the cell envelope. Gram-positive bacteria, including *B. subtilis*, have a cell envelope consisting of a thick layer of peptidoglycans, which are polysaccharides cross-linked by polypeptides. These biomacromolecules likely hydrolyze to simple sugars and amino acids that would reside within the aqueous-phase product. Past research has shown that continued hydrothermal processing of water-soluble amino acids and carbohydrates can form organic-solvent-soluble products [35, 105]. The 1 min reaction time for fast HTL may have been long enough to form these water-soluble products yet too brief to allow for their re-polymerization into biocrude components. Such processes could account for the higher biocrude yield at isothermal HTL conditions observed in Figure 3.2 for *B. subtilis*.

Fast HTL of *P. putida* and *S. cerevisiae* produced the most biocrude with yields of 41 $\pm$ 4 and 39 $\pm$ 8 wt %, respectively. The high yield of biocrude from *S. cerevisiae* may also be linked to the cell structure of the yeast, in this case improving the yield, unlike the result from *B. subtilis*.

The larger margin of error in the yields from fast HTL probably arises from the lower biomass loadings. There is less material to recover in these experiments, and transfer losses become more significant, on a relative basis, compared to isothermal HTL [33]. The reaction conditions did not affect the total yield of biocrude for both types of *E. coli*. Figure 3.2 shows that fast HTL always produced a higher fraction of heavy biocrude than light biocrude, regardless of the biomass feedstock. This trend is also true for the fast HTL of the microalga *Nannochloropsis* sp. [33]. Figure 3.2 shows that, with the exception of *B. subtilis*, the yield of total biocrude produced at isothermal HTL conditions was fairly consistent, ranging between 24 and 32 wt % on a dry basis for the different microorganisms.

Table 3.2 shows the yield of solid (water- and DCM- insoluble), aqueous-phase, and gas products for both fast and isothermal HTL of each organism. The aqueous-

phase product was translucent amber in color for all of the different microorganisms. More than 42 wt % of the biomass is converted to aqueous phase products. The solids were gray powders that settled at the bottom of the test tube. Solid yields were always < 9 wt %, with the exception of *E. coli* MM treated with fast HTL. *E. coli* differentially expresses genes that affect the cell structure when grown in minimal versus rich medium [106]. The milder reaction conditions in fast HTL may not have been sufficient to break down certain components in the *E. coli* cell, especially when grown in MM. The data in Table 3.2 suggest that the residual solids remaining after fast HTL likely form mostly aqueous phase products when reacted under the more severe isothermal HTL conditions.

Table 3.2: Yields of solid, aqueous-phase, and gas products (wt % dry basis)

	Solids		Aqueous-Phase		Gas	
	Fast	Isothermal	Fast	Isothermal	Fast	Isothermal
E. coli TB	8.5 ± 2.5	2.1 ± 0.3	66 ± 2	72 ± 1	[a]	1.2 ± 0.1
E. coli MM	26 ± 2	5.0 ± 0.3	46 ± 3	64 ± 1	0.38	1.6 ± 0.5
P. putida	4.3 ± 1.1	1.8 ± 0.3	53 ± 5	63 ± 2	1.7	4.8 ± 1.2
B. subtilis	3.4 ± 0.6	3.6 ± 0.3	91 ± 0	80 ± 2	1.8	1.3 ± 0.3
S. cerevisiae	5.6 ± 0.2	4.6 ± 0.6	42 ± 7	61 ± 4	6.9	2.4 ± 0.4
[a] - Not detected						

Table 3.2 shows that < 7 wt % of the biomass is converted to gas. The differences in the composition of the gas products from HTL of each biomass were not statistically significant. Therefore, Figure 3.3 shows the average composition of the gas products from both fast and isothermal HTL. The gas products from fast HTL contained 64 ± 15 mol % CO_2, 19 ± 11 mol % CO, 8 ± 3 mol % CH_4, 2 ± 0.3 mol % C_2H_4, and 2 ± 1 mol % C_2H_6. The gas phase from isothermal HTL contained, on average, 93 ± 6 mol % CO_2 (significantly more than in the gas from fast HTL), with the balance being H_2, CO, CH_4, C_2H_4, and C_2H_6, all present in smaller quantities than observed in the gas from fast HTL. At more severe reaction conditions, CO_2 is a common product

from the hydrothermal decomposition of amino acids [107].

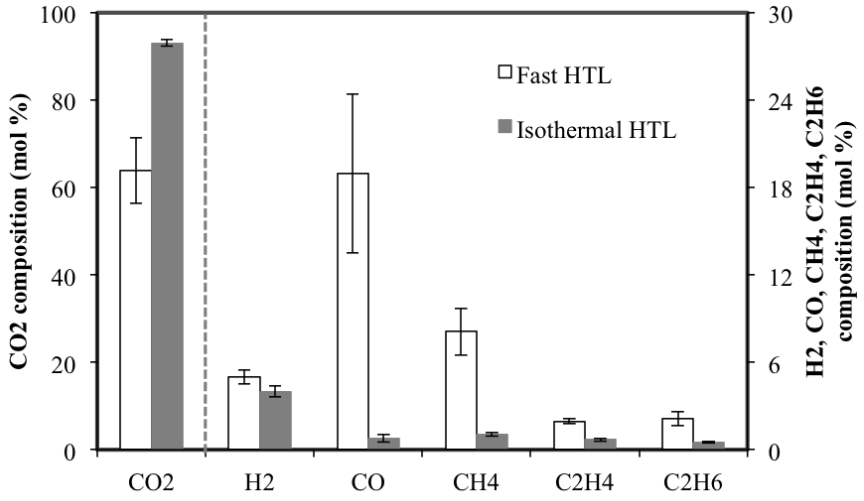

Figure 3.3: Average composition of the gas-phase products from fast and isothermal HTL (CO_2 on left axis, all other gases on right axis)

3.3.3 Elemental Composition of Light and Heavy Biocrudes

Figure 3.4 shows the C, N, O, and S contents (wt %) of the light and heavy biocrudes for each organism (exact values are included in Tables B.2 to B.6 in the Appendices). Elemental ratios of H/C, N/C, O/C, and S/C in the light and heavy biocrudes are also presented in Appendix B (Figures B.1 to B.4). Figure 3.4a shows that, regardless of the HTL reaction conditions, the light biocrude always had a higher weight percent of C than the heavy biocrude, similar to the results obtained previously for HTL of *Nannochloropsis* sp. [31, 33]. Fast HTL biocrudes, both light and heavy, always had a lower weight percent of C than did the biocrudes from isothermal HTL. Figures 3.4b and 3.4c show that the light and heavy biocrudes from fast HTL are always richer in N and O contents than their counterparts from isothermal HTL. Previous results for HTL of *Nannochloropsis* sp. showed that increasing the reaction severity, that is increasing the holding time and/or increasing the reaction temperature, reduces the O content in the biocrude [31]. The results in Figure 3.4c show the

same trend. Even so, the N and O contents in these biocrudes are roughly an order of magnitude greater than those in most petroleum crude oils [108] and may present challenges when upgrading the biocrude to a fungible hydrocarbon fuel. All of the biocrudes, however, have a reduced O content compared to the original biomass.

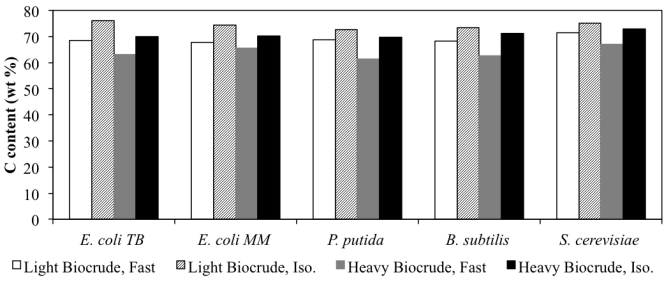

a Composition of C in the light and heavy biocrudes

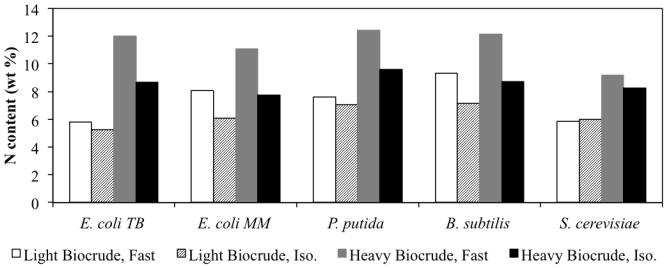

b Composition of N in the light and heavy biocrudes

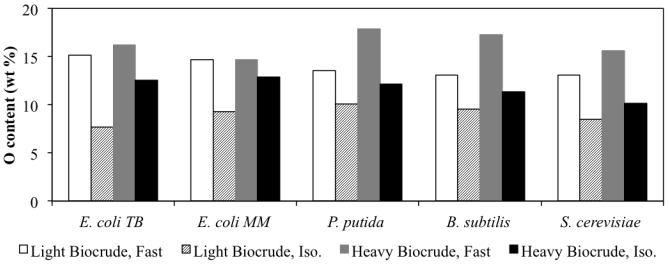

c Composition of O in the light and heavy biocrudes

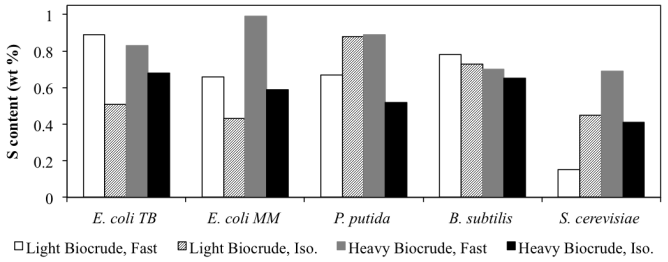

d Composition of S in the light and heavy biocrudes

Figure 3.4: Elemental composition of the light and heavy biocrudes

Figure 3.4d shows that the S content in the biocrude varies among the different organisms, but it is always < 1 wt %, putting it within range of the S content of most petroleum crudes [80]. The heavy biocrude from fast HTL is always richer in S than the heavy biocrude from isothermal HTL. The S content in the light biocrude from *S. cerevisiae* treated by fast HTL was the lowest at 0.15 wt %.

3.3.4 Ammonia in the Aqueous Phase

Figure 3.5 shows the percentage of the total N from the biomass that is present as dissolved ammonia in the aqueous phase. Isothermal HTL of the biomass favors the near-complete conversion of water-soluble N products into ammonia. As reaction severity increases, more of the N in the biomass is converted into ammonia [31]. Converting N-containing molecules into dissolved ammonia makes the N more bioavailable for use by most microorganisms. This conversion facilitates the recycling of N in a biorefinery, which is an important consideration for environmental sustainability.

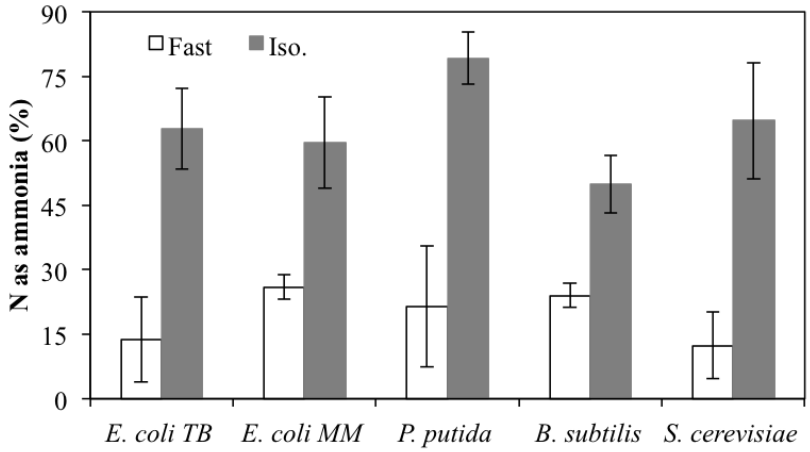

Figure 3.5: Percentage of N as ammonia in the aqueous phase

3.3.5 Elemental Distribution

Knowing the gravimetric yields and the elemental composition of each product allows one to calculate how the various elements are distributed among the product fractions. C and N are of most interest because the C content strongly influences the HHV, and N recycling is essential for a sustainable biorefinery. The present results (see Figures B.5 and B.6 in Appendix B) show that, at most, 58 % of C in the biomass goes to the biocrude. *B. subtilis* had the lowest C distributed to the biocrude, while *P. putida* and *S. cerevisiae* had the highest distribution of C because of their higher yields of biocrude. Similar to the results from the HTL of microalgae, the majority of N (80 % or more for isothermal HTL) resides in the aqueous phase and solids [31]. This outcome is desirable because it facilitates recycling of the N-containing compounds as nutrients for cultivation of additional biomass. Less than 35 % of the total N from the biomass is distributed to the biocrude for all HTL reaction conditions examined.

3.3.6 Heating Value and Energy Recovery

Table 3.3 shows the HHVs of the light and heavy biocrudes and the percentage of the chemical energy in the biomass that is recovered in the biocrude. The HHV of the light biocrude was always higher than that of the heavy biocrude, and biocrudes produced at isothermal HTL conditions had higher HHVs than biocrudes from fast HTL. These trends are simply a manifestation of the trends in the C and O contents of the various biocrude fractions. Regardless of the biomass feedstock processed, the variation in the HHV for a given biocrude (light or heavy) fraction from a given HTL approach (fast or isothermal) is always $\leq$ 2 MJ/kg. It appears that the processing conditions and product separation protocol play a larger role in determining the HHV than the biomass feedstock [29].

The last column of Table 3.3 shows the percentage of the energy recovered in

Table 3.3: HHV and energy recovery of the biocrude

		HHV (MJ/kg)		
		Light Biocrude	Heavy Biocrude	Energy Recovery
E. coli TB	Fast	34.09	30.42	36 ± 4
	Isothermal	38.48	33.32	40 ± 2
E. coli MM	Fast	33.14	31.14	38 3
	Isothermal	37.08	33.75	46 ± 2
P. putida	Fast	34.15	29.11	53 ± 5
	Isothermal	35.83	33.07	47 ± 3
B. subtilis	Fast	33.22	29.36	5 ± 1
	Isothermal	35.99	33.76	25 ± 3
S. cerevisiae	Fast	35.10	31.19	58 ± 12
	Isothermal	37.43	34.66	51 ± 5

the biocrude from the original biomass. *S. cerevisiae* and *P. putida* had the highest energy recovery values for both fast and isothermal HTL. *B. subtilis* had the lowest energy recovery (recall that it also produced the lowest yields of biocrude). The energy recoveries in biocrude from HTL of bacteria and yeast are not as high as those often observed from HTL of microalgae, where values exceeded 70 % at the same processing conditions [31, 33]. Of course, microalgae typically have lipid contents that are an order of magnitude higher than those of the bacteria and yeast used in this study. Higher lipid contents tend to correlate with higher biocrude yields [21] and higher energy recoveries in the biocrude. Nevertheless, Table 3.3 shows that HTL can produce energy-dense biocrudes containing 36 % or more of the chemical energy in the microbial biomass (with the exception of *B. subtilis*).

3.3.7 Molecular Composition of the Light Biocrude

We analyzed the light biocrude using a gas chromatograph with mass spectrometry (GC-MS). Table 3.4 shows the components in the light biocrude for which the GC-MS software gave at least a > 50 % match factor with a compound in its mass spectra

library and the relative abundance of these compounds quantified by peak area. Not all of the compounds in the biocrude could be identified because of the large number of low-intensity peaks present in each chromatogram. All chemical identities in Table 3.4 remain tentative, because we used no authentic standards to obtain positive identities. The peak areas listed in Table 3.4 provide a qualitative representation of the relative abundance of their respective compounds in the light biocrude.

Table 3.4 shows that the fast HTL biocrude was less likely to contain heterocycles and aromatics. The N-containing heterocycles, such as substituted indoles and amines, are possibly derived from the decomposition of porphyrins or the proteins that are abundant in the microorganisms [109]. Such N-containing heterocycles are not uncommon in petroleum crude, but the presence of these compounds in higher concentrations in the biocrude could make it more difficult to upgrade to a hydrocarbon fuel. Free fatty acids appear in Table 3.4, and these are common products in biocrudes from microalgae HTL [27]. For the microbial biomass studied here, free fatty acids are likely predominantly derived from the cell membrane. The biocrudes from fast HTL contain a higher percentage of fatty acids than the biocrudes from isothermal HTL, potentially showing that lipids in the cell hydrolyze faster than other biomolecules. Fatty acid amides are more common in the isothermal HTL products, suggesting that the higher concentration of NH_3 present in the reactor facilitates replacing the hydroxyl group of the fatty acid. Table 3.4 shows that more of the cyclic proline dimer [110], a likely decomposition product of proteins, is found in the fast HTL biocrude, suggesting the incomplete decomposition of proteins to amino acids at milder conditions.

Table 3.4: Tentative identities and relative abundance of different compounds in the light biocrude

Name	% Total Area									
	E. coli TB		*E. coli* MM		*P. putida*		*B. subtilis*		*S. cerevisiae*	
	Fast	Iso.	Fast	Iso.	Fast	Iso.	Fast	Iso.	Fast	Iso.
4-methylphenol	[a]	2.43	-	-	-	1.82	-	5.7	-	1.14
4-ethylphenol	-	1.88	-	1.4	-	1.41	-	4.09	-	0.58
piperidin-2-one	-	0.8	-	0.44	-	0.79	-	2.72	-	0.29
hexahydro-2H-azepin-2-one	-	0.81	-	-	-	0.56	-	2.66	-	0.31
indole	-	0.75	1.32	0.49	1.04	0.57	1.78	1.65	-	0.12
(3,5, or 7)-methylindole	-	1.46	1.07	1.1	0.55	1.08	1.24	3.32	0.49	0.56
N-alkyl-benzamine	-	1.67	1.24	1.68	-	1.59	-	3.62	0.67	0.85
2,3-dimethylindole	-	0.57	-	0.57	-	0.44	-	1.21	-	0.51
N-(2-phenylethyl)-ethanamide	-	0.42	1.3	0.48	1.01	-	1.61	2.24	0.91	0.22
dodecanoic acid	2.77	0.58	1.07	0.52	3.03	0.58	-	-	0.77	0.37
2-(indol-3-yl) acetaldehyde	-	0.64	-	0.67	-	0.61	-	1.6	-	0.43
1-(3-methylindol-1-yl)ethanone	-	0.57	-	0.69	-	0.53	-	-	-	0.41
1-phenylmethyl-2-pyrrolidinone	-	0.3	-	0.36	-	0.28	-	0.96	-	-
tetradecanoic acid	1.56	1.39	4.86	2.17	3.24	1.15	14.24	12.41	2.2	1.19
tetradecanamide	0.28	0.52	-	0.64	0.53	0.64	-	-	-	-
9H-carbazole	-	0.56	0.86	0.58	0.96	0.44	-	0.81	1.01	0.33
hexadecanenitrile	-	0.81	1.24	1.41	-	0.63	-	-	0.62	0.84
cycloheptan indole	-	0.58	3.84	0.7	1.01	0.17	7.49	-	-	-
9-hexadecenoic acid	3.63		-	0.32	1.67	0.42	-	-	21.07	4.81
cyclic proline dimer	3.56	0.64	3.18	0.75	2.43	0.83	-	-	7.67	1.23
hexadecanoic acid	30.02	3.97	12.32	3.48	7.17	2.13	3.35	-	9.75	5.19
9-octadecenoic acid	2.01	1.85	1.83	1.37	-	0.66	-	-	1.4	0.55
1-Methyl-9H-beta-carboline	-	0.6	0.8	0.27	1.04	0.54	-	0.65	-	0.74
octadecenamide	1.84	0.24	-	0.13	3.05	0.57	1.43	1.29	-	-
acridine	-	0.26	-	0.41	-	0.3	-	0.79	-	1.87
thiazole	0.82	-	0.82	-	1.31	-	-	-	-	2.38
hexadecanamide	5.22	5.46	3.72	7.81	2.23	3.83	-	-	1.38	4.2
dimethyl hexadecanamide	-	2.47	0.76	4.01	0.59	2.07	-	-	-	1.18

[a] - not detected

3.4 Conclusions

We demonstrated the feasibility of using microbial monocultures as a feedstock for biocrude production via HTL. The high N and O contents of the biocrude, for all organisms and all HTL reaction conditions, necessitates additional treatment of the biocrude before its use as a fungible liquid transportation fuel. The cultivation of bacteria with aqueous-phase byproducts from HTL of microalgae [93] provides an opportunity to improve the overall use of nutrients and total biocrude output in an algal biorefinery.

E. coli cultivated in the TB (nutrient-rich) media was higher in ash and lower in lipid than the *E. coli* cultivated in MM. The growth media used to cultivate the bacterium did not significantly affect the elemental composition of the harvested biomass. The biocrude yields produced at both fast and isothermal HTL conditions were not significantly different for the two different cultivation media. This insensitivity of the HTL outcomes to the growth media suggests that aqueous-phase product streams that are nutrient-depleted or contain certain substrates that are not easily metabolized [93] may nevertheless be suitable for biocrude production via *E. coli* cultivation.

The Gram-positive organism, *B. subtilis*, provided the lowest yield of biocrude from HTL compared to all other microorganisms in this study. Its modestly lower lipid content is probably not fully responsible for the reduced yield because *E. coli* TB had a similar lipid content but significantly higher biocrude yields. The *B. subtilis* biomass did decompose during HTL, however, as the yield of residual solids was only about 4 wt %. The decomposition products were primarily water-soluble, which might be in part due to the cell envelope of this Gram-positive bacterium containing a thick peptidoglycan layer.

HTL of the yeast, *S. cerevisiae*, yielded more biocrude on average than did HTL of any of the bacterial biomass. These higher yields also resulted in higher average recovery of the energy in the biomass to the biocrude product. However, *P. putida*

had similar yields and is capable of growing on media lacking nutrients and containing possible toxins that can inhibit growth, specifically the aqueous-phase product from the HTL of microalgae [93].

As the literature and results presented herein indicate, fast HTL can, in many cases, lead to higher total biocrude yields than isothermal HTL [33]. The shorter reaction time necessary for fast HTL would reduce reactor size and capital costs in a continuous industrial process. However, in exchange for these benefits, fast HTL biocrudes appear to have a less desirable composition. For example, a higher percentage of the total biocrude from fast HTL exists as heavy biocrude than observed in the biocrude from isothermal HTL. Fast HTL biocrudes also have higher O, N, and S contents, which make these biocrudes less desirable for use as a biofuel or biofuel precursor compared to those from isothermal HTL. More N in the isothermal HTL aqueous phase is converted to NH_3, making N more bio-available as a nutrient for algae cultivation [91]. Further analysis of these economic and environmental trade-offs, possibly via life cycle assessment (LCA) as Orfield et al. recently reported for the HTL of *Nannochloropsis* sp. [111], is required to determine which of these processes is preferable for the conversion of biomass to biocrude.

CHAPTER IV

Effects of Processing Conditions on Biocrude Yields from Hydrothermal Liquefaction of Microalgae

This chapter describes the examination of various reaction conditions (including algae species, reaction time, and reactor loading) and their effects on the biocrude yield from HTL of microalgae. All fast HTL reaction times were $\leq$ 2 min. The highest biocrude yield obtained at the reaction conditions included in this chapter was 67 $\pm$ 5 wt % (600 ℃ sand bath, 1 min, 5 wt % solids in slurry, 10 vol % water, standard error). With all other process variables fixed, increasing the reaction time in a 600 ℃ sand bath by 15 s increments led to a rapid increase in biocrude yield between 15 - 45 s. After longer reaction times, the biocrude yield decreased. Low reactor loadings generally gave higher biocrude yields than did higher loadings. The low reactor loadings may facilitate biocrude production by facilitating cell rupture and/or increasing the effective concentration of algal cells in the hot, compressed water in the reactor.

4.1 Introduction

In Chapter II, we described a variation on the HTL process and termed it fast HTL [33]. Fast HTL requires just a short reaction time (up to a few min) but rapid heating rates (150 - 300 ℃/min), which facilitate the production of biocrude from microalgae with yields comparable to or higher than those from isothermal HTL [33]. More recently, there have been investigations of fast HTL of macroalgae [52], microalgae HTL in a continuous flow system [13], and in Chapter III we described the fast HTL of other micro-organisms (bacteria and yeast) [66]. These studies demonstrated the robustness of this fast HTL approach but much about this promising HTL variation remains unknown. To fill some of these gaps, we explore herein the effects of different aspects of reactor loading and reaction time on fast HTL of four species of microalgae: *Nannochloropsis* sp., *Chorella vulgaris*, *Botryococcus braunii*, and *Neochloris oleoabundans*.

4.2 Materials and Methods

Materials used in this work are identical to those described in Chapter II [33] and were purchased and/or constructed in the same manner. Most data reported herein describe batch reactions using *Nannochloropsis* sp. from Reed Mariculture, Inc., although we also compare results from HTL of *Nannochloropsis* sp. to those from *Chorella vulgaris*, *Botryococcus braunii*, and *Neochloris oleoabundans* cultivated at the University of Dayton Research Institute (UDRI). Batch mini-reactors were loaded with algae and deionized water (see Tables C.1 to C.5 in Appendix C for loading details) and sealed to 45 ft-lbs using a torque wrench. Sealed reactors, accompanied by a thermocouple-equipped proxy reactor (as depicted in Figure 2.2), were submerged in a fluidized sand bath preheated to 600 ℃ for fast HTL, and 350 ℃ for isothermal HTL. The reaction time was defined to begin at the instant reactors were submerged

and to end at the instant reactors were quenched in a cold water bath.

Cooled reactors were opened and the products collected by pouring the reactor contents into a glass centrifuge tube, rinsing the reactor with 9 mL of DCM, and collecting these rinsings in the same test tube. The biocrude (organic phase), solid, and aqueous-phase products were separated with centrifugation and manual transfer via pipette as described in Chapters II [33] and III [66]. Once separated, the biocrude products were dried under N_2. After drying, the masses of the biocrude products were recorded. We report biocrude yields as the mass of biocrude divided by the mass of dry algae loaded into the reactor (wt % dry basis).

4.3 Results and Discussion

This section presents the effects of algae species, reaction time, and reactor loading on biocrude production from HTL of microalgae. The first subsection includes four species of microalgae, but all subsequent subsections focus on results from the HTL of *Nannochloropsis* sp.

4.3.1 Algae Species

Figure 4.1 depicts biocrude yields (in dry wt %) from fast (600 ℃ sand bath for 1 min) and isothermal (350 ℃ sand bath for 60 min) HTL of four species of microalgae. The standard error from at least three replicates of each reaction condition is represented by the error bars on this figure and all others in this work, unless otherwise indicated. The biocrude yield produced from isothermal HTL of *Nannochloropsis* sp. depicted in Figure 4.1 is taken from previous work (Chapter II, [33]) and is based on an HTL reaction singleton.

For all species of microalgae examined in the present work, fast HTL produces biocrude yields comparable to those from isothermal HTL. Fast HTL of *Botryococcus braunii* and *Nannocholoropsis* sp. produced more biocrude on a dry weight basis

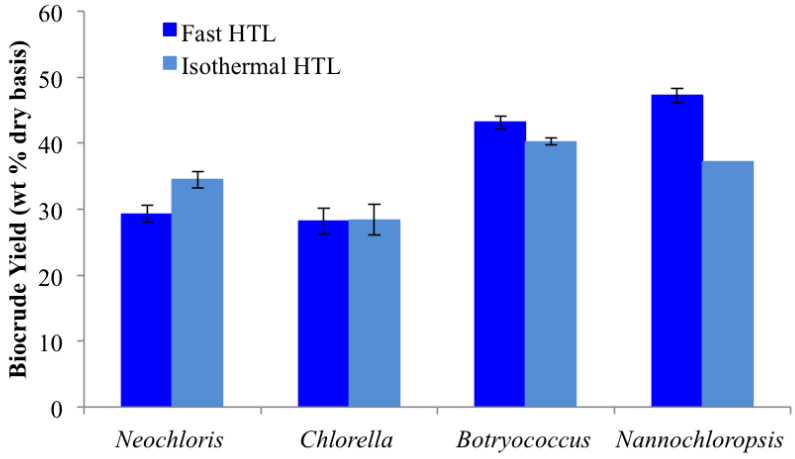

Figure 4.1: Biocrude yields from fast (600 ℃ sand bath, 1 min, 30 vol % water loading) and isothermal (350 ℃ sand bath, 60 min, 55 vol % water loading) HTL of different algae species, 15 wt % solids in slurry

than did isothermal HTL. Along with the previous work investigating fast HTL of bacteria and yeast [66], these results are a testament to the robustness of fast HTL as a biomass conversion process for microorganisms. The differences in biocrude yields between different algae species may reflect the differences in biochemical composition (i.e. protein, lipid, carbohydrate, ash for isothermal HTL) and/or cellular structure (i.e. cell wall strength, cell shape, cell size for fast HTL) between species.

4.3.2 Reaction Time

Figure 4.2 depicts the biocrude yields and corresponding maximum reactor temperatures for a series of reaction times examined at a sand-bath set-point temperature of 600 ℃. The biocrude yields increase rapidly between 0.25 - 0.75 min and decrease with further increases in reaction time. A maximum biocrude yield of 55 wt % is obtained after only 0.75 min in the 600 ℃ sand bath. The reactor temperature was 188 ℃ at 0.75 min.

The rapid increase in biocrude yield between 0.25 - 0.75 min may be due to cell breakage, which could occur at different characteristic temperatures for different

algal species [47] and possibly be accelerated by rapid heating. Cell breakage would release triglycerides and other biomolecules that may contribute to high biocrude yields. Decreasing biocrude yields with increasing reaction time beyond 0.75 min is likely the result of hydrothermal degradation of cellular components to water-soluble and gaseous products, with the latter becoming more significant at temperatures exceeding the critical point of water (374 ℃). The biocrude yields in Figure 4.2 appear to decrease more rapidly after increasing temperature beyond the critical point.

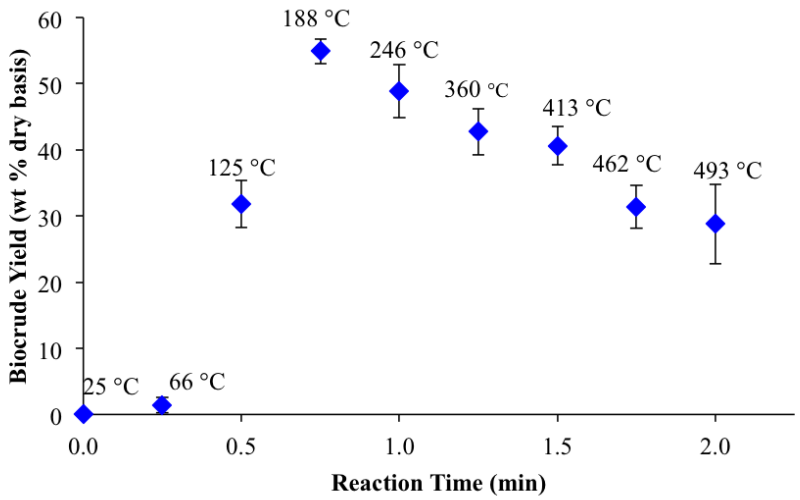

Figure 4.2: Biocrude yields and maximum reactor temperatures from fast HTL of *Nannochloropsis* sp. at different reaction times. Sand-bath temperature = 600 ℃, 15 wt % solids in slurry, 11 vol % water loading at room temperature

4.3.3 Reactor Loading

There are three ways to systematically vary the contents of the mini batch reactor during fast HTL. One way is to use a fixed amount of water in each reactor, but vary the amount of algae. A second way is to load different amounts of algae slurry with a fixed solids content (e.g., 15 wt %). The third way is to use a fixed amount of dry algal biomass in each reactor but vary the amount of water added. This section examines each of these methods.

These variations in reactor loading will be reported and discussed in terms of two key variables: the percentage of the reactor volume occupied at room temperature by the water loaded into the reactor (hereafter referred to as volume % water or vol % water) and the solids content (wt %) in the algae slurry loaded in the reactor. These two variables control the "effective concentration" of algae solids in high-temperature liquid water at a given reaction temperature. As the reactor is heated, some of the liquid water must vaporize to maintain the saturation pressure, which leaves less water in the liquid phase. The lower the initial water loading, the higher the relative amount of water that must vaporize.

We define the effective concentration (wt %) of algae as the mass of dry algae in the reactor divided by the mass of algae plus the mass of liquid water in the reactor at a given temperature. The mass of liquid water in the reactor at a given temperature was calculated using mass balances and steam tables [112]. Figure 4.3 shows how the effective concentration at 266 ℃ varies with vol % water loading and solids content (wt %). Note that some conditions displayed in Figure 4.3 may represent physically irrelevant reactor loadings (i.e., too little mass for recovery, too much material for safe operation of the reactor). We include this range of conditions in Figure 4.3 to facilitate better understanding of the reactor loadings examined in this work.

4.3.3.1 Fixed Water Loading

Figures 4.4 and 4.5 illustrate how biocrude yields from fast HTL (600 ℃ for 1 min) of *Nannochloropsis* sp. algae change with respect to the slurry solids content when a fixed amount of water (either 10 or 30 vol %), respectively, was added to each reactor. The mass of algae added to each reactor was adjusted to obtain the desired wt % of dry algae solids.

At 10 vol % water (Figure 4.4), biocrude yields decrease from 67 wt % to 43 wt % as the solids content of the algal slurry increases (from 5 - 25 wt %). The highest

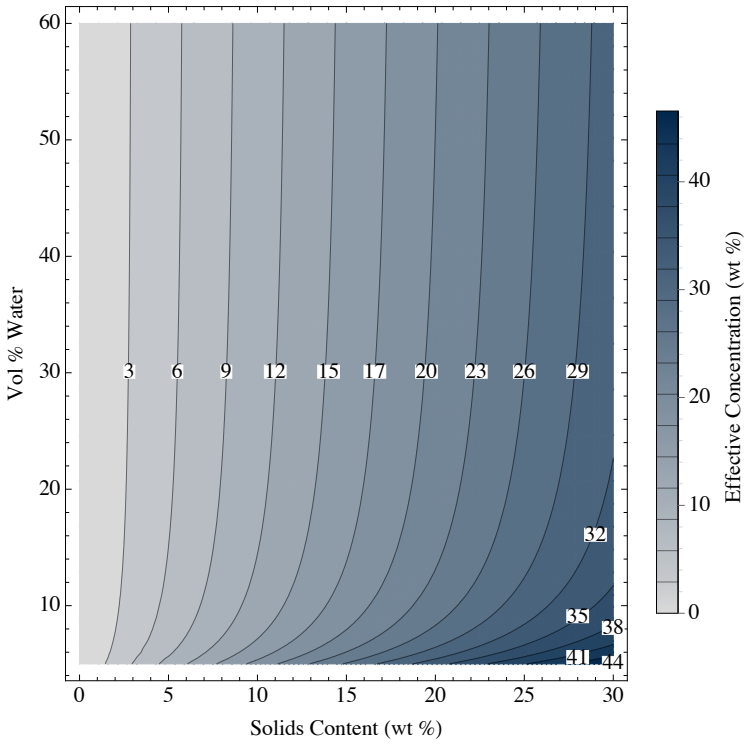

Figure 4.3: Effect of slurry solid content and vol % water on effective concentration at 266 ℃

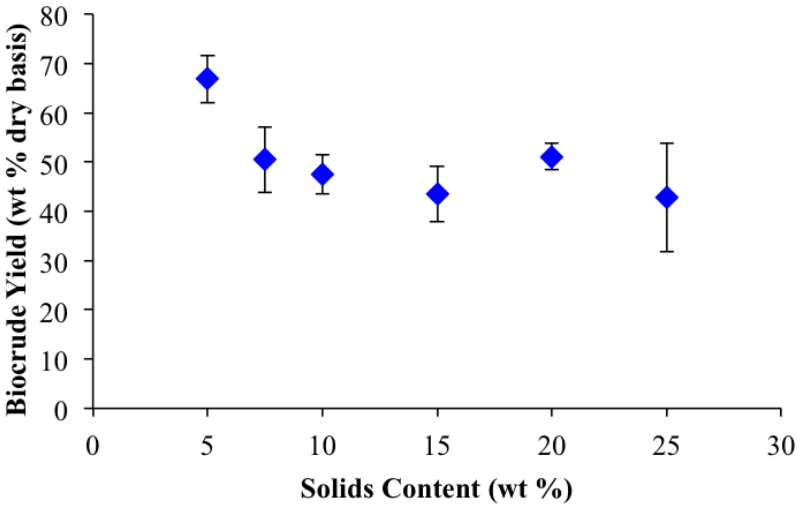

Figure 4.4: Biocrude yields from fast HTL at different slurry solids contents with fixed water loading. Sand-bath temperature = 600 ℃, 1 min, 10 vol % water loading

biocrude yield with 30 vol % water (Figure 4.5) is also observed after fast HTL of a reaction mixture containing 5 wt % algae solids. However, fast HTL reactions with

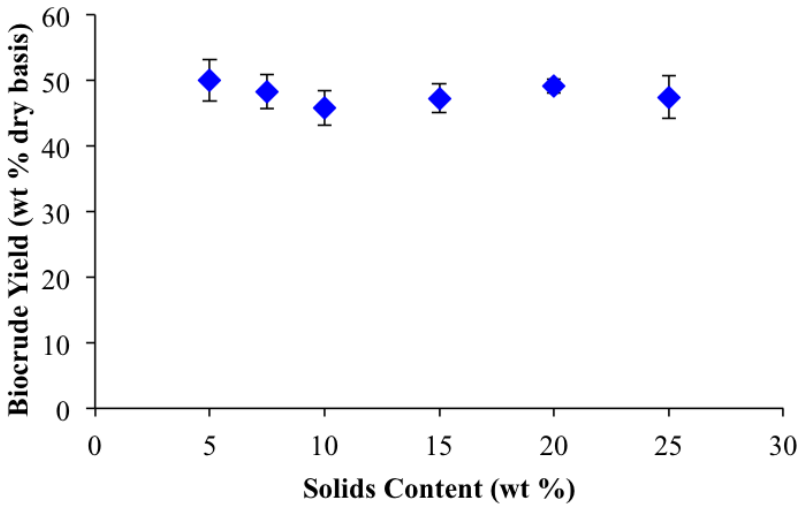

Figure 4.5: Biocrude yields from fast HTL at different algae solids content with fixed water loading, sand-bath temperature = 600 ℃, 1 min, 30 vol % water loading

30 vol % water resulted in all biocrude yields being within 5 wt % of the maximum biocrude yield for all solids contents examined. This difference in biocrude production between high and low water loadings may again be explained by an increase in effective concentration.

4.3.3.2 Fixed Solids Content

Figure 4.6 displays the biocrude yields from fast HTL of 15 wt % algae slurries with respect to the vol % water of each loading. To manipulate the vol % water in the reactor and maintain fixed solids content, both the algae and water loadings were varied. As the vol % water increases, biocrude yields decrease slightly, although plateaus are visible at both extremes.

As indicated in Figure 4.3, effective concentrations of algal biomass increase as mass loadings (and vol % water) decrease. Effective concentrations for the reactions included in Figure 4.6 increase from 15.4 to 18.8 wt % as the vol % water decreases from 60 % to 10 %. Since many biomolecules have high molecular weight, it is

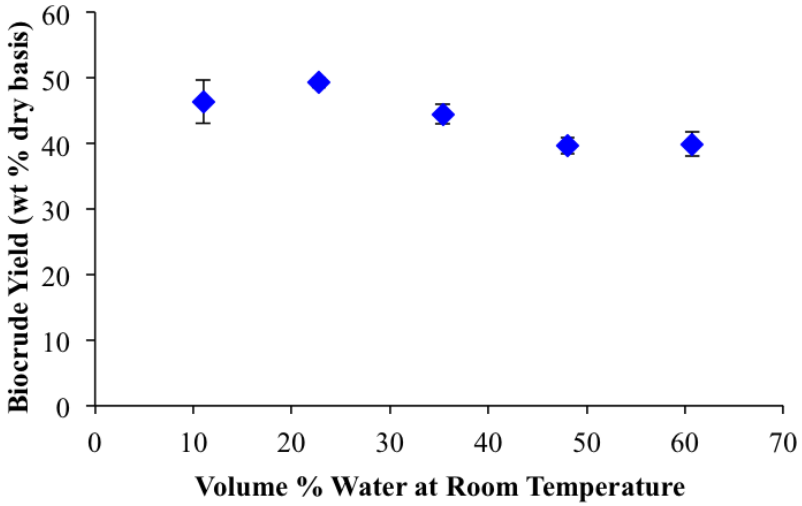

Figure 4.6: Biocrude yields from fast HTL at different reactor loadings with fixed 15 wt % slurry solids content, sand-bath temperature = 600 ℃, 1 min

unlikely that reactions with algal biomass occur in the gas phase. If the reactions of algal biomass to produce biocrude are greater than zero-order, an increase in the effective concentration of the reactant(s) in the liquid phase would increase the rate of biocrude production.

4.3.3.3 Fixed Biomass Loading

Figure 4.7 depicts biocrude yields obtained from experiments with varying water loading at a constant loading of dry algal solids. Note that we plot the biocrude yields with respect to effective concentration of the algae in liquid water at 266 ℃ since both the vol % water and slurry solids content change as a result of varying water loading. As the effective concentration increases, biocrude yields also generally increase. This observation further supports the idea that the effective concentration of algal biomass in the reaction mixture has an effect on biocrude production.

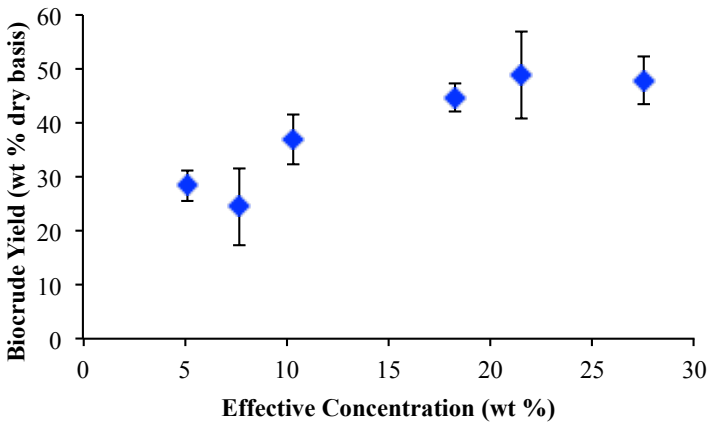

Figure 4.7: Biocrude yields from fast HTL at different reactor loadings with fixed (0.03 g) dry algae solids and variable water loading, with respect to effective concentration (wt %) at 266 ℃. Sand-bath temperature = 600 ℃, 1 min

4.3.4 Reaction Ordinate

Figure 4.8 displays the biocrude yields from Figures 4.2 and 4.6 of the current work and those reported in Chapter II [33], using reaction ordinate (R_0) as the basis for comparison. The same definition of reaction ordinate employed previously (Equation 2.2 [33]) is employed here to provide an equivalent comparison, and each point in Figure 4.8 represents a single experiment. Data reported in Figures 4.2 and 4.6 are included in Figure 4.8 because these experiments all used reaction mixtures consisting of 15 wt % algae solids, as did all experiments in the previous work.

Throughout the range of R_0 values explored in both works, the biocrude yields are mutually consistent. Figure 4.8 reinforces the idea from previous work that R_0 can be used to combine the effects of time and temperature into a single parameter for comparison of large data sets [33].

4.4 Conclusions

This study provides the most detailed examination to date of how fast HTL processing conditions (including biomass feedstock, reaction time, and reactor loading)

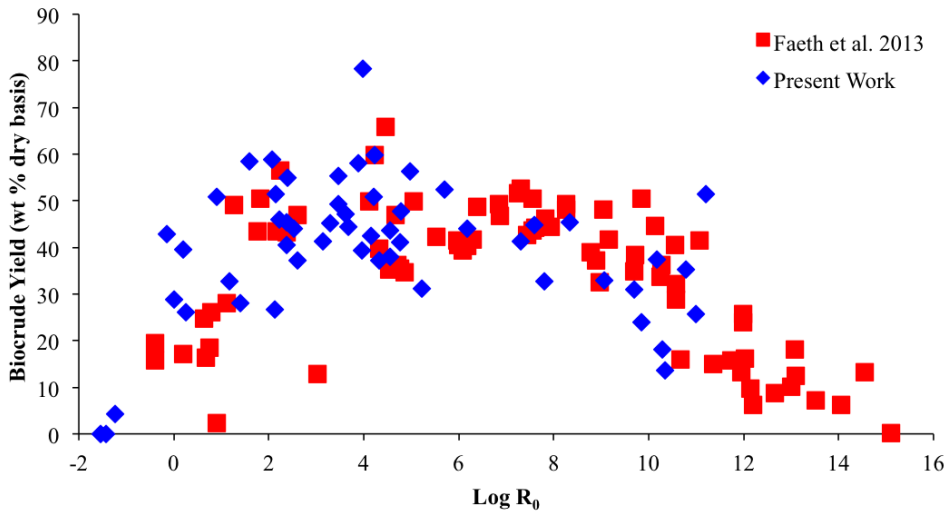

Figure 4.8: Variation of biocrude yields from fast and isothermal HTL of *Nannochloropsis* sp. with respect to reaction ordinate

affect biocrude yields. Fast HTL produced biocrude from four different species of microalgae with yields comparable to those available from isothermal HTL, further illustrating that fast HTL is a robust process. Investigation of short reaction times (0 - 2 min) revealed that the processes that produce biocrude from microalgal biomass are very fast. The highest biocrude yields from non-isothermal HTL of a 15 wt % algal slurry with 11 vol % water were obtained at a reaction time of 0.75 min (using a 600 ℃ sand-bath set-point temperature). Such rapid conversion may be explained by cell breakage that occurs at characteristic temperatures, possibly accelerated by high heating rates.

Different aspects of reactor loading also affect biocrude yields. Fast HTL of algal slurries with low solid contents can produce high biocrude yields when the vol % water in the reactor is low. Specifically, we observed a maximum biocrude yield of 67 wt % after HTL of a 5 wt % algal slurry, 11 vol % water in a 1 min in a 600 ℃ sand-bath. In contrast, variation in slurry solids content in reactions with high volume % water does not appear to have a clear impact on biocrude production via fast HTL. This observed increase in yield with low loading and low solids content

could be due to an increase in the effective concentration of algae cells in the liquid phase of the reaction, relative to an identical reaction with high loading.

Manipulation of reactor loading by fixing the solids wt % content and adjusting the total mass of the reaction mixture revealed a decrease in biocrude yields with increasing mass. Further, biocrude yields decreased as the vol % water increased (and solids content decreased) for fast HTL reactions with a fixed amount of dry algae biomass. Both of these trends reinforce the idea that increased effective concentration of algae in the liquid phase during rapid heating may facilitate biocrude production. Additionally, the volume % water appears to have a greater effect on biocrude yields than does the wt % of dry algae solids present in the slurry.

The results discussed in this chapter indicate that physical phenomena, in addition to chemical reactions, likely contribute to the improved biocrude yields obtained via fast HTL under certain operating conditions, and that further research in this area is needed to better understand the fast HTL process. We also affirm that R_0 may be used to quickly compare biocrude yields from HTL over a wide range of reaction times and temperatures.

CHAPTER V

Comprehensive Study of Fast and Isothermal Hydrothermal Liquefaction at Low and High Water Loading

In this chapter, we examine both fast and isothermal HTL at sand-bath set-point temperatures from 200 - 600 ℃ and reaction times from 30 - 3600 s with both low and high reactor loadings. The work described herein is the result of collaboration between the author of this dissertation, David Hietala, and Phillip Savage [68]. The goals of this study are to further probe the effects of water loading described in Chapter IV, and to generate a comprehensive data set including HTL at conditions leading to low biomass conversion for kinetic modeling (described in Chapter VII). Herein, we discuss the effects of reaction time, temperature, heating rate, and loading on the product yields from HTL. We found that reactor loading has little effect on product yields for reaction times $\geq$ 3 min. For reaction times $<$ 3 min, biocrude and gas product yields are higher and solid, dry aqueous-phase, and volatile product yields are lower after HTL with low loading than after HTL with high loading. Additionally, we found that biocrude product yields increase with increasing heating rate, although this effect diminishes with increasing quench temperature.

5.1 Introduction

HTL has been conventionally thought to depend primarily on two reaction variables: time and temperature. In the literature, reaction time is often assumed to begin at the instant the reactor begins to heat up and end the instant the reactor starts to cool down. Herein, we define time, t, as the instantaneous reaction time and t_q as the instant the reaction is quenched (removed from the sand bath and submerged in a water bath). For isothermal HTL, the most widely studied variation of the process, reaction temperature, T, is arguably more important than reaction time in terms of effect on biocrude production [31, 42]. T is often assumed to be constant once the reaction vessel has reached the desired set-point temperature, T_{sp}, hence the isothermal descriptor. Throughout the context of the present work, we define temperature as follows: $T(t)$ is the time-dependent reaction temperature, $T_q = T(t_q)$, the temperature inside the reactor when quenched, and $T_o = 25$ °C.

The primary focus of this study (which encompasses both fast and isothermal HTL reaction conditions) concerns a third variable that is arguably as, if not more, important than reaction temperature: heating rate, h. Throughout this study, we define different variations of heating rate as follows: $h(t) = \frac{dT}{dt}$, the instantaneous heating rate; h_0 is the initial heating rate spanning up to 70 % of the maximum possible temperature change ($h_0 = f\frac{T_{sp}-T_o}{t_{70}}$, where $f = 0.7$ or $\frac{T_q-T_o}{T_{sp}-T_o}$ (whichever is less), t_{70} such that $T(t_{70}) = \frac{7(T_{sp}-T_o)}{10} + T_o$); and $\bar{h}$, the average heating rate over the duration of heat up (defined as 95 % of the temperature change, analogous to h_0). Table 5.1 lists the values of h_0 and $\bar{h}$ used in the present work.

To date, the effect of heating rate has been scarcely explored in the HTL literature. Moreover, many different sizes and types of batch reactors have been described in the literature, each with different rates of heat transfer that are largely ignored. In Chapters II, III, and IV, however, we employed small reactors to maximize heat transfer, measured the temperature throughout HTL reactions, and indirectly ma-

T_{sp} [℃]	h_0 [℃/min]	$\bar{h}$ [℃/min]
200	79	49
250	101	63
300	123	77
350	146	91
400	168	106
450	191	121
500	213	134
550	236	148
600	258	162

Table 5.1: Initial heating rate (h_0) and average heating rate ($\bar{h}$) at various sand-bath set-point temperatures (T_{sp}) for 1.67 mL stainless steel batch reactors.

nipulated the heating rate by manipulating T_{sp}. We found that high heating rates lead to similar or higher biocrude yields, compared to isothermal HTL. This finding presents a significant opportunity for capital cost and energy savings in a continuous industrial process, since fast HTL could facilitate equivalent throughput with smaller reactors and processing equipment.

Others have demonstrated similar results for batch HTL of corn stover (5 ℃/min $< \bar{h} <$ 140 ℃/min) [113], pine sawdust and cellulose (2 ℃/min $< \bar{h} <$ 20 ℃/min) [114], bacteria and yeast ($\bar{h} \leq$ 216 ℃/min) [66], and macroalgae (146 ℃/min $< \bar{h} <$ 585 ℃/min) [52], and for continuous HTL of microalgae (we estimate 200 ℃/min $< \bar{h} <$ 400 ℃/min [13], and 235 ℃/min $< \bar{h} <$ 990 ℃/min [115], based on given information). These approaches facilitated better understanding of how HTL product yields evolve with time, especially during non-isothermal reactions and HTL with short reaction times. Currently, there exists no comprehensive examination of product evolution with respect to T, t, and h that also describes HTL kinetics at low algal biomass conversion. This gap in the literature presents an opportunity to explore these process variables and, in doing so, generate a suitable data set for empirical kinetic modeling.

5.2 Materials and Methods

A slurry of 31.4 ± 0.2 wt % (standard error) preservative-free *Nannochloropsis* sp. and water was purchased from Reed Mariculture. The ash content for this alga was previously reported to be about 6.3 wt % [33]. We constructed 1.67 mL mini batch reactors from a $^3/_8$ in. Swagelok® port connector and two caps, all of 316 stainless steel construction. We loaded each reactor with enough algae slurry (0.140 - 0.588 g) and deionized water (0.160 - 0.662 g) to constitute a 15 wt % slurry of algae in water (see Tables D.1, D.2, and D.3 in the Appendices for reactor loading details). The low reactor loading at each reaction condition was defined by the minimum possible loading, constrained by the following: dry algae loading $\geq$ 0.045 g (to avoid the limit of detection for gravimetric analysis), and a minimum water/algae ratio of 5:1 (m/m) at the reaction quench temperature (at least 5 parts liquid water present for each part algae, even after some water vaporizes to maintain saturation). Maximum reactor loadings were calculated such that reactor pressures would not exceed 408 bar at the reaction quench temperature, and the total mass of the 15 wt % slurry would be $\leq$ 1.25 g. After loading, reactors were sealed to 45 ft-lbs. using a torque wrench.

Additional proxy reactors for temperature measurements were constructed using a $^3/_8$ in. port connector, one cap, and one bored-through reducing union (reducing the internal diameter from $^3/_8$ in. to $^1/_8$ in.). An Omega Engineering, Inc. $^1/_8$ in. diameter 18 in. long stainless steel-clad K-type thermocouple was inserted into the $^1/_8$ in. end of the reducing union such that the tip of the thermocouple resided in the middle of the reactor body when closed. An Omega Engineering, Inc. HH309A Datalogger recorded the temperature measured by the thermocouples in the proxy reactors every 3 s.

Two loaded and sealed reactors (one with low and one with high loading) and two proxy reactors were simultaneously submerged in a Techne IFB-51 fluidized sand bath preheated to the specified T_{sp} (200 - 600 ℃). At $t = t_q$ (or $T = T_q$, for some of

the reactions with high h_0), reactors were removed from the fluidized sand bath and quickly quenched in cold water. After the thermocouples reported temperatures $<$ 25 ℃, the reactors and proxy reactors were removed from the water batch and dried with paper towels.

After quenching and drying, reactors were weighed, tapped forcefully on the bench top three times, opened to release gases, and weighed again. We calculated the mass of gas evolved, m_G, as the difference between these two reactor masses. This process was carried out within a few hours of quenching the reaction to prevent carbon dioxide gas from dissolving in the water inside the reactor, which would have reduced the mass of gaseous products detected. We estimate a flux of carbon dioxide on the order of 10^{-10} mol/hr across the gas-liquid interface (based on information in reference [116]), so very little CO_2 would dissolve in only a few hours.eed Biocrude, aqueous-phase, and solid products were recovered according to the procedure described previously [31]. This procedure involves pouring the reactor contents into a glass conical centrifuge tube, rinsing the reactor with 9 mL of DCM ($>$ 95 % Optima grade, Fisher Scientific) in small aliquots, and collecting these rinsings in the same glass tube. This tube was then mixed using a vortex mixer and centrifuged to facilitate phase separation.

Following centrifugation, the organic (DCM-soluble) phase was manually collected using a pipette and transferred to a pre-weighed glass tube. The remaining aqueous-phase and solid products were again mixed using a vortex mixer and centrifuged. The aqueous phase was transferred to a pre-weighed vial via pipette and the residual solids were left in the original glass tube. Tubes containing the DCM-dissolved organics, remaining solids, and wet aqueous phase were each dried under N_2 (99.998 %, Metro Welding Supply Corp., using a Labconco® RapidVap® Vertex™ Dry Evaporator with a solid aluminum heating block) and weighed until two consecutive cycles of drying and weighing produced tube masses varying by $<$ 2 mg. The heating block was maintained at a constant temperature of 70 ℃ for aqueous-phase samples and 35

℃ for all other samples.

We define the masses of dried biocrude (organic), solid, and aqueous phases to be m_B, m_S, and m_{DA}, respectively. Furthermore, we define volatiles to be the compounds primarily dissolved in aqueous phase but lost due to evaporation upon drying [31]. Together, dry aqueous-phase and volatile products constitute what we term the aqueous phase, the sum of all water-soluble products prior to drying. Product yields were calculated by dividing the mass of the product, m_i, by the mass of dry algae initially loaded in the reactor, and multiplying by 100 to obtain wt % yields, on a dry basis. To determine product yields at room temperature, we loaded reactors (for one trial) and glass tubes (for a second trial) with the minimum and maximum loadings of algae slurry and separated the various products using the same procedure outlined in the preceding paragraphs (loadings and product yields for these control experiments are reported in Table D.1 of the Appendices).

5.3 Results and Discussion

This section discusses the yields of gas, solid, biocrude, dry aqueous-phase, volatile, and aqueous-phase products from both fast and isothermal HTL with low and high reactor loadings. Throughout the discussion of product yields, we describe the effects of quench temperature, heating rate, quench time, and reactor loading. Unless otherwise noted, discussion of the effects of heating rate are limited to $t_q \leq 3$ min and discussion of the effects of reaction time are limited to $t_q > 3$ min.

5.3.1 Product Yields

Figures 5.1 to 5.6 depict the various product yields from HTL of *Nannochloropsis* sp. at low and high reactor loadings (displayed in the plots on the left and right, respectively). The curves on the plots represent typical temperature profiles for each of the sand-bath set-point temperatures examined in the present work. Each individual

point represents the actual quench time (t_q) and temperature (T_q) of a single HTL experiment with the product yield represented by the color of the point (color scales are depicted on the right of each figure). Product yields from room temperature control experiments are represented by a single point in the bottom left corner of each plot. It is important to note that t_q is represented on a log scale.

Figure 5.1 depicts the gas product yields over the reaction conditions examined in the present work. At quench times < 3 min, gas yields from HTL with low loadings are higher than those from HTL with high loadings. At quench times > 3 min, reactor loading does not appear to have a significant effect on gas product yields. Little gas is formed from HTL with T_q less than 150 ℃, regardless of heating rate or t_q. However, gas yields increase with heating rate at T_q 150 - 220 ℃. For $t_q > 20$ min and $T_q \geq 250$ ℃, gas yields appear to increase as t_q increases. This trend at long reaction times is fairly consistent with the gas product yields reported by Valdez et al. [31], though the gas yields in the present work are higher than those reported previously. This difference in observed gas product yields may be a consequence of the methods used to measure gas yields (by mass difference before and after opening the reactor in the present work, and by GC analysis in the previous work).

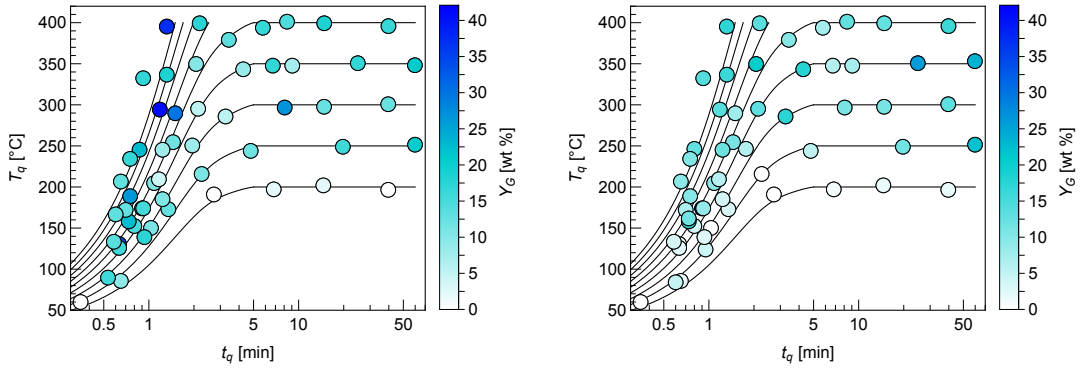

a low loading b high loading

Figure 5.1: Gas product yields from HTL of *Nannochloropsis* sp. with a - low and b - high loading at different times and temperatures. Curves depict typical temperature profiles for different set-point temperatures.

Figure 5.2 depicts solid product yields. It is important to note that this is the

first known demonstration of HTL at low algal cell conversion, which is of paramount importance to kinetic model development. As expected, solid yields are highest at short t_q and low T_q and lowest at long t_q and high T_q. Solid yields decrease with heating rate (for a certain t_q or T_q) throughout the entire range of HTL reaction conditions examined until a minimum (on the order of wt % ash) is reached. This minimum is observed at $T_q > 250$ and $T_{sp} \geq 450$ ℃. At reaction times > 3 min and $T_{sp} = 250$ ℃, solid product yields decrease with increasing t_q, though complete conversion is not observed within the range of reaction times examined. Solid yields decrease dramatically with increasing T_q (and T_{sp}) within this time frame, likely indicating that chemical hydrolysis of algal cell biomass becomes kinetically favorable at temperatures 225 - 250 ℃. Garcia Alba et al. [47] reported visible cell wall breakage (via scanning electron microscopy (SEM) imaging) of *Desmodesmus* sp. within the same range of HTL reaction temperatures.

As observed with gas yields in Figure 5.1, solid product yields from HTL at both low and high loadings are consistent at quench times > 3 min. At reaction times $<$ 3 min, solid product yields from HTL with low loadings are lower than those from HTL with high loading, indicating improved conversion of algal biomass into other products during HTL with low loadings compared to HTL with high loadings, at least at short timescales. This observation is consistent with the trend depicted in Figure 4.6 in Chapter IV, supporting the theory that low loadings (vol % water) can affect the rate at which algae is converted to other products.

Figure 5.3 displays biocrude product yields. Biocrude product yields from HTL with low loadings are greater than those from HTL with high loadings at quench times < 3 min. This difference in biocrude product yields between low and high loadings diminishes with increasing quench time. Among reactions with $t_q < 3$ min, biocrude yields increase as heating rate increases for $T_q \leq 250$ ℃. The trend of increasing biocrude yields with increasing heating rate is consistent with previous results from

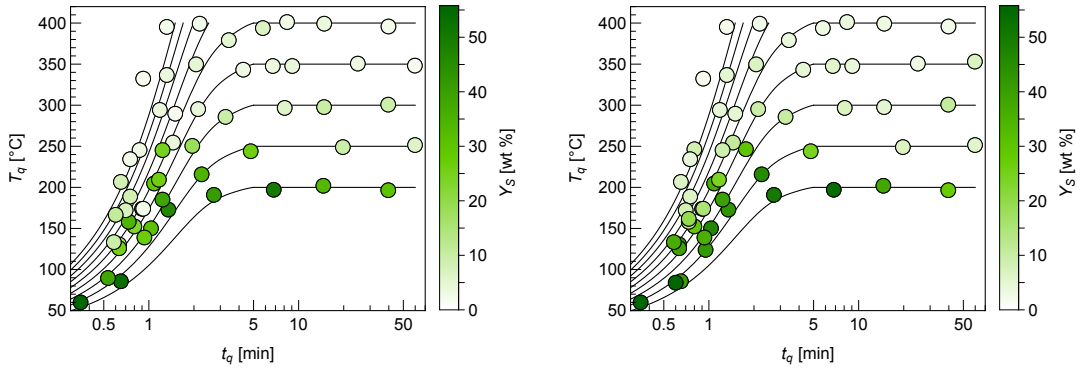

a low loading b high loading

Figure 5.2: Solid product yields from HTL of *Nannochloropsis* sp. with a - low and b - high loading at different times and temperatures. Curves depict typical temperature profiles for different set-point temperatures.

fast HTL [33, 52, 66, 115, 117]. The effect of heating rate was so significant within this range that biocrude yields of 30 - 45 wt % were observed after HTL with T_q 150 - 225 ℃, the first such report (to the best of our knowledge). However, biocrude yields appear to decrease with increasing heating rate for $T_q > 250$ ℃ and $T_{sp} > 500$ ℃. Further increases in heating rate ($T_{sp} > 600$ ℃) were not possible with this experimental system, so this trend could not be explored more thoroughly.

Within the range of reaction times characteristic of isothermal HTL, biocrude yields generally increase as T_q increases from 200 - 250 ℃, reach a maximum for T_q 300 - 350 ℃, and decrease slightly with further increases in T_q. High biocrude yields for isothermal HTL are often observed for reaction temperatures 300 - 350 ℃, the range that seems to be considered the standard for isothermal HTL in the literature (previously discussed in Chapter I and in references [15, 31, 36, 37, 49, 118]). Additionally, biocrude yields decrease with increasing t_q for $T_q = 400$ ℃. Decreasing biocrude yields with increasing time at $T_q > 350$ ℃ has also been observed previously [31, 42].

Figure 5.4 depicts dry aqueous-phase product yields. Dry aqueous-phase product yields are slightly higher after HTL with high loading at quench times < 3 min, and this difference again diminishes with increasing quench time. At long times

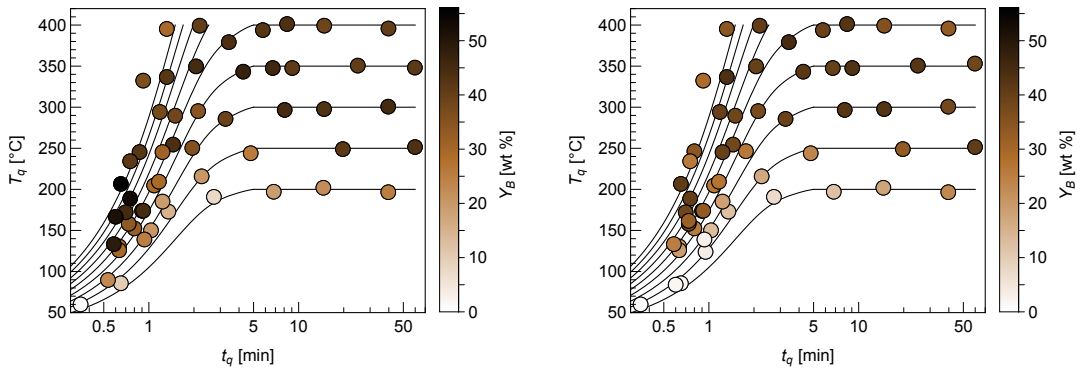

a low loading

b high loading

Figure 5.3: Biocrude product yields from HTL of *Nannochloropsis* sp. with a - low and b - high loading at different times and temperatures. Curves depict typical temperature profiles for different set-point temperatures.

($t_q > 3$ min), Y_{DA} increases with increasing time for $T_q = 200$ ℃. For $T_q \geq 300$ ℃, dry aqueous-phase product yields decrease with increasing t_q. These trends are consistent with those reported for water-soluble products (equivalent in definition to the dry aqueous-phase products in the present work) by Valdez et al. [31]. Morever, for $T_q \geq 250$ ℃ and $t_q > 3$ min, the yields of dry aqueous-phase products from HTL decrease with increasing quench temperature. This decrease is likely due to the production of water-soluble volatile compounds that evaporate during drying, as discussed by Valdez et al. [31].

For short reaction times ($t_q < 3$ min), maximum Y_{DA} occurs at a heating rate of about $h_0 = 168$ ℃/min (following the $T_{sp} = 400$ ℃ line). This maximum is sustained with increasing T_q until a temperature of about 300 ℃; above this temperature Y_{DA} decreases significantly at all heating rates. It is interesting to note that the decrease in dry aqueous-phase yields with increasing heating rate is observed at T_q as low as 200 ℃, a temperature at which significant degradation of dry aqueous-phase products does not appear to be favorable based on the previously described trends in Y_{DA} at $t_q > 3$ min.

Since all other product yields were measured directly, we calculated the volatile product yields by difference. Figure 5.5 illustrates the calculated volatile product

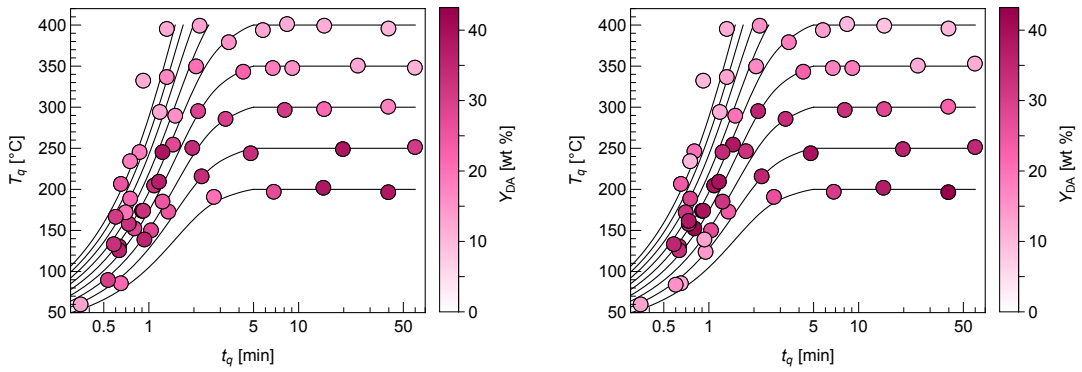

a low loading b high loading

Figure 5.4: Dry aqueous-phase product yields from HTL of *Nannochloropsis* sp. with a - low and b - high loading at different times and temperatures. Curves depict typical temperature profiles for different set-point temperatures.

yields. Volatile product yields are quite low at $T_q < 250$ °C and increase both with increasing T_q and t_q. Based on the observed decrease in dry aqueous-phase product yields with increasing temperature discussed previously, increasing volatile yields with increasing temperature is expected. Furthermore, Valdez et al. also reported increases in volatile products with increasing T_q and t_q [31]. At short times, volatile yields are low for $h_0 < 168$ ($T_{sp} \geq 400$ °C), and increase with further increases in heating rate. Exceptions to these trends are likely due to experimental error in gas measurements, which are highly sensitive to error thanks to low product masses and the accuracy of the balance used to measure mass.

Figure 5.6 depicts the sum of the measured dry aqueous-phase product yields and the calculated volatile product yields, which we term aqueous-phase product yields (i.e. $Y_A = 100 - Y_S - Y_B - Y_G$). We present the aqueous-phase product yields because previous research indicated that volatile products are produced almost entirely from water-soluble products [31]. Aqueous-phase product yields are fairly insensitive to t_q across the reaction conditions examined, although slightly lower after HTL with low loading and quench times < 3 min. This decrease in aqueous-phase products exists despite the increase in algal solid conversion (decreased solid yields) depicted in Figure 5.2. We speculate that this decrease in aqueous-phase product yields is

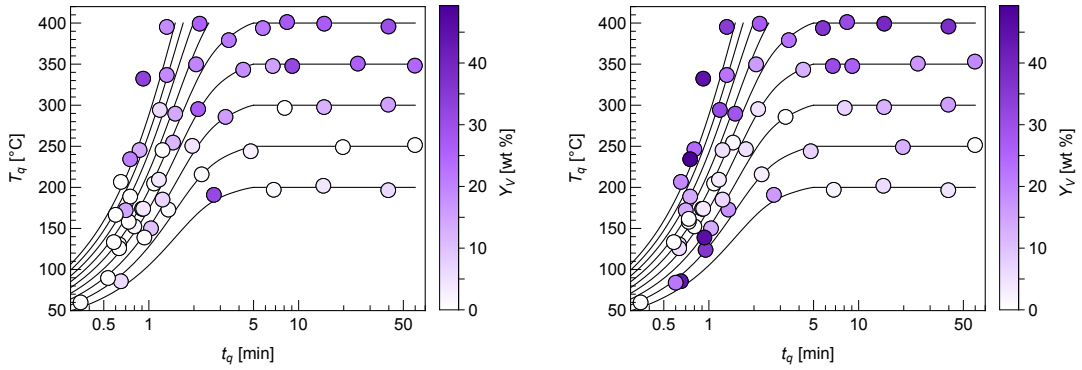

a low loading b high loading

Figure 5.5: Volatile product yields from HTL of *Nannochloropsis* sp. with a - low and b - high loading at different times and temperatures. Curves depict typical temperature profiles for different set-point temperatures.

due to increased production of biocrude from algal biomass in this range of reaction conditions, as indicated in Figure 5.3. The concurrent decline in aqueous-phase product yields and increase in biocrude yields suggests increased N incorporation into the biocrude. Elemental analysis of the dry aqueous-phase and biocrude products from fast HTL with low and high loadings (in Chapter VI) reveals higher N content in biocrudes and lower N content in dry aqueous-phase products from fast HTL with low loading, supporting this theory.

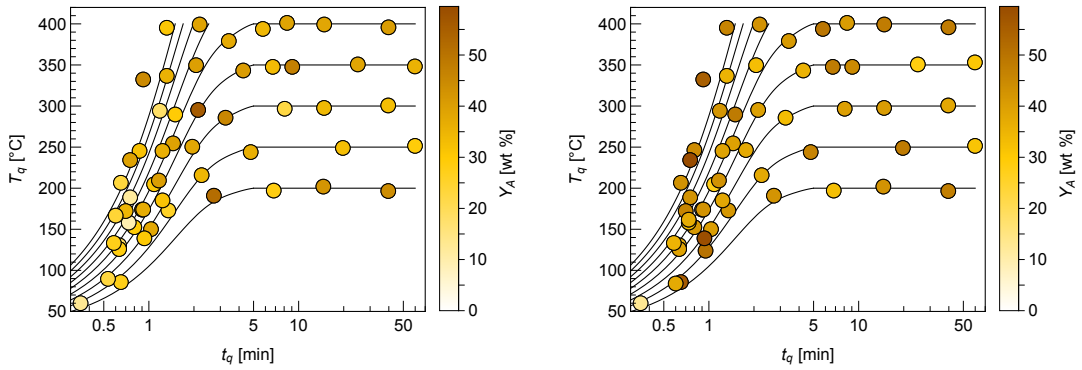

a low loading b high loading

Figure 5.6: Aqueous-phase product yields from HTL of *Nannochloropsis* sp. with a - low and b - high loading at different times and temperatures. Curves depict typical temperature profiles for different set-point temperatures.

In summary, gas product yields increase with h_0 and T_q and are higher than re-

ported previously for HTL of the same algae [31]. As h_0, T_q, and t_q increase, solid product yields decrease rapidly to a minimum yield on the order of the ash content of the original algal biomass. Biocrude yields increase rapidly with set-point temperature (and therefore h_0) at $t_q < 3$ min, but reach a maximum at T_q between 300 - 350 ℃ for $t_q > 3$ min. Dry aqueous-phase products increase with set-point temperature (and therefore h_0) up to a maximum after HTL with $T_{SP} = 400$ ℃ ($h_0 = 168$ ℃/min), then decrease with further increases in T_{SP} (and h_0). At long times, dry aqueous-phase yields decrease with increasing temperature for $T_q \geq 250$ ℃. Volatile product yields increase with increasing temperature for $T_q \geq 250$ ℃, which is logical, as volatile products are almost exclusively derived from the aqueous phase. The aqueous-phase product yields do not vary much overall, though these yields are slightly higher after HTL with high loading.

This trend in dry aqueous-phase product yields with heating rate (maximum yield obtained at a mid-range T_{SP} and h_0) is only the second known report of such findings (with the first from Bach et al. [52]). It is curious that we observe a decrease in dry aqueous-phase product yields after HTL with $h_0 > 168$ ℃/min, even though T_q is lower than 300 ℃, the temperature at which dry aqueous-phase product yields begin to decrease after isothermal HTL. This trend is paralleled by the increase in volatile product yields after HTL with $h_0 > 168$ ℃/min. Volatile products are derived predominantly from products soluble in water [31], which seems to indicate that the dry aqueous phase is degrading in some way to form volatile products at lower temperatures than expected.

5.3.2 Effects of Heating Rate

As described in the previous section, the data in Figure 5.3 suggest that biocrude production is strongly affected by heating rate. Figure 5.7 more clearly illustrates this effect. In Figure 5.7, we plot biocrude yield, Y_B, as a function of the initial heating

rate, h_0, for reactions with T_q in three different ranges (120 - 160 ℃, 160 - 200 ℃, and 200 - 220 ℃). These plots clearly show monotonic trends of increasing biocrude yield with increasing heating rate.

Moreover, because the reactions in each of the plots in Figure 5.7 are all quenched at approximately the same T_q, this trend cannot be explained by Arrhenius kinetics, which predicts that, for reactions proceeding at equivalent temperatures, those with longer reaction times should progress to a greater extent. Figure 5.7 shows the opposite, with the shorter reactions (fastest heating rate) producing the most biocrude. This suggests that heating rate affects biocrude yield production in some way other than (or in addition to) Arrhenius kinetics.

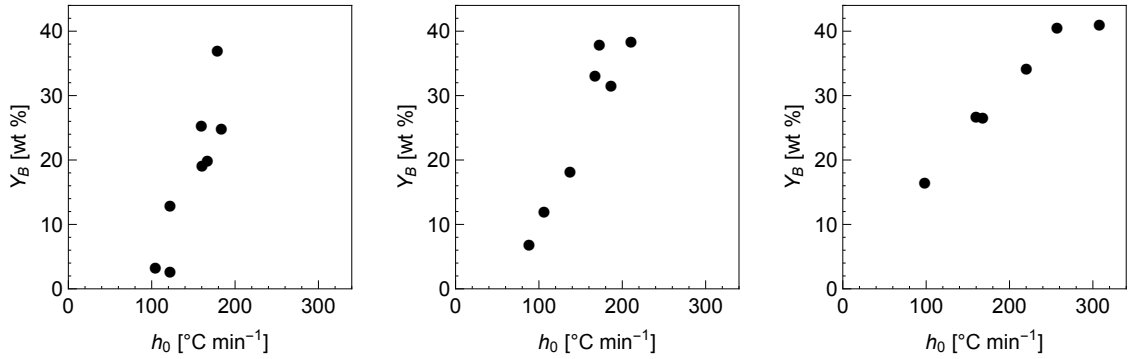

a $120 < T_q < 160$ ℃ b $160 < T_q < 200$ ℃ c $200 < T_q < 220$ ℃

Figure 5.7: Biocrude yield, Y_B, as a function of initial heating rate, h_0, grouped by quench temperature, T_q, produced from the HTL of *Nannochloropsis* sp.

We postulate that heating rate has such a significant impact on HTL product formation because it facilitates physical disruption of the algal cells. As the temperature increases during heat-up, the bulk liquid water inside the reactor expands freely; however, because the cell walls of microalgae are fairly rigid structures [119], the water within the cells likely has less room to expand relative to the bulk high-temperature water. This limitation on intracellular water expansion could cause pressure gradients to develop between the inside of the cells and the bulk high-temperature water. Further, differences in thermal conductivity may exist between the cell contents and

the bulk water, enabling the formation of temperature gradients and, therefore, pressure gradients across cell walls. These pressure differentials would in turn drive water flow out of the cells at an increasing rate until the pressure differentials exceed the tensile strength of the cell walls, and lysis occurs. This phenomenon would be similar to cytolysis, in which a cell bursts due to osmotic imbalance, except instead due to mechanical stress resulting from a thermally induced pressure gradient.

This theory provides a possible explanation for the observed trend in dry aqueous-phase product yields (maximum observed at moderate h_0). For HTL at lower heating rates, the various organelles and other cell contents were presumably ensconced inside the cell walls and therefore not accessible for reaction with the bulk volume of water in the reactor. However, if these contents were released upon rapid heating, they would be free to react with the bulk volume of water. It is possible that slower destruction of cell walls via hydrolysis could obscure the true temperature at which compounds in the dry aqueous-phase product fraction actually start to decompose into volatile products.

Some studies in the HTL literature include SEM analysis of algal biomass before HTL and of solid residues after HTL, reporting a decreasing resemblance between the solid residue and whole algal cells with increasing HTL reaction temperature [13, 47]. Further, Biller et al. report increasing biocrude yields with increasing heating rate and verified that the algae feedstock consisted of intact cells [115], lending some credence to our theory of cell wall disruption, though no imaging of residual solids was reported. Furthermore, we are not aware of any studies investigating the HTL of algal cells that are already ruptured, perhaps via sonication. Microscopic visualization and/or HTL of sonicated cells may support or refute our cell rupture theory. In summary, we believe rapid heating causes the rate of intracellular pressure increase (relative to the bulk liquid water) to exceed the rate of water expulsion achievable by the cell wall and lipid bilayer cell membrane, such that cells undergo mechanically induced lysis. This

physical phenomenon is, of course, in addition to the chemical reaction that occurs as the high-temperature water hydrolyzes the cell wall and/or membrane [117].

As the range of T_q depicted in each plot increases from Figure 5.7a to Figure 5.7c, the slope of the increase in biocrude yield with increasing heating rate decreases. This trend may indicate that heating rate has the most influence on biocrude yield at low T_q, and this effect diminishes with increasing T_q. The diminishing effects of heating rate with T_q may be the result of increasing rates of chemical reactions (like hydrolysis), which likely assert increasing influence on biocrude production with increasing T relative to the proposed cell rupturing effects.

5.4 Conclusions

We examined a broad range of HTL reaction conditions, culminating in the generation of a comprehensive data set describing how the yields of different products from HTL change with time, temperature, and heating rate. To the best of our knowledge, this experimental data set is the first true demonstration of algal HTL at low biomass conversion. Reactor loading was not observed to have a significant effect on product yields from HTL at reaction times ≥ 3 min. At reaction times < 3 min, gas and biocrude product yields are higher after HTL with low loadings, and solid, dry aqueous-phase, and volatile product yields are higher after HTL with high loadings.

We also confirm that heating rate has a significant impact on biocrude yields, even for similar quench temperatures, and we postulate that these effects are the results of increased cell rupturing with increased heating rate. Observed differences in product yields between HTL at low and high loadings (for reaction times < 3 min) may be caused by an increase in effective concentration at low loading conditions, initially discussed in Chapter IV.

CHAPTER VI

Characterization of Products from Fast and Isothermal Hydrothermal Liquefaction of Microalgae

In this chapter, we discuss the characterization of biocrude and aqueous-phase products from fast and isothermal HTL of *Nannochloropsis* sp. Biocrude yields ranged from 36 - 45 wt % (dry basis), with the highest yield obtained after fast HTL with low mass loading. This condition also produced the biocrude with the lowest HHV, which indicates there are compromises to be made between biocrude quantity and quality. The aqueous-phase and biocrude product fractions were characterized using elemental analysis and Fourier Transform Ion Cyclotron Resonance Mass Spectroscopy. This detailed level of analysis identified more than 30,000 unique molecular products. The aqueous-phase products included compounds with the same molecular formulae as known herbicides, which may inform efforts in genetic engineering of algae and/or bacteria for cultivation on the aqueous phase. This detailed molecular-level characterization provides some clues regarding the types of reactions that may take place during HTL.

6.1 Introduction

The methods used to characterize products from HTL include elemental analysis, simulated distillation, total organic and inorganic carbon analysis, and ammonia analysis, none of which provide comprehensive information about the molecular composition of the HTL products. Some studies investigating isothermal HTL reported molecular characterization of product fractions using GC-MS, but this method provides information only about the more volatile compounds that can elute from the GC. FT-ICR MS, on the other hand, provides a much more complete molecular characterization of the products. FT-ICR MS has been used to characterize petroleum crude oils [120–126], some products of biomass conversion processes [15, 127–137], and the processing water from oil sands [138] in molecular detail.

To the best of our knowledge, analysis of the biocrude and/or aqueous-phase products of HTL of microalgae using FT-ICR MS has been reported previously only by Sudasinghe et al. [15, 128] and Sanguineti et al. [129], though Levine et al. used FT-ICR MS to characterize the aqueous-phase byproduct from hydrothermal carbonization of microalgae [127]. This present study is the first to apply FT-ICR MS characterization to the products from fast HTL of microalgae and is also the first to provide a detailed characterization and comparison of products from both fast and isothermal HTL of microalgae. Herein we characterize the biocrude and aqueous-phase product fractions from both isothermal and fast HTL using FT-ICR MS and elemental analysis. These data provide new information about the composition of these complex mixtures and illustrate the potential advantages and disadvantages of each biomass conversion process for the production of biocrude from microalgae.

6.2 Materials and Methods

6.2.1 Materials

Nannochloropsis sp., was purchased as a paste from Reed Mariculture Inc. The algae were from the same lot as reported in Chapter II [33], and therefore contain 32.5 wt % solids in the paste and 6.25 ± 0.23 wt % ash in the dry solids. All chemicals were purchased from the same sources and are identical to those used previously (Chapters II [33] and IV [31]). Reactors were constructed from $^1/_2$ in. Swagelok® 316 stainless steel port connectors. A $^1/_2$ in. cap sealed one end of the port connector, and a $^1/_2$ to $^1/_8$ in. reducing union sealed the other side. The $^1/_8$ in. end of the reducing union was connected to 8.5 in. of $^1/_8$ in. stainless steel tubing and a High Pressure Equipment Co. high pressure valve with grafoil packing. The internal reactor volume, including the gas valve assembly, was 4.6 mL. After assembly, reactors were conditioned before use. To do this, reactors were loaded with deionized water such that 95 % of the reactor volume would be occupied by liquid water at reaction conditions, sealed, and submerged in a preheated Techne IFB-51 fluidized sand bath with a Eurotherm 3216 PID controller at 350 ℃ for 1 h. Then the reactors were cooled and cleaned. This procedure removed any residual material inside the reactors prior to use in HTL reactions.

6.2.2 Experimental Methods

Either 0.25 or 1.54 g of algae slurry (32.5 wt % solids) were loaded into a pre-conditioned reactor. An additional 0.29 or 1.74 mL of deionized water was added to dilute the slurry to 15 wt % solids. Reactor loadings are reported in Table E.1 in Appendix E. Both loadings were used in fast HTL experiments and only the higher loading was used in isothermal HTL. The low loading resulted in 10 % of the reactor volume being occupied by water at ambient conditions and the high loading

corresponded to 60 %. The headspace contained ambient air, which was sealed inside the loaded reactor. Loaded, sealed reactors were submerged in a preheated fluidized sand bath, set at 300 ℃ for isothermal HTL and 600 ℃ for fast HTL. The reaction time was defined to start as soon as the reactor was submerged in the sand bath. Reaction times were 1 min for fast HTL and 20 min for isothermal HTL.

After the specified reaction time, reactors were immediately quenched in cold water and allowed to equilibrate at room temperature for 15 min. Table 6.1 shows the reaction conditions explored in this work. Temperatures were recorded using two thermocouple-equipped proxy reactors, constructed as described previously (Figure 2.2 in Chapter II, [33]), but from the same size Swagelok® parts as those used to construct the reactors in the present work ($^1/_2$ in. inner diameter). These proxy reactors provided a direct estimate of the temperatures experienced by the reactors during HTL. The average of the data from these two proxy reactors provided the characteristic temperature profile for that respective reaction condition. The pressure and headspace volume fractions in Table 6.1 were calculated using steam tables and the experimental temperature data. The reaction ordinate (R_0), a single parameter that describes the reaction severity, was calculated for the entire reaction time (not including quench), as described previously (Equation 2.2 in Chapter II [33]).

Figure 6.1 displays the reactor temperature profiles. The fast HTL reactors reached 186 ℃, and the isothermal HTL reactors reached 279 ℃. This ultimate reactor temperature for the isothermal run differs from the set-point temperature, which illustrates the importance of using a direct measurement of the reactor temperature. The careful reader will note that the temperature profiles in Figure 6.1 differ from those in our earlier work (Chapter II, [33]). This difference arises from the use of larger reactors in the present study.

Table 6.1: Reaction conditions for fast and isothermal HTL

	Fast, Low Loading	Fast, High Loading	Isothermal
Set-point Temperature	600	600	300
Reaction Time (min)	1	1	20
Maximum Reaction Temperature	186 ± 14	186 ± 14	279 ± 1
Log Reaction Ordinate (Log[R_0])	2.01	2.01	6.41
Pressure at Maximum Reaction Temperature (bar)	11.9 ± 3.7	11.9 ± 3.7	62.9 ± 0.5
Headspace Volume Fraction at Maximum Reaction Temperature	0.888 ± 0.002	0.306 ± 0.006	0.208 ± 0.001

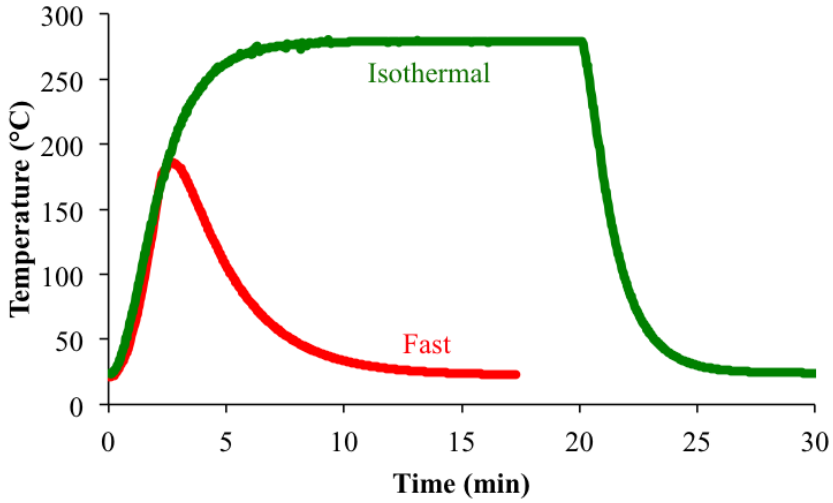

Figure 6.1: Temperature profiles for fast and isothermal HTL

6.2.3 Product Recovery and Elemental Analysis

Gaseous products were analyzed using an Agilent Technologies model 6890 GC equipped with a TCD, as described by Brown et al. [27]. The N_2 initially present in the headspace of the sealed reactor (calculated using the ideal gas law) served as an internal standard to determine the yields of H_2, CO, CO_2, CH_4, C_2H_6, and C_2H_4. Once gas analysis was complete, the valve assembly was removed and the contents of the reactor were poured into a borosilicate glass conical centrifuge tube. The reactor

was rinsed with 9 mL of DCM, and the rinsings were collected and added to the same centrifuge tube. The procedure for separating the aqueous phase, organic phase, and residual solids was described previously and involves centrifugation and manual transfer of phases using a glass pipette [31].

The product fractions were dried under N_2 using a Labconco® RapidVap® Vertex™ Dry Evaporator. The solvent-free DCM-soluble organic phase is identified as the biocrude. The masses of each dried sample were recorded and divided by the mass of dry algae initially loaded in the reactor to calculate the gravimetric yields of each product fraction on a dry basis. All reactions were carried out in duplicate. One of the dried aqueous phase samples and one of the biocrude samples from each set of duplicates were sent to Atlantic Microlabs, Inc. for analysis of C, H, N, and S. O was calculated by difference. The remaining dried aqueous phase and biocrude samples were sent to the National High Magnetic Field Laboratory for analysis by FT-ICR MS, as described in the next subsection.

6.2.4 Fourier Transform Ion Cyclotron Resonance Mass Spectrometry Analysis

Dried aqueous-phase samples were prepared for analysis by positive and negative mode ESI at a concentration of 500 μg/mL 50/50 (v/v) water/methanol. Dried biocrude samples were prepared for analysis at a concentration of 250 μg/mL 50/50 (v/v) DCM/methanol. For positive mode ESI, 1 % (v/v) formic acid was added to aid in protonation. For negative mode ESI, 1 % (v/v) ammonium hydroxide solution (28 % in water) was added to aid in deprotonation.

Samples were analyzed with a custom-built 9.4 T Fourier transform ion cyclotron resonance mass spectrometer [139]. Data collection was facilitated by a modular ICR data acquisition system (PREDATOR) [140]. Multiple (75-150) individual time-domain transients were co-added, half-Hanning-apodized, zero-filled, and fast Fourier

transformed prior to frequency conversion to mass-to-charge ratio (m/z) to obtain the final mass spectrum in absorption mode [141, 142]. ICR frequencies were converted to ion masses based on the quadrupolar trapping potential approximation [120].

External calibration of the instrument is performed monthly by use of ESI tuning mix (Agilent, Santa Clara, CA) to correct for temporal drift of the magnetic field. Internal calibration of the spectrum was possible with the use of homologous series which repeat by 14.01565 Da (or CH_2 units). All of the negative mode spectra (for both aqueous-phase and biocrude samples) and the positive mode spectra for aqueous-phase samples were manually calibrated on multiple homologous series because no one series spanned the entire m/z range. However, the positive mode spectra for biocrude samples included a homologous series that did span the entire m/z range so these spectra were calibrated by "walking calibration" [143, 144]. To capture the most abundant compounds in the samples from HTL of *Nannochloropsis* sp., FT-ICR MS excite and detect parameters were adjusted such that ions below 200 m/z were not collected.

IUPAC mass can be converted to Kendrick mass (Kendrick mass = IUPAC mass $\times$ (14/14.01565)) to sort compounds that differ in mass by 14.01565 Da (mass of CH_2) [145]. Mass spectral peaks with signal magnitude greater than six times the baseline root-mean-square (rms) noise level were assigned elemental compositions with custom-built software (MIDAS). Peak assignments and data visualization were performed with PetroOrg software [146]. For all mass spectra, the achieved spectral resolving power approached the theoretical limit [120] over the entire mass range: for example, average resolving power, $m/\Delta m_{50\%}$, in which $\Delta m_{50\%}$ is mass spectral peak full width at half-maximum peak height, was $\sim$ 1,000,000 - 1,300,00 at m/z 500.

6.3 Results and Discussion

The product yields from each HTL reaction condition are reported in this section, along with the molecular and/or elemental characterization of the gaseous, aqueous-phase, and biocrude products. The results from FT-ICR MS analysis are displayed in a variety of different formats, including broadband spectra, van Krevelen Plots, heteroatom density plots, and isoabundance contour plots (visualized using PetroOrg software [146]).

6.3.1 Product Yields and Elemental Analysis

Table 6.2 provides the average product yields for each reaction condition. The gas, aqueous-phase, biocrude, and solid product yields are largely comparable to those observed in previous studies of the same algae processed with similar reaction severity [31, 33]. An exception is the biocrude yield from fast HTL with the high loading, which was slightly lower than expected based on the variation of biocrude yield with reaction ordinate (R_0) reported by Faeth et al. [33]. This departure from the trend reported previously may be the result of increased mass loading in the present work. Fast HTL with low loading produced the most biocrude, and fast HTL with high loading produced approximately the same amount of biocrude as did isothermal HTL. Higher gas yields were also obtained after fast HTL at the low loading, consistent with the results in Figure 5.1 in Chapter V. These observations support the theory that mass loading (and effective concentration of algal biomass in the liquid phase) has a significant effect on product formation, first discussed in Chapter IV.

6.3.1.1 Gas Analysis

Table 6.3 highlights the molar yields of gaseous products per gram of dry algae loaded into the reactor. Only gases containing C and/or H are included in Table 6.3, as

Table 6.2: HTL product yields on a wt % dry basis

	Fast, Low Loading	Fast, High Loading	Isothermal
Biocrude	44.9 ± 1.0	36.9 ± 0.1	37.5 ± 0.9
Aqueous	49.0 ± 10.2	45.9 ± 7.1	49.8 ± 3.3
Solid	10.2 ± 0.5	12.4 ± 1.4	5.4 ± 0.4
Gas	4.3 ± 0.4	1.6 ± 0.2	1.4 ± 0.3
Total	108.5 ± 11.3	100.7 ± 4.5	96.7 ± 0.3

these are produced by the reaction. For all reaction conditions, CO_2 is the dominant product with yields $\geq$ 0.3 mmol/g dry algae. CO is the second most abundant product, contributing up to 0.12 mmol/g algae. Comparing the gases from the two fast HTL reaction conditions with those from isothermal HTL reveals that isothermal HTL results in more completely oxidized gases and no C_2 gases. Oxidation of propane and other short-chain hydrocarbons in subcritical water has been observed previously [147], which provides a possible explanation for the gas products from isothermal HTL. Similar yields of CO_2 are observed after HTL at both of the high loading reaction conditions, which may indicate that the mass loading in the reactor has more influence on CO_2 production than does the reaction severity. This observation further supports the idea that mass loading affects product formation during HTL.

Table 6.3: Yield (mmol/g dry algae) of gaseous products from HTL

	Fast, Low Loading	Fast, High Loading	Isothermal
H_2	0.035 ± 0.001	0.009 ± 0.001	0.0002 ± 0.00002
CO	0.120 ± 0.024	0.075 ± 0.043	0.002 ± 0.0004
CH_4	0.046 ± 0.0004	0.012 ± 0.0003	0.001 ± 0.0001
CO_2	0.857 ± 0.080	0.301 ± 0.011	0.317 ± 0.075
C_2H_4	0.043 ± 0.008	0.009 ± 0.001	Not Detected
C_2H_6	0.013 ± 0.0001	0.004 ± 0.0005	Not Detected

6.3.1.2 Elemental Composition of Aqueous Phase and Biocrude

This section provides the elemental composition of the dried aqueous-phase and biocrude product fractions. HHVs were calculated from the elemental compositions using the Boie formula (Equation 2.1 [74]). We also calculated the recovery of C, N, and S in the dried aqueous-phase and biocrude samples, according to Equation 6.1 and displayed in Figures E.1 and E.2 in Appendix E.

$$\text{Recovery of Element X (\%)} = \frac{\text{Wt \% X in Product} \times \text{Mass of Product}}{\text{Wt \% X in Dry Algae} \times \text{Mass of Dry Algae Loaded}} \tag{6.1}$$

Table 6.4 displays the elemental compositions for the dried aqueous-phase samples from all three experimental conditions. All three aqueous-phase samples have similar H and S content, but fast HTL with the low loading appears to produce an aqueous-phase product with less C and N than the other two conditions.

Table 6.4: Elemental composition (wt %) of dried aqueous phase samples from HTL

	C	H	N	S
Fast, Low Loading	22.54	7.00	6.30	0.48
Fast, High Loading	31.03	7.49	9.09	0.49
Isothermal	29.47	7.59	7.79	0.46

The lower C and N content in the aqueous phase from fast HTL with low loading may be due to the presence of a different reaction environment. With the lower water loading and larger headspace volume, proportionately more water would partition into the vapor phase and the algal biomass would be more concentrated in the liquid phase. This increase in effective concentration of the algae in the liquid water phase during HTL seems to facilitate reactions that favor partitioning of C- and N-containing compounds into the biocrude rather than into the aqueous phase, which is consistent with both the increase in biocrude yield and decrease in C and N content of the

aqueous phase from fast HTL at the low loading HTL condition.

In contrast, fast HTL with the high loading produced the aqueous-phase product with the highest C and N content. The amount of C and N in the aqueous phase at this condition accounts for 31.5 % of the C and 54.6 % of the N in the algal biomass loaded into the reactor (see Figure E.1 in Appendix E). The higher C content of the aqueous-phase sample produced here may be caused by rapid hydrolysis of proteins into water-soluble amino acids and/or amino acid chains (peptides and polypeptides), followed by a rapid quench before further reaction [148]. Fast HTL with the low loading may increase the rate at which these dissolved protein components react, thanks to the aforementioned increase in effective concentration of reactants. Isothermal HTL likely also facilitates reactions of these dissolved protein components via an extended reaction time.

Fast HTL with the high loading led to the highest recovery of N in the aqueous phase, which is desirable as it reduces heteroatoms in the biocrude and facilitates nutrient recycling to algae cultivation ponds or bioreactors. This condition also led to a higher C recovery in the aqueous phase, which is undesired as it partially deprives the biocrude fraction of C. These results clearly indicate that trade-offs exist between minimizing C and maximizing N in the aqueous phase.

Table 6.5 shows the elemental composition of the biocrude samples. The biocrude from fast HTL at the high loading contains the least N and O. The low N content, which represents just 25.7 % of the N in the algal biomass, is consistent with fast HTL with the high loading favoring rapid solubilization of protein-derived (and likely N-containing) products that partition into the aqueous phase. Further, biocrude from fast HTL with the low loading contained the most N (44.5 % of the N in the algal biomass feedstock) and exhibited the lowest HHV of all three biocrude samples. As energy density and N content can be proxies for biocrude quality, this condition produced the lowest quality biocrude. Recall, however, that this reaction condition

also resulted in the highest biocrude yield.

Table 6.5: Elemental composition (wt %) of biocrude samples from HTL

	C	H	N	S	O	HHV (MJ/kg)
Fast, Low Loading	66.69	8.78	8.21	0.70	15.62	32.51
Fast, High Loading	70.20	9.38	5.76	0.68	13.98	34.47
Isothermal	69.04	9.22	6.10	0.51	15.13	33.75

Fast HTL with the low loading leads to the highest C recovery (61.0 % of the C in the algae) in the biocrude of the reaction conditions examined, but it also leads to the highest N (44.5 %) and S (48.6 %) recoveries (see Figure E.2 in Appendix E). Heteroatoms decrease the energy content of a fuel (specifically O) and produce harmful substances upon combustion (specifically N and S). In exchange for lower N and S recoveries in the biocrude, fast HTL with the high loading and isothermal HTL also led to a lower C recovery. Again, we observe competing effects of the HTL conditions on the C and heteroatom recoveries in the biocrude, and between biocrude yield and quality. These trade-offs point to the need to optimize HTL reaction conditions to obtain high quality products at acceptable yields.

6.3.2 Fourier Transform Ion Cyclotron Resonance Mass Spectrometry Analysis

The preceding section identified trade-offs between the recovery of C and the recovery of heteroatoms to both the aqueous-phase and biocrude products, and between yield and quality of the biocrude. This section reports on the use of high-resolution FT-ICR MS analysis to better understand how the different reaction conditions affect HTL product yields and compositions.

6.3.2.1 Distribution and Ionization of Product Molecules

The high resolution of FT-ICR MS permitted assignment of molecular formulae to up to 95 % of the peaks in the broadband MS spectra (see Table E.2 in Appendix E for further details on peak assignment). Figure 6.2 depicts the positive ESI FT-ICR MS broadband spectra for the aqueous-phase samples. These spectra illustrate relative abundances of the various compounds present over the range of molecular weights analyzed. Large peaks appear in the 300 - 400 m/z region for all three HTL reactions. The most abundant compounds in the aqueous phase from isothermal HTL (spectrum C) are concentrated in a lower range of m/z than are the most abundant compounds in the aqueous-phase samples from fast HTL. Fast HTL with the high loading (spectrum B) produced more water-soluble compounds with high m/z than did the other reaction conditions. Additionally, the highest number of assignable peaks was in the spectrum for the aqueous phase from fast HTL with low loading (spectrum A). Figures E.3 to E.5 in Appendix E provide additional broadband spectra for the aqueous phase (negative ESI) and biocrude (positive and negative ESI).

Using both positive and negative ESI FT-ICR MS, we identified more than 13,000 unique molecular formulae in each of the aqueous-phase samples and over 25,000 unique molecular formulae in each of the biocrude samples. These counts exceed those reported by Sudasinghe et al. by at least a factor of three [128]. The relative number of molecular formulae identified by positive ESI and negative ESI are depicted using Venn diagrams in Figure 6.3 [149]. The size of the left circle of each diagram corresponds to the number of unique molecular formulae identified using positive ESI alone. The overlapping (middle) and right sections of each diagram correspond to the number of unique molecular formulae identified using both ESI methods and negative ESI alone, respectively. The labels of each of these portions indicate the actual number of peaks identified by positive, negative, or both methods of ionization. Please note that the circles in Figure 6.3 scale within a given sample type (aqueous

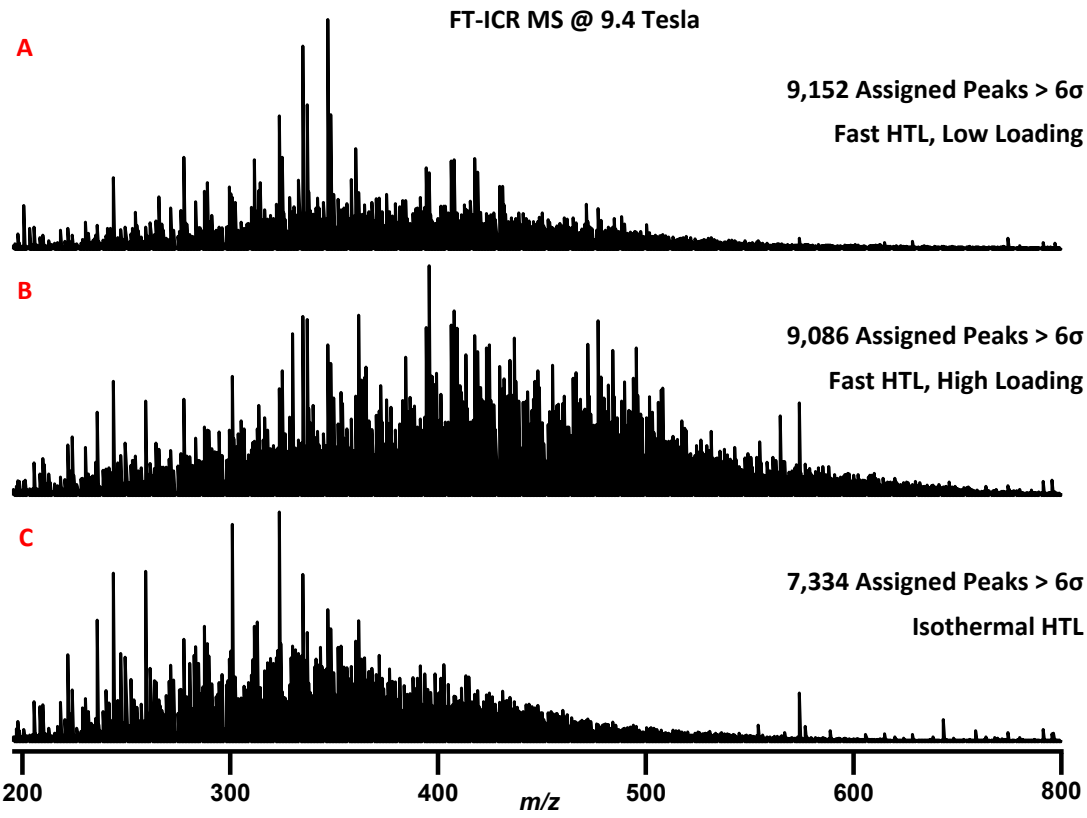

Figure 6.2: Positive ESI FT-ICR MS broadband spectra of aqueous-phase samples from HTL (a - Fast HTL with low loading, b - Fast HTL with high loading, c - Isothermal HTL)

phase or biocrude), but not across different types of samples.

Figure 6.3a shows that more unique compounds in the aqueous-phase samples were identified using negative ESI than with positive ESI for all HTL processing conditions in this work. Compounds readily detected by negative ESI include those with acidic functional groups (like carboxylic acids) and those containing O atoms [150]. Compounds readily detected by positive ESI include those with basic functional groups (like pyridine and related compounds) and those containing N atoms [150]. More compounds in the aqueous phase being identified by negative ESI (rather than positive ESI) likely indicates that the aqueous-phase samples examined in this study contain more compounds with acidic functional groups (or with more O atoms) than with basic functional groups.

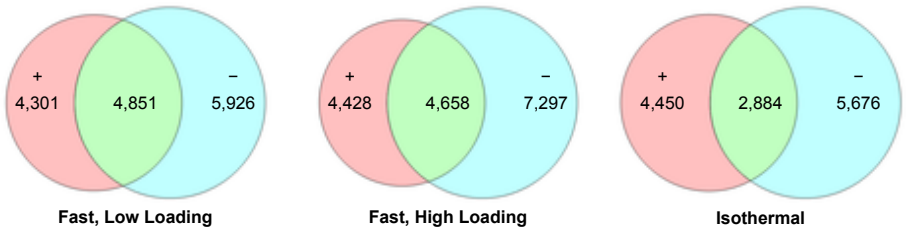

a Aqueous-Phase Samples

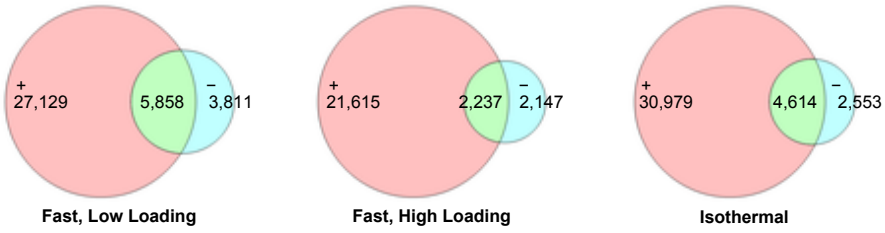

b Biocrude Samples

Figure 6.3: Venn diagrams illustrating relative numbers of unique molecular formulae identified in HTL products by FT-ICR MS (left = positive ESI, overlap = both, right = negative ESI)

It is clear from Figure 6.3b that a large majority of the unique compounds identified in the biocrude samples produced under all three reaction conditions were ionized using positive ESI. Based on the likely composition of the compounds identified using each ionization method, the biocrude samples are likely to contain a larger fraction of compounds with basic, rather than acidic, functional groups than do the aqueous-phase samples. This result is consistent with the observations of Sudasinghe et al. [128].

Of the acidic compounds identified in the biocrude, the most abundant are C16 - C20 compounds. Figure 6.4 depicts the relative abundance fraction of compounds of each C number in the biocrude, analyzed using negative ESI. The three C numbers with the most abundant compounds are 20, 16, and 18, in decreasing order. These C numbers also correspond to the most abundant fatty acids in *Nannochloropsis* sp. [151]. In fact, we identified a compound with molecular formula $C_{20}H_{30}O_2$ and a

double bond equivalent (DBE) of 5 in all three biocrude samples analyzed using negative ESI. The DBE represents the degree of unsaturation of a molecule, with the number indicating the sum of rings and double bonds. For example, cyclohexane has a DBE of 1 to represent 1 ring, while benzene has a DBE of 4, representing 1 ring and 3 double bonds. This molecular identification matches that of eicosapentaenoic acid (EPA, C20:5ω-3) the most abundant fatty acid detected in a different study with *Nannochloropsis* sp. biomass [151]. We also note that some compounds in the C16 - C20 range contain multiple N and O atoms and have molecular formulae consistent with chains of amino acids.

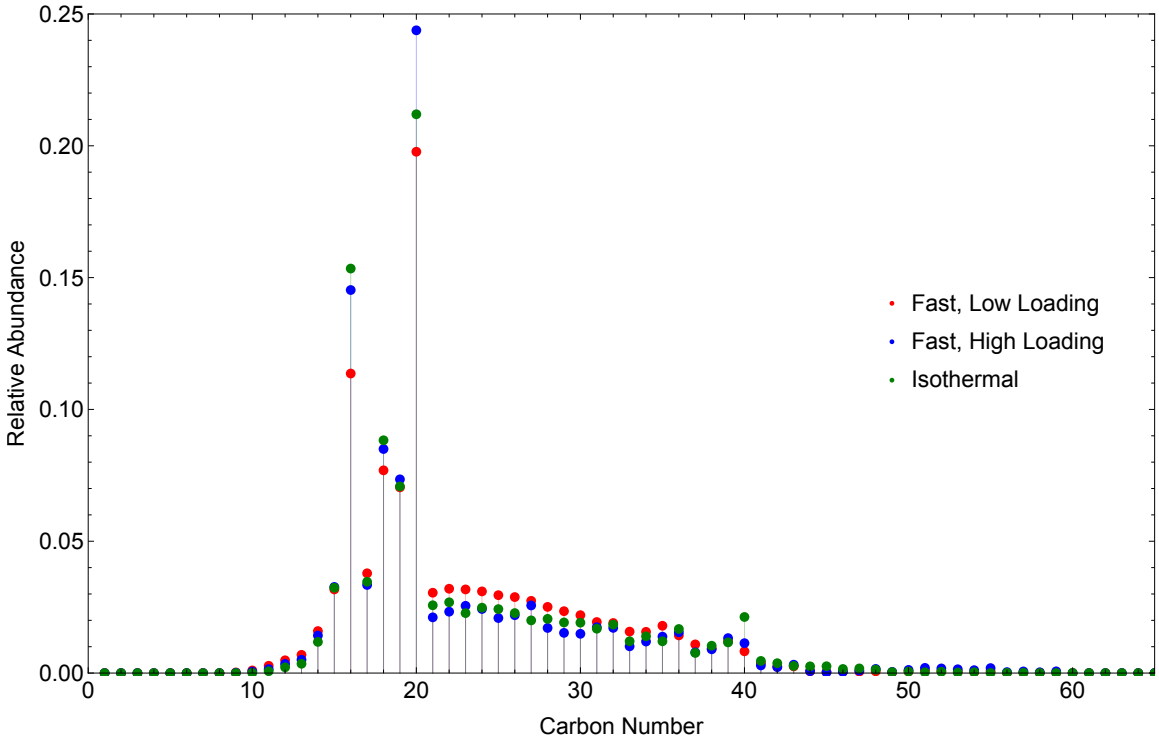

Figure 6.4: Carbon number distributions for negative ESI analysis of biocrude samples

Compounds with 16 - 20 C atoms are also among the most abundant in the aqueous-phase samples analyzed using negative ESI, as Figure 6.5 depicts. These compounds may include free fatty acids, but many of them contain several heteroatoms.

In fact, the aqueous phase from fast HTL with high loading contains C20 compounds with up to 8 N atoms and 6 O atoms. Such compounds are consistent with chains of 4 amino acids, indicating that many of the water-soluble compounds with C numbers of 16 - 20 may be derived from proteins. C number distribution plots for the aqueous phase and biocrude analyzed using positive ESI are included in the Appendices (Figures E.6 and E.7).

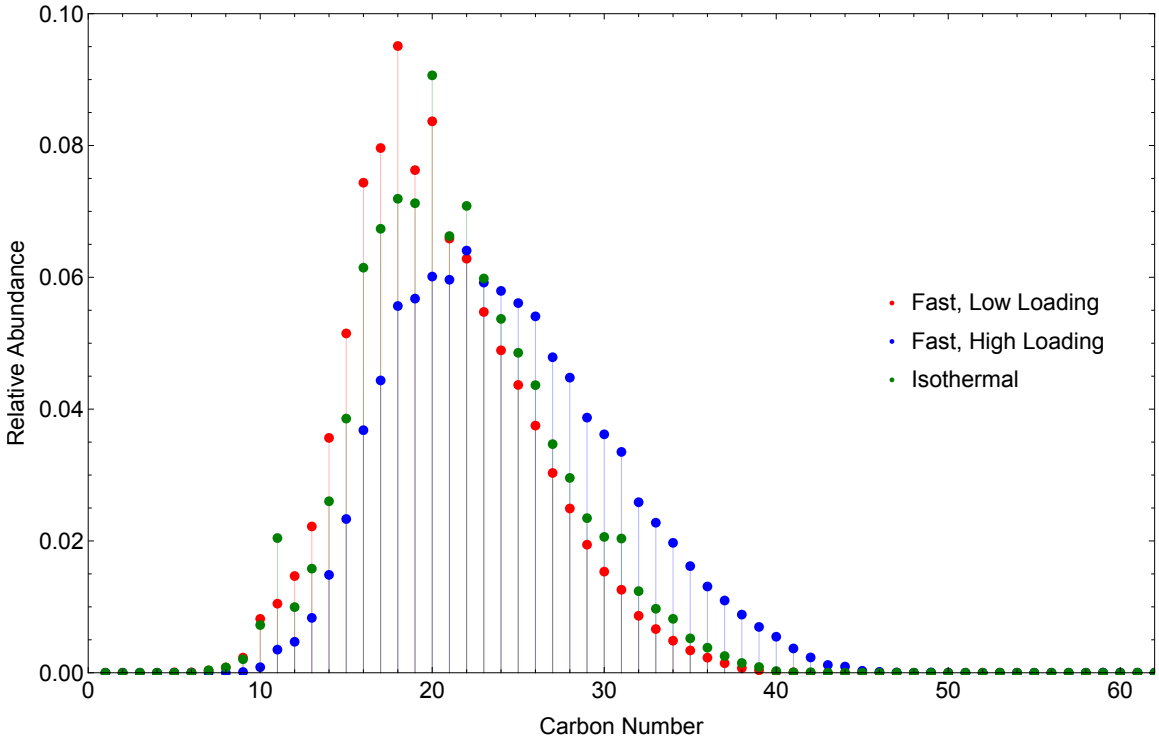

Figure 6.5: Carbon number distributions for negative ESI analysis of aqueous-phase samples

6.3.2.2 Heteroatoms

This section provides information about the heteroatom content and distribution in the products from the three HTL conditions examined. We first explore O-containing compounds, followed by compounds containing both N and O, N-containing compounds, Na-containing compounds, and S-containing compounds. Since more

compounds in the aqueous-phase samples were identified using negative ESI, the remainder of the aqueous-phase analysis in this work is restricted to negative ESI unless indicated otherwise. Likewise, more compounds in the biocrude samples were identified using positive ESI, so the remainder of the analysis of biocrude samples in this article is restricted to positive ESI unless otherwise indicated.

Oxygen-Containing Compounds

One way to visualize FT-ICR MS results for O-containing compounds is via the van Krevelen plot, which displays the H/C ratio of each compound with respect to its O/C ratio [152]. Different types of compounds appear in different regions of the plot, which can help characterize the composition of the samples. Biocrude and aqueous-phase samples produced via HTL of microalgae may contain lipids, proteins, phenolic polymers, unsaturated hydrocarbons, aromatics, and products derived therefrom. Lipids generally have H/C from 1.7 - 2.2 and O/C from 0.0 - 0.2. Proteins lie between 1.5 - 2.2 H/C and 0.2 - 0.6 O/C, phenolic polymers between 0.6 - 1.7 H/C and 0.1 - 0.6 O/C, unsaturated hydrocarbons between 0.7 - 1.5 H/C and 0.0 - 0.1 O/C, and aromatics between 0.3 - 0.7 H/C and 0.0 - 1.0 O/C [127]. Further, different collections of data points on a van Krevelen plot can identify chemical reactions that relate the compounds in the group. For example, a grouping of points on a line with a slope of 2 may indicate compounds that are related to each other by hydration or condensation, and a horizontal line indicates compounds related by oxidation or reduction [152, 153].

Figure 6.6 depicts a van Krevelen plot of the compounds identified via negative ESI of the aqueous-phase samples from HTL. All three samples contain many compounds that appear in the regions expected for phenolic polymers and proteins. Some compounds also fall into the lipid region on these plots, which may indicate some sol-

ubility in water for energy-dense compounds like lipids. Based on the arrangement of points on these plots, there appear to be compounds related by oxidation/reduction, hydrogenation/dehydrogenation, methylation/demethylation/alkyl chain elongation, hydration/dehydration, and carboxylation/decarboxylation reactions (as described above, and in greater detail in references [152] and [153]).

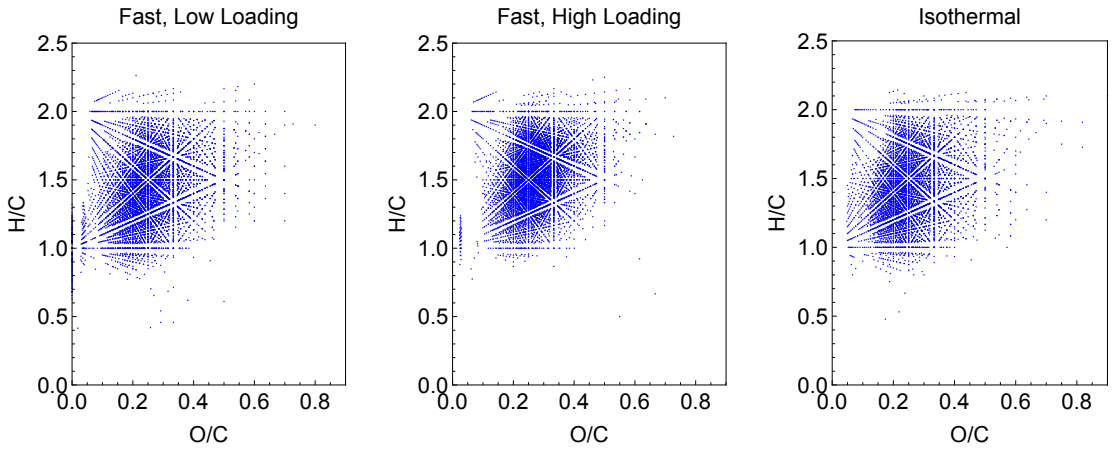

Figure 6.6: van Krevelen Plot (H/C and O/C ratios) for negative ESI analysis of aqueous-phase samples

Figure 6.7 depicts van Krevelen plots for biocrude samples analyzed by positive ESI FT-ICR MS. All three biocrude samples contain many compounds within the regions representing phenolic polymers, lipids, and unsaturated hydrocarbons. Figure 6.7 shows fewer compounds with O/C ratios > 0.3, than were present in the aqueous-phase samples. Table 6.6 displays counts of the few compounds that do appear in this region. Positive ESI identified the most compounds with high O/C ratios in the biocrude from isothermal HTL, though all three HTL processing conditions yield similar numbers of compounds with high O/C. However, isothermal HTL produced far fewer acidic (identified using negative ESI) compounds with O/C ratios > 0.3 than did fast HTL. The additional reaction time (and greater reaction severity) may provide additional time for reactions between compounds, possibly converting acidic

compounds to more basic ones through the addition of N.

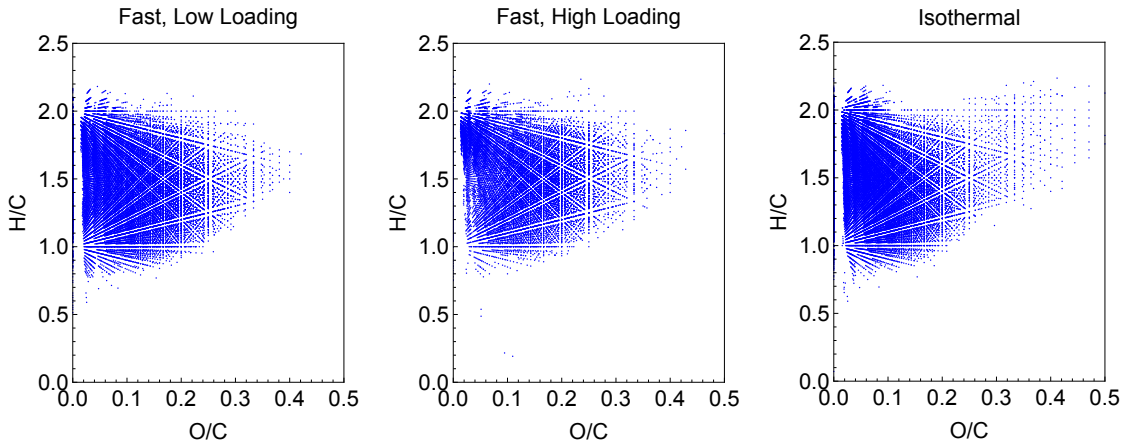

Figure 6.7: van Krevelen Plots (H/C and O/C ratios) for positive ESI analysis of biocrude samples

Table 6.6: Number of O-containing compounds with O/C ratios > 0.3 in the biocrude

	Fast, Low Loading	Fast, High Loading	Isothermal
Positive ESI	241	273	317
Negative ESI	329	139	51

N_xO_y Compounds

Since N and O are the most abundant heteroatoms, we examine how these two elements are combined in the various compounds identified. Figures 6.8 and 6.9 depict the relative abundance (color scale) of distinct compounds in different heteroatom classes (O on the horizontal axis and N on the vertical axis) for the aqueous-phase and biocrude samples, respectively. In FT-ICR MS, relative abundance does not correspond directly to a mass or molar basis, but is a function of how many ions move past the detector, the distance between the ions and the detector, and how long the ions can be detected. As a result, the relative abundance resulting from

FT-ICR MS analysis is a qualitative representation of the sample composition.

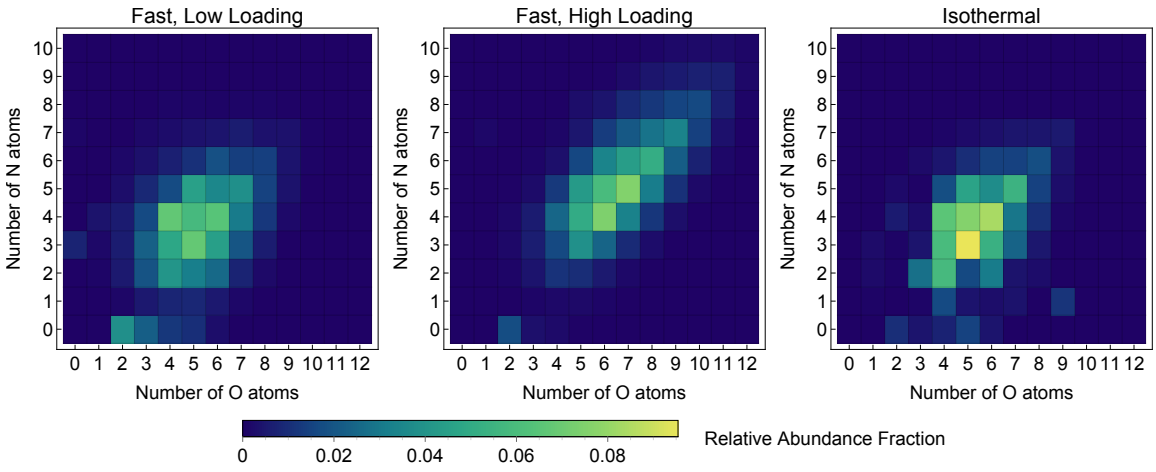

Figure 6.8: Heteroatom density graph for aqueous-phase samples (negative ESI)

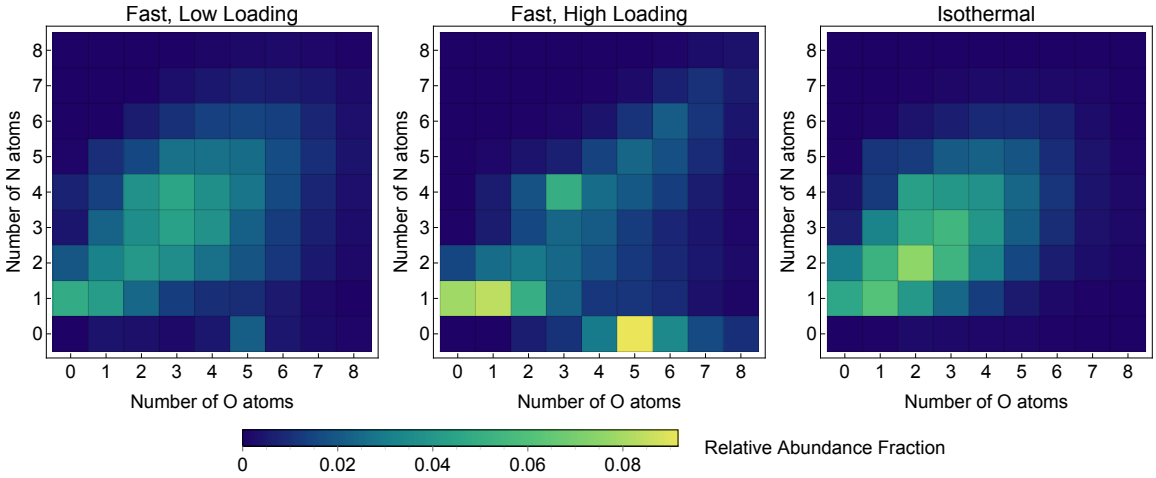

Figure 6.9: Heteroatom density graph for biocrude samples (positive ESI)

Figure 6.8 shows that fast HTL with high loading produced aqueous-phase compounds that contained the highest number of N and O atoms ($N_{10}O_{12}$), compared to the other two reaction conditions (for which N_8O_9 is the highest heteroatom class observed). Though the mass loadings are the same, the product distributions in Figure 6.8 for fast HTL with high loading and isothermal HTL are quite different. The most abundant compounds in the aqueous phase from isothermal HTL belong to the N_3O_5

class and classes within one or two N and/or O atoms. It seems that the compounds that formed initially during fast HTL underwent additional hydrolysis or decomposition to form compounds with fewer N and O atoms. Figure E.8 in Appendix E depicts similar trends.

Figure 6.9 depicts heteroatom density graphs for the biocrude samples analyzed using positive ESI. Several compounds with no N atoms are present in the biocrudes from fast HTL, but all compounds in the biocrude from isothermal HTL contain at least 1 N atom (after analysis by positive ESI). Sudasinghe et al. observed several compounds with no N atoms and 4 O atoms in their biocrude, which they believed to be polymerized fatty acids [128]. It is possible that the compounds with no N and 3 - 7 O atoms identified in the biocrude samples produced via fast HTL are also polymerized fatty acids with varying levels of oxygenation. Since none of these compounds are present in the biocrude produced via isothermal HTL, it is likely that the extended reaction time facilitated reactions of fatty acids and/or polymerized fatty acids with amino acids, ammonia, or other N-containing compounds. This scenario is consistent with the observation from Table 6.6 that the high O/C compounds in the biocrude from isothermal HTL are primarily ionized by positive ESI (which ionizes N-containing and basic compounds). Sudasinghe et al. observed an increase in the relative abundance of compounds containing both N and O with increasing temperature [15], which may also contribute to the paucity of compounds deemed likely to be polymerized fatty acids in the biocrude from isothermal HTL. As indicated in Table 6.1, the maximum reaction temperatures increased from 186 ℃ for the fast HTL reactions to 279 ℃ for the isothermal HTL reaction.

The negative ESI analysis of the biocrude samples from all three reaction conditions contained several compounds with 2 O atoms and no N atoms. In fact, such compounds contribute 33 - 44 % of the total relative abundance. Figure E.9 in Appendix E depicts the vast abundance of compounds with 2 O atoms in the biocrude

analyzed by negative ESI. Many of these compounds are likely fatty acids, which indicates that reactions of N-containing compounds with fatty acids and/or polymerized fatty acids do not consume all of these compounds, even after isothermal HTL.

Isoabundance contour plots provide yet another way to depict characteristics of the numerous compounds containing both N and O atoms. As a representative example, Figure 6.10 displays isoabundance contour plots for the heteroatom class N_3O_4. The number of C atoms present in a particular compound is on the horizontal axis, and the DBE is on the vertical axis. The color scale indicates the relative abundance of the compounds. Isoabundance contour plots of heteroatom class can build a comprehensive "fingerprint" of the samples analyzed by FT-ICR MS. This fingerprint provides a very detailed accounting of the size of the compounds, degree of unsaturation, and the distribution of different types of compounds, all of which can be very useful when considering these samples for upgrading.

The plots in the top row (panels A, B, and C) of Figure 6.10 depict results for the aqueous-phase samples, and the plots in the bottom row (panels D, E, and F) show results for the biocrude, both analyzed using positive ESI. The biocrudes contain a more diverse distribution of compounds in this particular heteroatom class than do the aqueous-phase samples, perhaps because of the larger number of compounds present in the biocrudes relative to the aqueous phase. The plots of both the aqueous phase and the biocrude from fast HTL at the high loading have two small regions of high relative abundance instead of a single "hot spot" as observed in the other plots. The results for the samples produced using isothermal HTL and fast HTL with low loading are quite similar. Recall that the heteroatom density plots for these samples were also similar.

Nitrogen-Containing Compounds

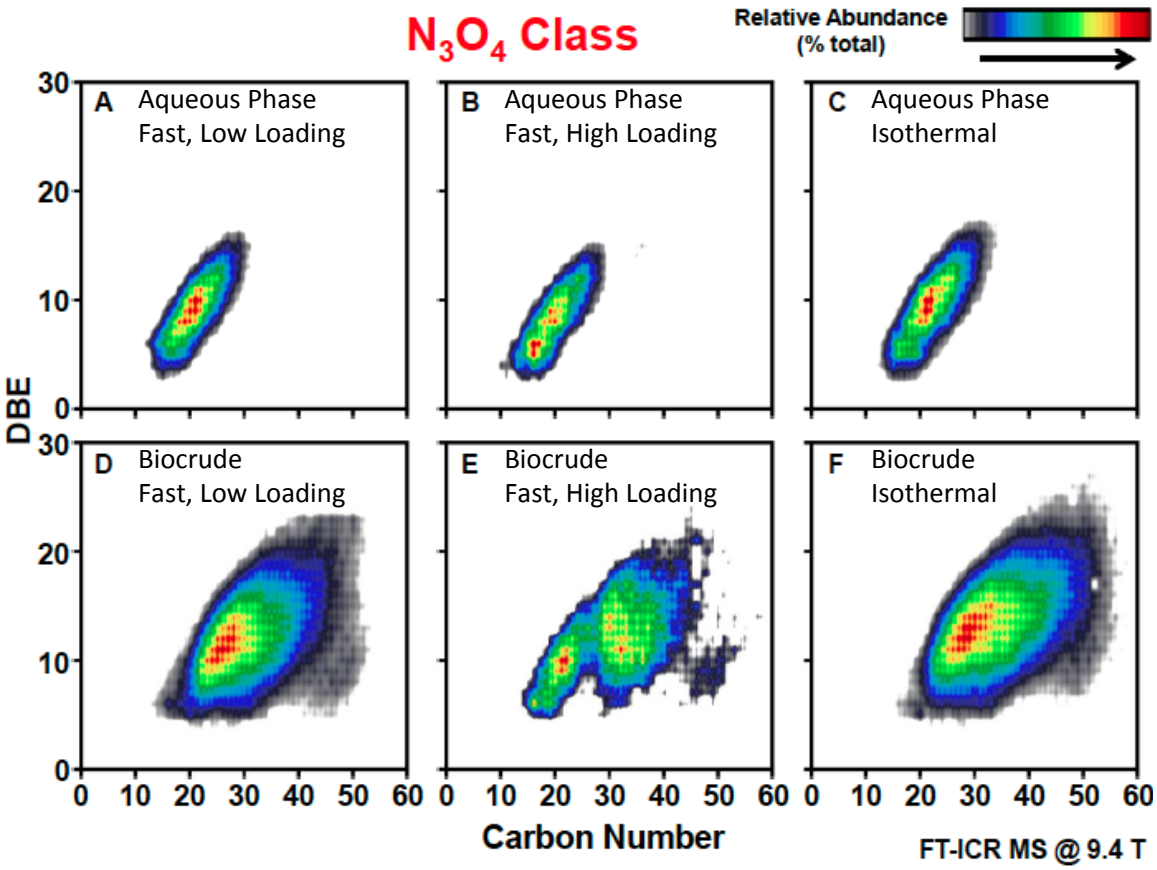

Figure 6.10: Isoabundance contour plots for aqueous-phase and biocrude samples (positive ESI)

N is abundant in protein-rich biomass, such as many algal species. It is important to understand how N is included in the various compounds in the aqueous phase and biocrude from HTL to facilitate upgrading of these compounds to usable nutrient sources and fuels. Figure 6.11 depicts the N/C ratios plotted with the molecular weight in units of atomic mass unit (AMU) for the aqueous-phase samples. This plot illustrates how N is incorporated into molecules of different sizes in the aqueous phase. Most compounds in all three samples have molecular weights between 200 - 800 AMU and the compounds with the highest N/C ratios are within the 250 - 500 AMU range. The aqueous phase from fast HTL with the high loading is the only aqueous phase sample analyzed by negative ESI that contains compounds with molecular

weights > 800 AMU. These compounds primarily have N/C ratios of 0.1 - 0.3. Select molecular formulae of compounds with molecular weights > 800 AMU and their respective DBE values are consistent with those of various polypeptide chains. This tentative identification supports the idea that fast HTL with high loading facilitates solubilization of peptides and/or polypeptides, and that the reaction is quenched prior to significant decomposition of these products.

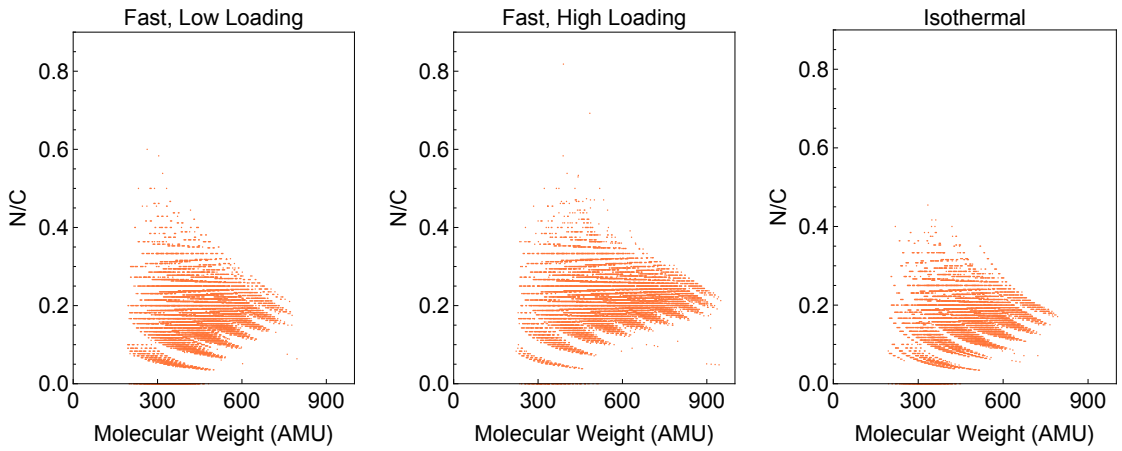

Figure 6.11: N/C ratios vs. average molecular weight for negative ESI analysis of aqueous-phase samples

Most N-containing compounds in the biocrude samples also have molecular weights < 800 AMU (see Figure E.10 in Appendix E). Table 6.7 shows that the biocrude samples generated under high loading conditions from both fast and isothermal HTL include the most N-containing compounds at molecular weights above 800 AMU. However, elemental analysis (Table 6.5) revealed that the biocrude from fast HTL with the high loading contains the least N overall, followed closely by the biocrude from isothermal HTL. Therefore, the N that is retained in the biocrude from fast HTL with the high loading is concentrated in some of the heavier compounds. We speculate that the high molecular weight compounds identified in the biocrude from fast HTL with high loading are residual cellular components that were not readily soluble

in the aqueous phase. Since isothermal HTL is the most severe of the reaction conditions examined, oligomerization and/or condensation reactions involving dissolved protein components that could produce higher molecular weight compounds may be more likely, explaining the large number of N-containing high molecular weight compounds. One likely example of such a reaction was postulated by Sudasinghe et al.: the formation of amides from reactions of carboxylic acids with ammonia (a water-soluble product of protein decomposition) [128].

Table 6.7: Number of N-containing compounds with molecular weight > 800 AMU in the biocrude (positive ESI)

Fast, Low Loading	Fast, High Loading	Isothermal
1,139	2,013	3,303

6.3.2.3 Sodium- and Sulfur-Containing Compounds

FT-ICR MS analysis identified several compounds in the products of HTL that contain Na and/or S, as Table 6.8 indicates. Such compounds are of interest because they are potential catalyst poisons in an algal biorefinery. To the best of our knowledge, this is the first detailed report including identification of molecular formulae containing Na and S in both the aqueous-phase and biocrude products of algal HTL. Na- and S-containing compounds were preferentially ionized by different ESI modes; positive ESI did not identify any S-containing compounds, but it identified more Na-containing compounds than did negative ESI. Identification of S-containing compounds solely with negative ESI indicates that the S present in molecules with molecular weights > 200 in both the aqueous-phase and biocrude samples is likely incorporated into acidic compounds. Amino acids and thiols are examples of acidic S-containing compounds.

Table 6.8 indicates that the most Na-containing compounds were identified in the aqueous phase from fast HTL with the low loading. This reaction condition was

Table 6.8: Number of compounds containing Na or S in the aqueous-phase and biocrude product fractions

	Aqueous Phase		Biocrude	
	Na	S	Na	S
	Positive ESI	Negative ESI	Positive ESI	Negative ESI
Fast HTL, Low Loading	2,938	1,341	5,629	83
Fast HTL, High Loading	2,384	1,234	7,960	27
Isothermal HTL	1,783	1,108	5,590	54

also the only one for which compounds with 2 Na atoms were identified. Such compounds were identified in both the aqueous-phase and biocrude products, as Figure E.11 illustrates in Appendix E. Figures 6.12 and 6.13 depict the Na/C ratios with respect to the average molecular weights of the aqueous-phase and biocrude compounds containing Na.

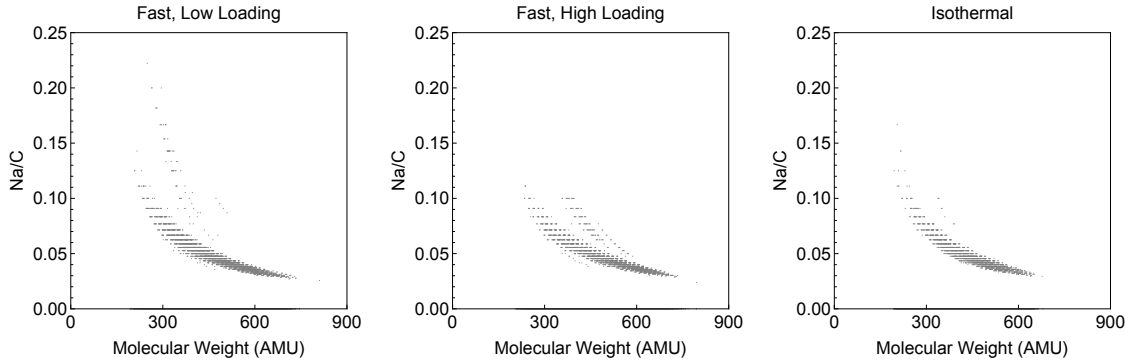

Figure 6.12: Na/C ratios vs. average molecular weight for aqueous-phase samples (positive ESI)

These figures reveal two distinct "bands" for the products from fast HTL with low loading. The Na-containing compounds in the biocrude may include mono- or di-sodium organo-metallic salts with sufficient hydrocarbon character to be soluble in DCM. Sudasinghe et al. reported adducts of Na with acylglyerol lipids in biocrudes from low-temperature isothermal HTL [15], so similar products may also be present in the biocrude samples examined in the present work. The presence of Na in fuels

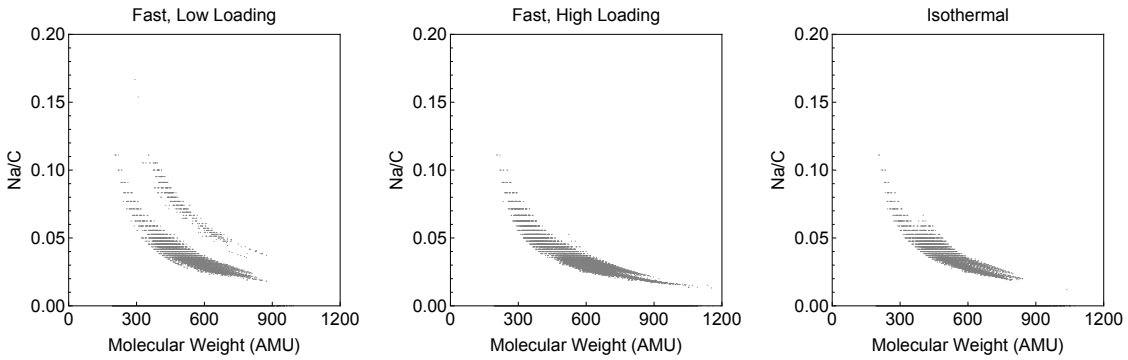

Figure 6.13: Na/C ratios vs. average molecular weight for biocrude samples (positive ESI)

can be problematic [154], so upgrading of biocrudes from HTL of microalgae would need to include removal of Na in addition to N, O, and S.

Figure 6.14 depicts the S/C atomic ratios with respect to the average molecular weight of the S-containing compounds in the aqueous phase samples from HTL. All of the compounds contain just a single S atom. The aqueous phase from fast HTL with high loading appears to contain the fewest compounds with S/C ratios > 0.1. As Table 6.8 indicates, very few S-containing compounds were identified in the biocrude samples from HTL of *Nannochloropsis* sp. in this study. Figure E.12 in Appendix E shows that the S-containing compounds present were most abundant at the lower molecular weights. The biocrude contained about 0.5 wt % S, so much of this sulfur seems to exist in smaller (MW < 200) molecules not detected by FT-ICR MS.

6.3.2.4 Herbicides as Byproducts

Given the wealth of data obtained for molecular formulae of reaction products, we searched for molecular formulae of known herbicides in the aqueous-phase samples. The molecular formulae and DBEs for imazamethabenz ($C_{15}H_{18}N_2O_3$), imazaquin ($C_{17}H_{17}N_3O_3$), and imazapyr ($C_{13}H_{15}N_3O_3$) matched those of products in the aqueous phase. Although we do not know for certain whether these herbicides are, in fact,

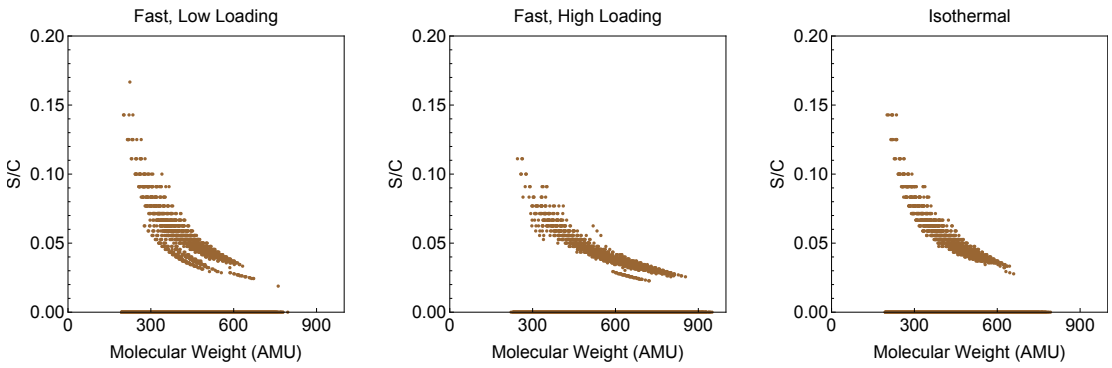

Figure 6.14: S/C ratios vs. average molecular weight for aqueous-phase samples (negative ESI)

the species in the samples analyzed by FT-ICR MS, the matching molecular formulae and DBEs provides circumstancial evidence.

From a sustainability point of view, it would be preferable to use the aqueous phase as source of N and P for algae cultivation. However, previous studies indicated toxicity effects when the aqueous phase is used to grow algae [59]. The possible presence of known herbicides may shed some light on why these toxic effects are observed. Some kind of treatment, perhaps biological [93] or thermochemical [32], can likely mitigate the toxicity of the aqueous phase for algae cultivation.

6.4 Conclusions

This chapter provides the first FT-ICR MS characterization of the aqueous-phase and biocrude products from fast HTL of microalgae. It also provides the first comparisons between fast and isothermal HTL at identical loadings and between different reactor mass loadings for fast HTL. Fast HTL with low loading produced higher biocrude yields than did isothermal HTL and fast HTL with high loading. However, the quality of biocrude produced via fast HTL with low loading appears to be less desirable than the biocrude produced via isothermal HTL or fast HTL with high

loading. Closely related to this trade-off between quality and quantity is the trade-off between the desirable recovery of C and the undesirable recovery of heteroatoms in the biocrude. Fast HTL with the low loading gave the highest C recovery to the biocrude, but it also gave the highest recovery of N and S to the biocrude, which would necessitate more aggressive upgrading in an industrial implementation of this process.

The trade-offs associated with elemental recovery extend to aqueous-phase products as well. HTL with high reactor loading (including both fast and isothermal HTL) leads to high recovery of N in the aqueous phase, which would be desirable for recycling N for algae cultivation. However, HTL with high reactor loading also promotes high recovery of C in the aqueous phase, which diverts C away from the biocrude. The trade-offs identified here provide many opportunities for the optimization of HTL processing conditions.

These trade-offs exist because rapid heating, mass loading, and reaction severity promote different reaction paths. For example, during HTL at the low loading, the algae and products derived therefrom experienced a higher effective concentration in the liquid water phase at reaction conditions because more of the water is partitioned to the vapor phase at this condition.

High molecular weight compounds in the aqueous-phase product from fast HTL with high loading are consistent with the molecular formulae and saturation levels of polypeptide chains, indicating that solubilization of these peptides and/or polypeptides into liquid water takes place very quickly. Far fewer high molecular weight compounds consistent with polypeptides are identified in the aqueous-phase products of fast HTL with low loading and isothermal HTL, which may indicate that such polypeptides are subject to decomposition and other reactions at these other conditions. This finding also suggests that further research is needed to better understand the effects of mass loading, especially for HTL at very short times and with rapid

heating.

Analysis using FT-ICR MS revealed that biocrudes from fast HTL contain several compounds with no N but 3 - 7 O atoms. These compounds are likely free fatty acids and/or oligomerized or polymerized fatty acids. All O-containing compounds present in the biocrude from isothermal HTL (identified using positive ESI) also contain N, possibly indicating that isothermal HTL provides ample time for reactions between O-containing compounds and N-containing compounds (likely including the formation of amides from reactions of carboxylic acids with organic amines or ammonia). This idea is reinforced by the observation that many of the high molecular weight compounds in the biocrude from isothermal HTL are basic, while many of the high molecular weight compounds present in the biocrudes produced via fast HTL are more acidic. However, analysis by negative ESI revealed many compounds with 2 O atoms and no N atoms in the biocrude samples from all three reaction conditions, which likely indicates that reactions between N- and O-containing compounds do not consume all fatty acids, even after isothermal HTL.

The detailed data provided by FT-ICR MS analysis facilitated the tentative identification of herbicides in the aqueous phase. To the best of our knowledge, no other studies have suggested specific compounds in the aqueous-phase products from HTL that may contribute to the toxic effect of aqueous phase on algae cultivation. This information could be especially helpful for informing the treatment of the aqueous-phase products or the genetic engineering of bacteria and/or algae that are capable of tolerating, or even metabolizing, these compounds.

CHAPTER VII

Development of a Unified Empirical Kinetic Model Describing Fast and Isothermal Hydrothermal Liquefaction

In this chapter we describe the development of a unified kinetic model describing both fast and isothermal HTL, the result of a collaborative effort between David Hietala and the author of this dissertation. Using the product yields and temperature profiles from HTL with high loading generated in Chapter V, we developed a modified reaction network including a novel physical "activation" pathway for algal cells that incorporates the effects of heating rate. We used MATLAB® to calculate kinetic parameters for all pathways in this modified reaction network, and the resulting model accurately correlates calculated and experimentally observed product yields for both fast and isothermal HTL.

7.1 Introduction

Few attempts have been made to develop a quantitative model of reaction kinetics for HTL of microalgae. Biller and Ross examined the HTL of several model compounds and algae species and developed an additive, non-kinetic model based on the biocrude yields of biochemical components weighted by the biochemical composi-

tion of the microalgae [21]. This model predicted biocrude yields from HTL of green microalgae, but failed to predict biocrude yields from HTL of cyanobacteria and only described one specific reaction condition ($T_q = 350$ ℃, $t_q = 92.5$ min, $\bar{h} = 10$ ℃/min).

Valdez and Savage [35] developed a reaction network and kinetic model for the HTL of *Nannochloropsis* sp., a marine species of microalgae, encompassing a range of reaction temperatures ($250 < T_q < 400$ ℃), times ($10 < t_q < 90$ min), and heating rates ($77 < h_0 < 129$ ℃/min, $50 < \bar{h} < 83$ ℃/min). This model successfully correlated the yields of solid, biocrude, aqueous-phase, and gas products for the reaction conditions within the scope of the study. However, the data used to develop the model only included experiments with reaction times ≥ 10 min, with little to no data at low solids conversion and little to no variation in product distribution. This restriction on reaction times was imposed such that all reactions operated under predominantly isothermal conditions (reactor heat-up contributed to ≤ 50 % of the reaction time).

In Chapter II [33], however, we observed comparable or higher biocrude yields from HTL of microalgae after reaction times < 10 min, indicating that such reaction conditions are also important for kinetic modeling of HTL. In this chapter, we bridge the work of Valdez et al. [35] and Faeth et al. [33]. To do so, we used the experimental data set encompassing a broad range of HTL reaction temperatures ($100 < T_q < 400$ ℃), reaction times (30 s $< t_q < 60$ min), and heating rates ($79 < h_0 < 258$ ℃/min, $49 < \bar{h} < 162$ ℃/min, $200 < T_{sp} < 600$ ℃) initially discussed in Chapter V to develop a revised reaction network and kinetic model for the HTL of *Nannochloropsis* sp.

7.2 Calculations and Kinetic Modeling Methods

To facilitate kinetic modeling, we employed several corrections to achieve mass balance closure for all experiments. Given that we measured the mass of gas evolved by difference rather than by direct measurement, some values were higher than expected based on the data from experiments with similar reaction conditions. In those rare

cases, we recalculated gas masses by linear interpolation of data points at equivalent T_{sp} and with t_q immediately preceding and following.

For reactions with $T_q > 250$ ℃, we generally recovered at least 80 % of the original water mass (wet aqueous recovery = Y_{WA}, where $Y_{WA} = 100$ % × mass wet aqueous phase / mass initial water loaded). In cases where Y_{WA} was < 80 wt % and $T_q \leq 250$ ℃, there often was higher mass loss than normal, due to the increased presence of wet, unreacted algal cells. To adjust for this, we assumed that this lost mass was distributed between the solids and wet aqueous phases proportional to the masses we measured. More specifically, we calculated correction factors (z), weight fractions of product i (x_i) and yields of product i (Y_i) according to equations 7.2 - 7.7, respectively. Here $m_{S,0}$ and $m_{W,0}$ are the initial masses of dry algae and water, m_i is the recovered mass of product i, and $m_T = \sum_i m_i$ is the total mass of recovered products.

$$z = \frac{(m_{S,0} - m_T)}{m_S + m_{DA}} \tag{7.1}$$

$$x_G = \frac{m_G}{m_{S,0}} \tag{7.2}$$

$$x_S = \frac{m_S(1+z)}{m_{S,0}} \tag{7.3}$$

$$x_B = \frac{m_B}{m_{S,0}} \tag{7.4}$$

$$x_{DA} = \frac{m_{DA}(1+z)}{m_{S,0}} \tag{7.5}$$

$$x_{WA} = \frac{m_{WA}(1+z)}{m_{W,0}} \tag{7.6}$$

$$x_V = 1 - x_G - x_{TS} - x_B - x_{DA} \tag{7.7}$$

$$Y_i = x_i \times 100\% \tag{7.8}$$

Furthermore, if applying equations 7.1, 7.6, and 7.8 resulted in $Y_{WA} > 80$ wt %, we instead used equation 7.9 to set x such that $Y_{WA} = 80$ wt % and recalculated all

yields accordingly.

$$z = \frac{0.8 m_{W,0}}{m_{WA}} - 1 \tag{7.9}$$

We first reported the original experimental product yields in Chapter V, but we include both the original and adjusted product yields for the reaction conditions used for kinetic model development in Tables F.1 to F.3 of the Appendices for reference.

7.3 Results and Discussion

This section includes the adjusted product yields from HTL with the high loading of *Nannochloropsis* sp. at temperatures of $100 < T_q < 400$ ℃, times of 30 s $< t_q <$ 60 min, and heating rates of $79 < h_0 < 258$ ℃/min ($49 < \bar{h} < 162$ ℃/min, $200 < T_{sp} < 600$ ℃). These adjusted yields are depicted in Figure 7.1. The curves on the plot represent typical temperature profiles resulting from $200 < T_{sp} < 600$ ℃. Each individual point represents an HTL reaction singleton shaded by adjusted product yield and plotted at the quench point (t_q, T_q), with t_q on a log scale. The trends depicted in each of the plots in Figure 7.1 are consistent with those discussed in Chapter V and are not repeated here for brevity. Following the adjusted product yield profiles, we discuss our proposed reaction network and kinetic model.

7.3.1 Product Yields

Figure 7.1 depicts the various adjusted product yields from HTL of *Nannochloropsis* sp. Figures 7.1a to 7.1f depict the gas, solid, biocrude, dry aqueous-phase, volatile, and aqueous-phase product yields (recall $Y_A = 100 - Y_S - Y_B - Y_G$), respectively. We present the aqueous-phase product yields because previous research indicated that volatile products are produced almost entirely from water-soluble products [31]. Therefore, we treat the sum of these products as the total aqueous-phase products for the sake of kinetic modeling.

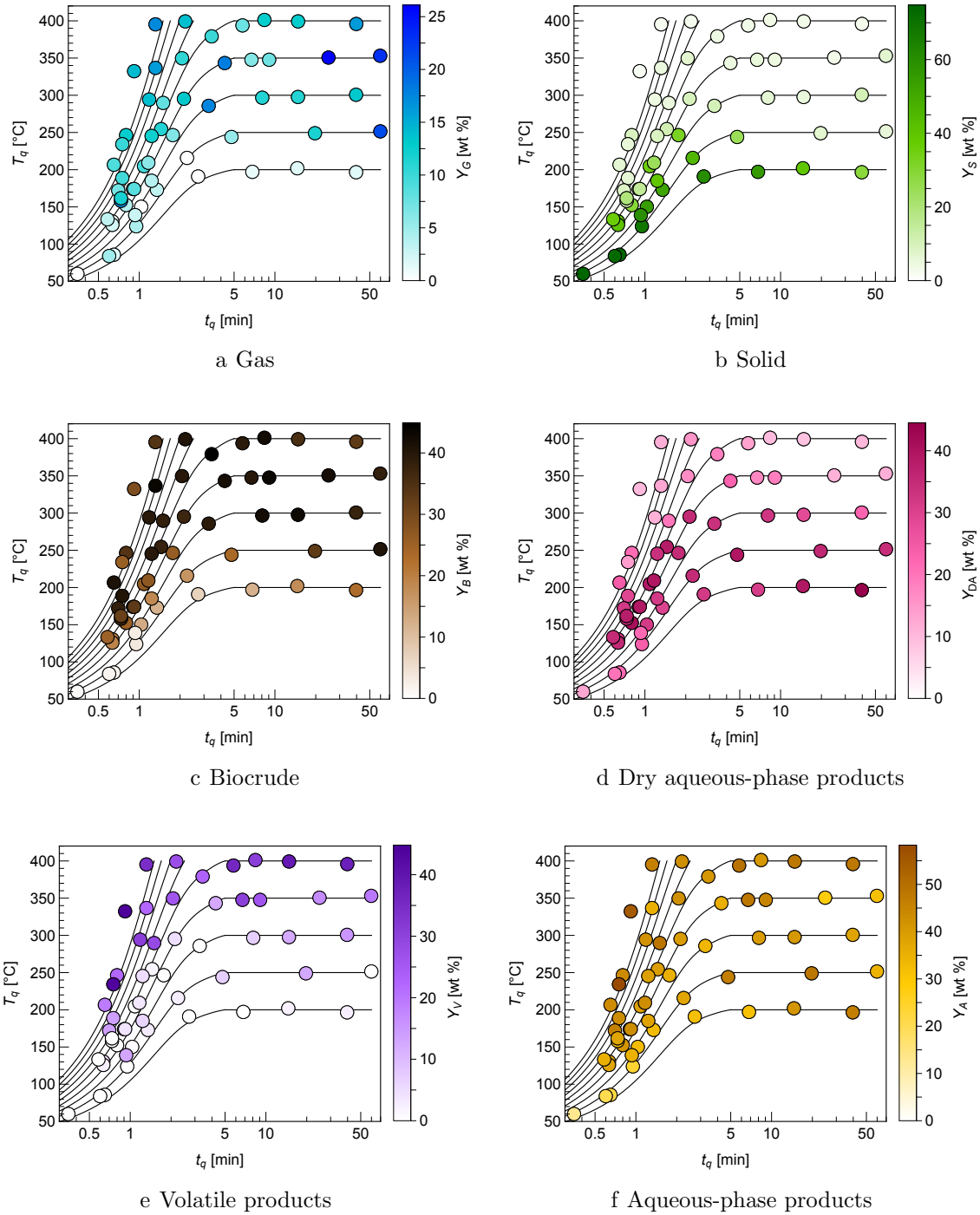

a Gas

b Solid

c Biocrude

d Dry aqueous-phase products

e Volatile products

f Aqueous-phase products

Figure 7.1: Adjusted product yields from the HTL of *Nannochloropsis* sp. plotted as functions of reaction quench temperature, T_q, and time, t_q. Solid lines represent typical temperature profiles based on sand-bath set-point temperatures of 200 - 600 °C.

7.3.2 Kinetic Model Development

We sought to derive a reaction network and develop a corresponding kinetic model that accurately describes the behavior of microalgal HTL over the entire range of temperatures (T_q), reaction times (t_q), and heating rates (h_0) employed. We began with the reaction network developed by Valdez and Savage [35] which was constructed from both traditional algal HTL reactions [31] as well as additional HTL reactions on the biocrude and aqueous-soluble products individually [35]. The results discussed in section 5.3.2 have significant implications on the structure of this reaction network, given the non-Arrhenius behavior of biocrude formation at short reaction times and rapid heating. Figure 5.7 illustrates a clear need for a solids-conversion pathway directly accounting for instantaneous heating rate, $\frac{dT}{dt}$. Moreover, it is well understood from literature that cellulose, a major component of cell walls, undergoes chemical transformations via hydrolysis in water at conditions relevant for HTL (240 - 310 ℃ [155], 290 - 400 ℃ [156], and 320 - 400 ℃ [157]).

To model these reaction pathways occurring in parallel, we introduce a new reaction intermediate, activated solids (S), that we theorize to represent both algal cells (C) that lysed by rapid heating (via the physical pathway) and algal cells whose cell walls chemically degraded by hydrolysis (via the chemical pathway) to the extent that the intracellular contents were exposed to the bulk high-temperature water. Figure 7.2 presents these new pre-treatment pathways in addition to the pathways established by Valdez and Savage [35] that lead to biocrude (B), aqueous-phase product (A), and gas (G) formation.

Similar to the network established by Valdez and Savage [35], we assumed each chemical reaction pathway in Figure 7.2 to be first-order following Arrhenius kinetics:

$$k_{ij}(t) = A_{ij} \exp\left(\frac{-E_{ij}}{RT(t)}\right) \tag{7.10}$$

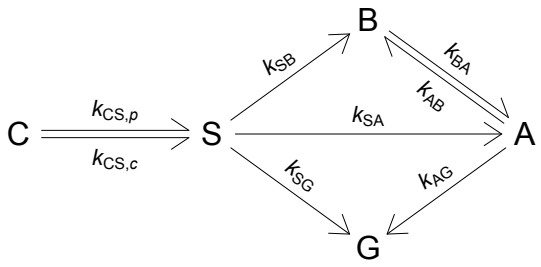

Figure 7.2: Reaction network for the HTL of *Nannochloropsis* sp. C, S, B, A, and G represent algal cells, activated solids, biocrude, aqueous-phase products, and gases, respectively.

Here, $k_{ij}(t)$ is the rate constant in 1/min, A_{ij} is the pre-exponential factor in 1/min, E_{ij} is the activation energy in kJ/mol, R is the gas constant in kJ/(mol K), and $T(t)$ is the time-dependent temperature. To model $k_{CS,p}$, the physical pathway that directly accounts for $\frac{dT}{dt}$, we tried adopting a modified version of the Arrhenius-based rate constant that replaces $-\frac{E_a}{RT}$ with $-\frac{B_{CS,p}}{{}^{dT}/_{dt}}$:

$$k_{CS,p}(t) = A_{CS,p} \exp\left(\frac{-B_{CS,p}}{{}^{dT}/_{dt}}\right) \tag{7.11}$$

We define $B_{CS,p}$ as a general constant with units ℃/min and ${}^{dT}/_{dt}$ is the instantaneous heating rate with units ℃/min. These rate coefficients along with the batch reactor design equation yield the following system of first-order ordinary differential equations (Equations (7.12) to (7.16)) with time-varying coefficients:

$$\frac{dx_C}{dt} = -(k_{CS,p} + k_{CS,c})x_C \tag{7.12}$$

$$\frac{dx_S}{dt} = (k_{CS,p} + k_{CS,c})x_C - (k_{SB} + k_{SA} + k_{SG})x_S \tag{7.13}$$

$$\frac{dx_B}{dt} = k_{SB}x_S + k_{AB}x_A - k_{BA}x_B \tag{7.14}$$

$$\frac{dx_A}{dt} = k_{SA}x_S + k_{BA}x_B - (k_{AB} + k_{AG})x_A \tag{7.15}$$

$$\frac{dx_G}{dt} = k_{SG}x_S + k_{AG}x_A \tag{7.16}$$

Using the temperature profiles and product yield data from each experiment, we calculated values for all kinetic parameters by simultaneously solving the system of first-order, ordinary differential equations in MATLAB® with the function `ode23s` and minimized the residual, calculated from eq. 7.17, with respect to those parameters using the function `lsqnonlin`. Here $\boldsymbol{p}$ is the array of kinetic parameters, n_e is the number of experiments, n_p is the number of products, and $Y_{i,j}^{obs}$ and $Y_{i,j}^{calc}$ are the measured and calculated yields of product j from experiment i, respectively.

$$r(\boldsymbol{p}) = \sum_{i}^{n_e} \sum_{j}^{n_p} (Y_{i,j}^{\text{obs}} - Y_{i,j}^{\text{calc}}(\boldsymbol{p})) \tag{7.17}$$

Table 7.1 contains the calculated parameters for the physical pathway from algal cells (C) to activated solids (S), and Table 7.2 displays all calculated Arrhenius parameters for the chemical reaction pathways.

Table 7.1: Model parameters for physical algal cells (C) → activated solids (S) pathway in Figure 7.2, with the form of Equation 7.11

Pathway	log(A) [log(s^{-1})]	B [°C min^{-1}]
C → S (p)	-0.5 ± 0.1	434 ± 30

Table 7.2: Arrhenius parameters for reaction pathways in Figure 7.2 with the form of Equation 7.10

Pathway	log(A) [log(s^{-1})]	Ea [kJ/mol]
C → S (c)	7.8 ± 0.5	99.6 ± 4.9
S → B	4.3 ± 0.5	46.8 ± 3.9
S → A	3.2 ± 0.3	37.5 ± 2.5
S → G	5.8 ± 0.5	63.9 ± 4.8
B → A	4.9 ± 0.7	98.6 ± 14.8
A → B	2.6 ± 1.4	71.1 ± 8.7
A → G	0.3 ± 0.1	55.6 ± 4.1

All activation energies for the chemical reaction pathways are greater than 37 kJ/mol, which is physically meaningful in that the chemical reactions described by these parameters do not result in significant conversion at room temperature. Some of the activation energies we calculated (namely for reactions of S → B, S → A, A

$\rightarrow$ G) are similar to those calculated by Valdez and Savage [35], but the activation energies for the reactions between biocrude and aqueous phase products (B $\rightarrow$ A and A $\rightarrow$ B) are far greater than those reported by Valdez and Savage (4.8 and 2.9 kJ/mol, respectively). The values reported by Valdez and Savage [35] would allow for significant reactions between these products, even at room temperature, which is inconsistent with physical intuition and control experiments.

For comparison, activation energies for the hydrolysis of amino acids in high-temperature water range from 46 - 191 kJ/mol [158]. Monoacylglyceride hydrolysis activation energies range from 75 - 105 kJ/mol, fatty acid hydrolysis activation energies range from 50 - 68 kJ/mol, and fatty acid ester hydrolysis activation energies range from 55 - 72 kJ/mol [158]. Reactions of carbohydrates (including cellulose, starch, and mono- and disaccharides) exhibit activation energies of 92 - 164 [158].

Figure 7.3 illustrates model-calculated yields (solid lines) alongside measured temperature profiles (red solid line) for four selected experiments, with points indicating the experimental product yields. These experiments were chosen such that they were representative of a typical model fit (and did not necessarily display an uncharacteristically good agreement between experimental and calculated yields); they also intentionally span roughly the entire range of conditions studied, with 60 s $< t_q <$ 60 min, $150 < T_q < 400$ ℃, and $123 < h_0 < 258$ ℃/min.

The calculated solutions demonstrated in Figure 7.3 display the ability of the model to accurately calculate yields for a variety of reaction conditions. These conditions span short (Figures 7.3a, 7.3c and 7.3d) and long (Figure 7.3b) t_q; low (Figures 7.3a and 7.3c) and high (Figures 7.3b and 7.3d) T_q; and slow (Figures 7.3a and 7.3b), moderate (Figure 7.3c), and fast (Figure 7.3d) h_0. Despite the large range of conditions explored, including a large range of conversions (or solids yields, Y_S), the model calculations match the experimentally observed yields remarkably well. The plots in Figure 7.3 are the first display of a model capable of calculating yields

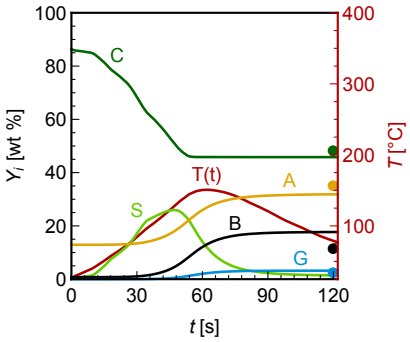

a Short t_q (61 s), low T_q (151 °C), slow h_0 (122 °C/min; T_{sp} = 300 °C)

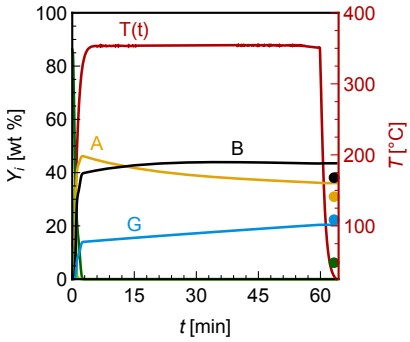

b Long t_q (60 min), high T_q (350 °C), slow h_0 (153 °C/min, T_{sp} = 350 °C)

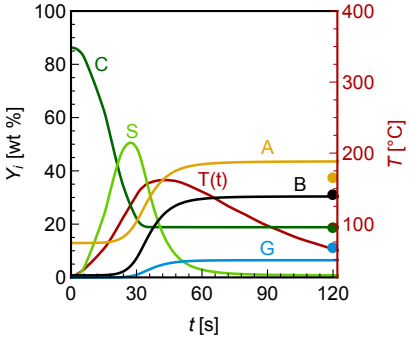

c Short t_q (44 s), low T_q (162 °C), moderate h_0 (186 °C/min, T_{sp} = 600 °C)

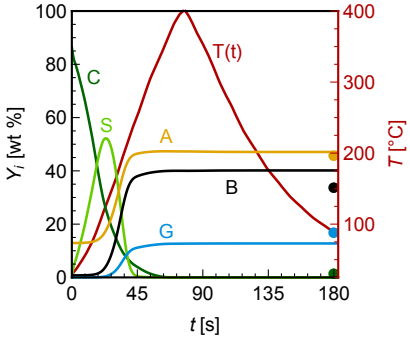

d Short t_q (77 s), high T_q (401 °C), fast h_0 (291 °C/min; T_{sp} = 550 °C)

Figure 7.3: Selected experimental product yields (circle), measured temperature profiles (red line), and model calculations (lines) for the HTL of *Nannochloropsis* sp. t_q, T_q, and h_0 values are experimentally observed values rather than typical values.

at isothermal HTL conditions (Fig. 7.3b, t_q = 60 min, T_q = 350 °C) as well as at fast HTL conditions (Figures 7.3a, 7.3c and 7.3d). Moreover, the model accurately calculates yields even at high solid yield, which presumably corresponds to low algal cell conversion (Figure 7.3a, Y_S^{obs} = 51 wt %).

Figure 7.4 depicts a parity plot of the observed and calculated yields from all reaction conditions examined. The dashed and dotted lines bordering the parity line represent one and two standard deviations (σ = 5.2 wt %), respectively. This standard deviation is approximately the same as our experimental error for replicate reactions conducted at T_q = 350 °C and t_q = 10 min (T_{sp} = 350 °C, data not shown), indicating

that the accuracy of the model is in line with our experimental uncertainty. The quality of the agreement between observed and calculated product yields throughout the entire range of reaction conditions, including both fast and isothermal HTL, is a testament to the robustness of our calculated kinetic parameters and revised reaction network.

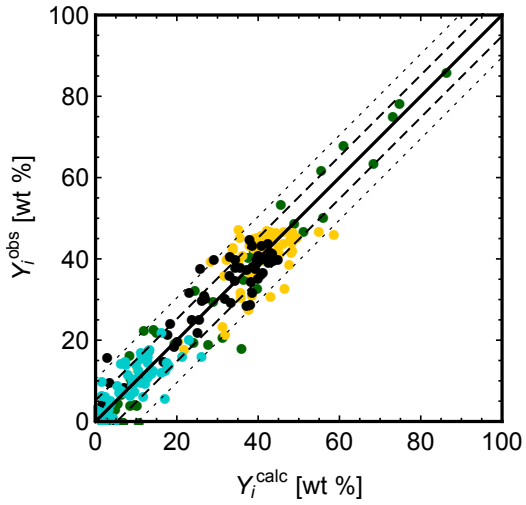

Figure 7.4: Parity plot of observed vs. calculated yields for total solids (algal cells + activated solids, green), aqueous-phase products (gold), biocrude (black), and gas (teal). Dashed and dotted lines represent one and two standard deviations (σ = 5.2 wt %), respectively.

7.3.3 Kinetic Model Implementation

With the establishment of a robust kinetic model, we now use it to improve our understanding of the underlying kinetics that govern microalgal HTL. Figure 7.5 depicts model-calculated product yields as functions of t and parametrized by typical temperature profiles resulting from several T_{sp} (labeled above each line). The dotted red arrows illustrate quench temperature isotherms, pointing in the direction of increasing h (and T_{sp}). We depict only the first 2 min of the profiles to highlight the HTL kinetics occurring over that timescale.

Figure 7.5a depicts the calculated yields of algal cells, Y_C^{calc}. For each temperature

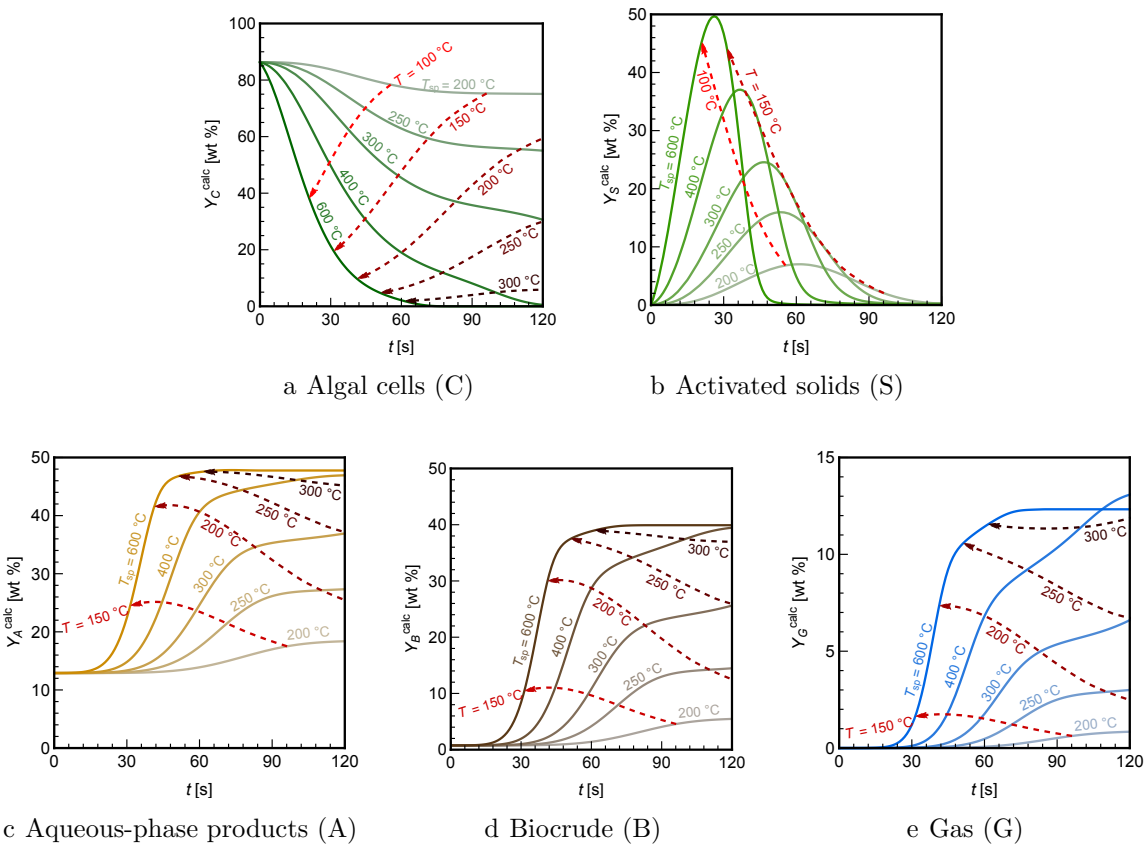

a Algal cells (C) b Activated solids (S)

c Aqueous-phase products (A) d Biocrude (B) e Gas (G)

Figure 7.5: Product yields as functions of reaction time. Solid lines represent yields from typical temperature profiles resulting from T_{sp} = 200, 250, 300, 400, and 600 ℃. Dashed red lines correspond to isotherms pointing in the direction of increasing heating rate.

profile (parametrized by T_{sp}), Y_C^{calc} decreases over time with increasing temperature. Y_C^{calc} also decreases monotonically with increasing heating rate (in the direction of the dashed arrows). For example, the 150 ℃ isotherm spans yields of about 80 wt % (t = 95 s, h_0 = 79 ℃/min, T_{sp} = 200 ℃) to about 20 wt % (t = 30 s, h_0 = 258 ℃/min, T_{sp} = 600 ℃). This sharp decrease in Y_C^{calc} with increasing h demonstrates the ability of the model to capture the phenomena seen in Figure 5.2, a direct result of the C → S (physical) pathway implemented in our reaction network.

Figure 7.5b illustrates the change in Y_S^{calc}, the model-calculated activated solids yields, over time. Only two quench temperature isotherms are depicted for clarity. This plot illustrates the role of the C → S (physical) pathway in our kinetic model.

The maximum Y_S^{calc} for each T_{sp} curve spans nearly an order of magnitude (6 - 50 wt%) as a function of h. The accumulation of activated solids creates the driving force for secondary reaction pathways to aqueous-phase products, biocrude, and gas. This allows the model to calculate product formation at lower temperatures, shorter times, and faster heating rates, which is consistent with experimental results presented in Figure 7.1. After 120 s, for all heating rates studied, the activated solids are essentially depleted, although this depletion time shortens with increasing h. After this depletion time, the activated solids reach pseudo-steady state, and converted algal cells immediately react to form secondary reaction products. This transition is coupled with increasing temperature, which renders the chemical pathways more readily accessible, leading to the reduced importance of the physical degradation pathway and a shift toward traditional reaction kinetics.

Figure 7.5c depicts the calculated yields of aqueous-phase products, Y_A^{calc}. All yield profiles exhibit a lag period before significant yield accumulation. The activation energy of the S $\rightarrow$ A pathway is high enough (E_a = 37.5 $\pm$ 2.5 kJ/mol) that the reaction rate (and consequently Y_A^{calc}) is appreciable only at elevated temperatures, which is consistent with experimental observations in Figure 7.1f. At a given t or nearly any given T, Y_A^{calc} increases monotonically with h. This trend is due to both the accumulation of activated solids (which increases with h) that drive the S $\rightarrow$ A reaction pathway and the increase of k_{SA}, the S $\rightarrow$ A rate constant, afforded by increasing temperature at an increasing rate (h). The exception to this general trend occurs at substantially high h_0 and low T, where Y_A^{calc} actually decreases slightly. Along the 150 ℃ isotherm, for example, Y_A^{calc} decreases slightly. Along the 150 ℃ isotherm, for example, Y_A^{calc} decreases slightly at h_0 >168 ℃/min (T_{sp} > 400 ℃). This optimum h_0 increases as T increases, to roughly 213 ℃/min (T_{sp} = 500 ℃) along the t_q = 200 ℃ isotherm, for instance.

Figure 7.5d shows Y_B^{calc}, the calculated biocrude yield, as a function of time. The

general trends for Y_B^{calc} are nearly identical to those of Y_A^{calc}. The 200 ℃ isotherm shows that Y_B^{calc} increases from about 14 wt % for $h_0 = 101$ ℃/min ($T_{sp} = 250$, $t =$ 110 s) to 30 wt % for $h_0 = 258$ ℃/min ($T_{sp} = 600$ ℃, $t = 38$ s). Thermodynamically speaking, both of these reaction conditions require the same amount of energy per unit mass because they reach the same temperature; however, the latter produces double the biocrude yield in about $^1/_3$ of the reaction time. Given a target throughput, the latter condition would also allow for smaller reactors and lower capital costs in flow systems. This type of comparison highlights the utility of this kinetic model to optimize processing conditions in terms of maximizing biocrude yield and minimizing energy requirements.

Figure 7.5e displays model-calculated gas yields, Y_G^{calc}, over time for several temperature profiles. Y_G^{calc} generally follows similar trends to Y_A^{calc} and Y_B^{calc}, although at $T_q > 250$ ℃ Y_G^{calc} decreases with increasing h_0. Collectively, all the product yield profiles depicted in Figure 7.5 capture the experimentally observed trend of increased Y_A, Y_B, and Y_G with increased heating rate.

Figure 7.6 demonstrates the effect of temperature and heating rate on the total rate constant, $k_{CS,T}$, of activated solids formation (top) and the relative contribution of the physical pathway, $k_{CS,p}/k_{CS,T}$ (bottom). At low temperatures (T $<$ 200 ℃), the physical pathway dominates, and the instantaneous heating rates entirely govern the overall rate. At intermediate temperatures (200 $\leq$ T $<$ 350 ℃), the relative contribution of the physical pathway is dependent on both heating rate and temperature. Finally, at high temperatures (T $\geq$ 350), the chemical pathway dominates, and the instantaneous temperature controls the overall rate.

Figure 7.7 depicts rate constants of pathway S $\rightarrow i$ relative to the total rate of disappearance of activated solids, $k_{Si}/k_{S,T}$, where $k_{S,T} = k_{SA} + k_{SB} + k_{SG}$, with respect to temperature. The selectivity of product formation from activated solids changes substantially with reaction temperature. The conversion of activated solids is most

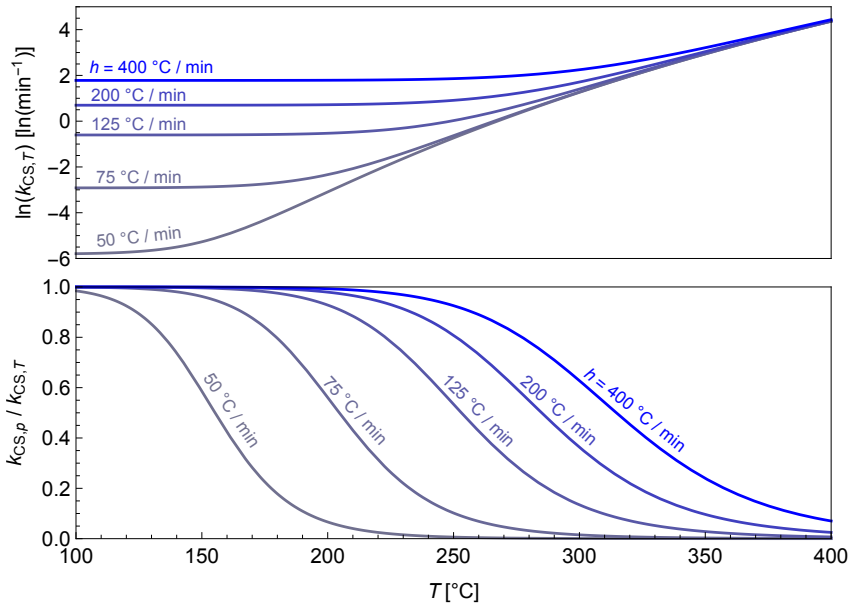

Figure 7.6: Plot of total algal cells (C) $\rightarrow$ activated solids (S) rate constant, $k_{CS,T} = k_{CS,c} + k_{CS,p}$, and fractional contribution of physical pathway, $k_{CS,p}/k_{CS,T}$, with respect to temperature and parametrized by heating rate.

selective toward the production of aqueous phase, biocrude, and gas over temperatures of $T < 150$ ℃, $150 \leq T < 340$ ℃, and $T \geq 340$ ℃, respectively. Selectivity to biocrude formation is greatest at 208 ℃, while the selectivity to aqueous-phase products decreases with increasing temperature. Selectivity to gaseous product formation increases monotonically with increasing temperature. Although the selectivity of the secondary reaction products changes with respect to temperature, the total rate of conversion, $k_{S,T}$, increases by three orders of magnitude with increasing temperature in the range $100 \leq T \leq 400$ ℃.

7.4 Conclusions

The experimental results presented in Chapter V and the present chapter comprise the most comprehensive study of temperature, reaction time, and heating rate effects on algal HTL product yields to date. By examining such a broad range of HTL reaction conditions, we also provide the first true demonstration of algal HTL

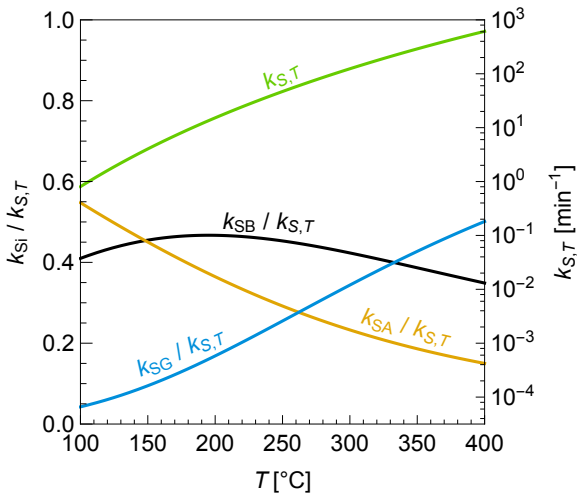

Figure 7.7: Plot of rate constants (k_{Si}) of secondary reaction pathway activated solids (S) $\rightarrow$ product i normalized by the overall rate of disappearance of S, $k_{S,T} = k_{SB} + k_{SA} + k_{SG}$, with respect to temperature. Yellow - aqueous phase (A), black - biocrude (B), blue - gas (G).

kinetics at low conversion, as previous efforts were limited to long reaction times. The dependence of biocrude yields on heating rate first explored by Faeth et al. [33] was confirmed by these results. Even at temperatures < 200 °C, we observed appreciable biocrude production, a result previously absent in the literature, to the best of our knowledge (Figure 7.3).

We accounted for these experimentally-observed phenomena by introducing activated solids (S) as a reaction intermediate and a "physical" pre-treatment pathway ($k_{CS,p}$, eq. 7.11) that directly incorporated the instantaneous heating rate ($\frac{dT}{dt}$), in addition to a traditional chemical kinetics pre-treatment pathway. These pathways, along with the addition of an activated solid to gas reaction pathway, led to a revised reaction network (Figure 7.2) adapted from the network posited by Valdez and Savage that served as the basis for the kinetic modeling in the present work [35].

We calculated physically meaningful kinetic parameters for all pathways (Tables 7.1 and 7.2). Product yields calculated using these kinetic parameters accurately describe the trends observed experimentally, throughout the entire range of reaction conditions (Figure 7.4), with a standard deviation of 5.2 wt %. The model accurately

captures the experimentally observed trend of increasing biocrude, aqueous-phase, and gas product formation with increasing heating rate, even at equivalent quench temperatures (Figure 7.3). This is the first kinetic model to accurately correlate calculated and experimental product yields from HTL for such a broad range of reaction times, quench temperatures, and heating rates. Such a model presents a clear opportunity for process optimization, especially to maximize biocrude yields while minimizing energy input.

CHAPTER VIII

Conclusions and Recommendations for Future Research

8.1 Conclusions

In this dissertation, we described the development of fast HTL (a variation on the HTL biomass conversion process), established the robustness of fast HTL through reactions of microbial biomass, and examined fast HTL processing conditions. Additionally, we explored molecular characterization of HTL products and developed a kinetic model that describes both fast and isothermal HTL.

In Chapter II, we examined short reaction times and high heating rates for HTL, leading to the development of a variant we term fast HTL. We obtained biocrude yields comparable to or greater than those observed after isothermal HTL, and results indicated that heating rate may contribute to this increase in biocrude yield. We compared biocrude yields from fast and isothermal HTL of different microorganisms (including other algae species, as well as bacteria and yeast) in Chapters III and IV. For all organisms examined, except the Gram-positive bacteria *B. subtilis* and the microalga *Neochloris oleoabundans*, biocrude yields from fast HTL were equivalent to or higher than those from isothermal HTL.

Also in Chapter III, we observed that biocrudes from fast HTL contain a greater

fraction of hexane-insoluble material than do the biocrudes from isothermal HTL, a trend that was consistent for all bacteria and yeast biomass examined. In a biorefinery, bacteria and/or yeast could be used to remove some of the organic C from the aqueous-phase product of algal HTL prior to recycling this aqueous phase for cultivation of additional microalgal biomass [66]. Remediation of the aqueous-phase product through bacterial growth could reduce the cost and land footprint of such a biorefinery [111].

In Chapter IV we examined the effects of reaction time, slurry solids content, and reactor loading and demonstrated that reaction time and reactor loading both affect biocrude yields, but the effect of changing the slurry solids content was minimal. To explain the observed increase in biocrude yield with decreasing reactor loading (or vol % water), we postulated that low reactor loadings facilitate an increase in the effective concentration of algal biomass in the liquid water. For reactions with low vol % water, more water (relatively) must vaporize to achieve saturation than would be required in a reactor with a high vol % water loading. To the best of our knowledge, this theory had not previously been introduced to the scientific community studying HTL. These results, along with those discussed in Chapters II and III, prompted the design of a comprehensive set of HTL experiments aimed at isolating and investigating the effects of reaction temperature, time, heating rate, and reactor loading.

This comprehensive study of reaction conditions (Chapter V) provided the first known demonstration of algal HTL at low algal cell conversion. We found that reactor loading effects are only relevant at short reaction times (≤ 3 min). Isolating the effects of heating rate by controlling the quench temperature (T_q), we directly confirmed the trend of increasing biocrude yield with increasing heating rate discussed previously (Chapter II). This trend led us to postulate that rapid heating induces pressure imbalances that facilitate cell rupture, a possible explanation for the observed trend in biocrude yield with increasing heating rate.

B. subtilis (a Gram-positive bacteria) is known to possess thick, peptidoglycan-based cell walls which may have prevented cell rupture at the heating rate examined in Chapter III, which could explain the observed low biocrude yield from fast HTL. It is possible that the *Neochloris oleoabundans* algae examined in Chapter IV also exhibit structural properties that prevented cell rupturing at the heating rates we were able to achieve experimentally. Even higher heating rates may be required to achieve the increases in biocrude from fast HTL of *B. subtilis* and *Neochloris oleoabundans* that we observed for several other microorganisms.

Elemental analysis and molecular characterization using FT-ICR MS revealed that biocrudes from fast HTL with low loading are of lesser quality than those from isothermal HTL or fast HTL with high loading due to differences in the recovery of heteroatoms to the biocrude (Chapter VI). However, fast HTL with low loading led to the highest biocrude yields, demonstrating a trade-off between biocrude quantity and quality. Such trade-offs indicate that there is a significant opportunity to optimize the HTL process. Compounds tentatively identified as herbicides were found in the aqueous-phase product, which provides a possible explanation for the toxicity of the aqueous phase from HTL and target compounds for genetically modified bacteria and/or algae to tolerate or metabolize.

The broad range of HTL reaction conditions examined in Chapter V generated a data set (including temperature profiles and product yields) that prompted modification to the reaction network previously described by Valdez and Savage [35]. To account for the observed increase in biocrude yield with increasing heating rate, we added two "activation" pathways, one describing chemical degradation of cell walls (e.g. hydrolysis) and the other the physical rupturing of algal cells resulting from rapid heating (Chapter VII). The kinetic parameters we calculated using this reaction network constitute the first known model to accurately correlate calculated and experimentally observed product yields from HTL of *Nannochloropsis* sp. across a

wide range of reaction conditions and algal cell conversions. Further, this model captures the increase in biocrude yields with increasing heating rates, supporting the idea that fast HTL cannot adequately be described solely by traditional reaction kinetics.

In addition to these intellectual merits, several students (many of whom can be considered historically underrepresented minorities in science, technology, engineering and math (STEM) fields) advanced in their professional development. Through outreach activities with elementary, middle, and high school students, the training and research efforts of undergraduate research assistants, and collaborations between graduate students, many individuals gained exposure to (and/or education in) chemical engineering. Such efforts are extremely important to the proliferation of STEM disciplines in the United States.

8.2 Recommendations for Future Research

The body of work described in this dissertation contributes meaningfully to the HTL literature. However, there is still much to be learned about fast HTL and the mechanism by which this HTL process variation produces biocrudes at comparable or higher yields than isothermal HTL, in a fraction of the time. Further, significant challenges exist in the upstream (algae cultivation and harvesting) and downstream (biocrude production, upgrading, and partitioning into fungible fuel products) operations for an algal biofuel process [159, 160]. In the following paragraphs, we first describe broad areas of research required for algal HTL to become a relevant biofuel production process, followed by recommendations for research directly related to HTL.

8.2.1 Broad Challenges for Biofuel Production via Hydrothermal Liquefaction

Figure 8.1 depicts the various process flows in a conceptual biorefinery design. There are multiple steps required to produce biofuels from algae, each of them with unique challenges. Sources of nutrients (especially N and P) for algae cultivation on a large scale present their own challenges, as easily-accessible sources of these essential elements are finite and are energy-intensive to convert to bio-available forms [159, 160]. Moreover, the sources of the nutrients for algae cultivation can impact the life cycle greenhouse gas emissions of the entire biofuel production process [159, 161]. Genetically engineering algae for expression of desirable traits, such as high lipid content or biomass productivity, can impact the life cycle greenhouse gas emissions of algal biofuel production processes [161]. Open ponds and closed photo-bioreactors may be used to cultivate algae, although further research and/or techno-economic analysis is needed to determine the cultivation system best suited for a particular biorefinery [160].

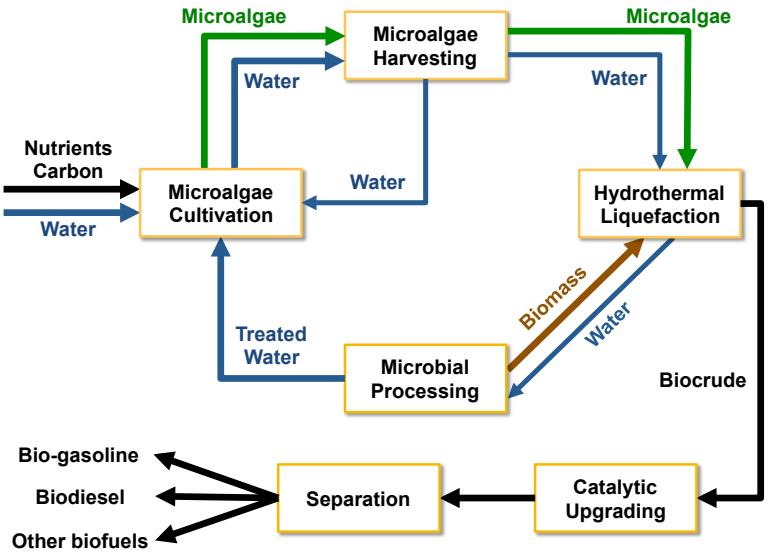

Figure 8.1: Schematic diagram of a biorefinery concept

Due to the size of microalgal cells and dilute nature of microalgal cultures, concentrating algal biomass for processing via HTL is necessary for commercial viability [8]. Different methods are available (i.e. flocculation, centrifugation, filtration) [159], but additional research could improve the efficiency of the harvesting stage in a biorefinery process. Pumping concentrated slurries is not a problem at large scales (flow rate $\geq$ 100 kg/h), though it can be challenging at bench- and pilot plant-scales [8], which are critical to the research and development of continuous HTL processes.

Recycling the aqueous-phase products from HTL is important for many reasons. As mentioned previously, the nutrients for algae cultivation are finite resources and are energy-intensive to produce, so recovery and recycling of said nutrients is of great importance. Moreover, the release of such nutrients into the environment could "feed" algal blooms in large bodies of water like Lake Erie and the Gulf of Mexico, which can subsequently cause hypoxic conditions and threaten other aquatic life [162]. However, we tentatively identified known herbicides in the aqueous-phase products from HTL (in Chapter VI) which could inhibit direct recycling of the concentrated aqueous-phase products directly to an algae pond or photobioreactor (although such compounds would not likely affect algal blooms as the toxins would be diluted by the large volume of water present). Treatment of this aqueous phase with bacteria or yeast, which are relatively easy to genetically engineer because such organisms are already used in many industrial processes [81–86], could mitigate the toxic effects of the concentrated aqueous phase from HTL.

The biocrude from HTL requires upgrading prior to use as a fuel product given that heteroatoms (especially O, N, and S) are abundant in biocrudes compared to petroleum crudes [19, 33, 40, 42]. Deoxygenation, denitrogenation, and desulfurization reactions are all necessary steps for commercialization, each likely requiring a different upgrading step. The upgrading of petroleum crude is well-studied and can serve as a starting point for research on removing heteroatoms from the biocrude

product of HTL.

8.2.2 Challenges Specific to Hydrothermal Liquefaction

Throughout this dissertation, we reported that heating rate has a significant effect on biocrude production during HTL and proposed that cell rupturing due to heating-induced pressure gradients may explain these observations. Chemical hydrolysis of cellulose, a major component of cell walls, is known to occur in water at conditions relevant for HTL (240 - 400 ℃ [155–157]) and the concept of cells lysing as a result of pressure imbalances is well understood [163, 164]. Therefore, cell rupturing due to rapid heating is a plausible explanation for the observed trend in biocrude yields. However, to the best of our knowledge, there is no direct evidence to support this claim. Further investigation of this hypothesis through microscopic imaging and/or HTL of cells that have been disrupted using sonication (to control for the non-homogeneity associated with intact cell walls, which prevent cell contents from interacting with the bulk reaction environment) would support or refute this claim. If our cell-rupturing theory can be verified, additional research into this phenomenon is warranted. Specific topics for such research could include investigating the effects of cell size and/or cell wall tensile strength and identifying characteristic heating rates required for cell rupture in different microorganisms.

The kinetic model we developed in Chapter VII accurately correlates the calculated and observed product yields for a given reaction time and quench temperature, but it lacks the level of detail necessary to estimate product quality, which we found to vary significantly with reaction conditions (in Chapter VI). The model is also restricted to describing product yields for a 15 wt % slurry of *Nannochloropsis* sp. algae at the maximum loading allowable by safety constraints, although we previously observed that reactor loading also affects product yields. Further refinement of the kinetic model to include the effects of loading, slurry solids content, and algal species

(or mixtures of several species of algae), and to simultaneously calculate product quality and quantity, would further inform possible future industrial implementation of an HTL process. These improvements would also enable process optimization to a greater extent than possible with the kinetic model discussed in this dissertation.

Although significant obstacles must be addressed prior to successful implementation of an industrial-scale algal biorefinery, the research included in this dissertation addressed several aspects of the HTL step in a biofuel production process. This body of work, along with the additional research proposed here, may help establish HTL as a viable algal biofuel production process that could, along with other biofuel processes, improve the sustainability of fuels used for transportation.

APPENDICES

APPENDIX A

Supplementary Information for Chapter II

This appendix contains reactor loadings (Table A.1), solid yields from fast HTL of *Nannochloropsis* sp. (Table A.2), and light and heavy biocrude composition (Table A.3), initially discussed in Chapter II.

Table A.1: Reactor loadings for fast HTL

Set-point Temp. (℃)	Holding Time (min)	Mass Algae Paste, 32.5 wt % Solids (g)	Mass Algae Solids (g)	Total Mass (g)	Weight % Algae Solids
300	1	0.6253 ± 0.0020	0.2032 ± 0.0006	1.3308 ± 0.0044	15.3
300	3	0.6249 ± 0.0008	0.2031 ± .0003	1.3291 ± 0.0035	15.3
300	5	0.6250 ± 0.0014	0.2031 ± 0.0005	1.3275 ± 0.0080	15.3
300	60	0.6247	0.2030	0.1903	15.5
350	1	0.5050 ± 0.0014	0.1641 ± 0.0005	1.0706 ± 0.0040	15.3
350	3	0.5060 ± 0.0009	0.1645 ± 0.0003	1.0726 ± 0.0032	15.3
350	5	0.5060 ± 0.0021	0.1645 ± 0.0007	1.0739 ± 0.0044	15.3
350	60	0.5075	0.1649	0.1546	15.4
400	1	0.4311 ± 0.0002	0.1401 ± 0.0001	0.9321 ± 0.0031	15.0
400	3	0.4317 ± 0.0004	0.1403 ± 0.0001	0.9354 ± 0.0021	15.0
400	5	0.4330 ± 0.0015	0.1407 ± 0.0005	0.9356 ± 0.0030	15.0
400	60	0.4345	0.1412	0.1324	15.1
450	1	0.2171 ± 0.0011	0.0705 ± 0.0004	0.4711 ± 0.0015	15.0
450	3	0.2171 ± 0.0015	0.0706 ± 0.0005	0.4695 ± 0.0026	15.0
450	5	0.2160 ± 0.0054	0.0702 ± 0.0002	0.4687 ± 0.0016	15.0
450	60	0.2183	0.0709	0.0665	14.9
500	1	0.1308 ± 0.0009	0.0425 ± 0.0003	0.2812 ± 0.0009	15.1
500	3	0.1306 ± 0.0006	0.0424 ± 0.0002	0.2806 ± 0.0008	15.1
500	5	0.1307 ± 0.0009	0.0425 ± 0.0003	0.2803 ± 0.0004	15.2
500	60	0.1323	0.0430	0.0403	15.3
550	1	0.1220 ± 0.0008	0.0396 ± 0.0003	0.2620 ± 0.0008	15.1
550	3	0.1218 ± 0.0008	0.0396 ± 0.0003	0.2617 ± 0.0006	15.1
550	5	0.1226 ± 0.0011	0.0399 ± 0.0004	0.2618 ± 0.0011	15.2
550	60	0.1206	0.0392	0.0367	15.1
600	1	0.1061 ± 0.0005	0.0345 ± 0.0002	0.2259 ± 0.0003	15.3
600	3	0.1051 ± 0.0012	0.0341 ± 0.0004	0.2245 ± 0.0020	15.2
600	5	0.1051 ± 0.0006	0.0342 ± 0.0002	0.2244 ± 0.0017	15.2
600	10	0.1044	0.0339	0.0318	15.0

Table A.2: Solid yields from fast HTL of *Nannochloropsis* sp.

Run	Set-point Temp. (℃)	Holding Time (min)	log(R_0)	Solids Yield (wt % dry basis)
0	25	0	N/A	N/A
1	300	1	0.806	61.9 ± 10.9
2	300	3	4.93	14.2 ± 1.1
3	300	5	5.91	6.2 ± 0.8
4	350	1	0.675	66.8 ± 9.9
5	350	3	6.19	5.6 ± 0.4
6	350	5	7.45	4.9 ± 0.3
7	400	1	0.680	34.5 ± 10.4
8	400	3	7.67	4.1 ± 0.1
9	400	5	8.60	3.7 ± 0.8
10	450	1	1.98	9.4 ± 2.2
11	450	3	8.80	2.3 ± 1.4
12	450	5	10.1	3.3 ± 0.7
13	500	1	3.16	6.7 ± 0.4
14	500	3	10.5	3.3 ± 1.8
15	500	5	11.4	1.7 ± 1.5
16	550	1	3.71	2.5 ± 0.5
17	550	3	11.5	1.4 ± 1.2
18	550	5	12.8	1 ± 0.9
19	600	1	5.14	6.2 ± 2.4
20	600	3	13.1	2.1 ± 1.3
21	600	5	14.4	3.7 ± 2.4
Note: Run numbers correspond to those in Table 2.1				

Table A.3: Elemental composition of light (LBC) and heavy biocrude (HBC)

Run	LBC C (wt %)	LBC H (wt %)	LBC N (wt %)	LBC S (wt %)	LBC O (wt %)	HBC C (wt %)	HBC H (wt %)	HBC N (wt %)	HBC S (wt %)	HBC O (wt %)
1	71.92	9.74	1.53	0.20	16.61	65.39	8.73	4.07	0.57	21.24
2	74.60	10.64	1.87	0.40	12.49	65.75	8.21	7.96	0.80	17.28
3	74.05	10.71	3.61	0.49	11.14	69.59	8.89	6.99	0.65	13.88
4	72.53	10.34	1.48	0.21	15.44	65.15	8.94	3.94	0.64	21.33
5	74.13	10.81	3.29	0.48	11.29	67.48	8.64	8.35	0.77	14.76
6	74.53	10.48	4.17	0.55	10.27	70.66	8.36	7.55	0.71	12.72
7	71.29	9.95	1.78	0.25	16.73	64.70	8.39	8.37	0.81	17.73
8	75.51	10.04	4.16	0.61	9.68	70.10	8.56	8.35	0.79	12.20
9	75.92	9.89	4.45	0.76	8.98	70.72	8.17	7.46	0.72	12.93
10	72.55	10.06	2.32	0.50	14.57	65.20	8.11	8.42	0.80	17.47
11	75.90	10.13	4.40	0.68	8.89	71.85	8.04	7.59	1.09	11.43
12	76.10	10.00	4.35	0.68	8.87	72.12	8.13	7.73	1.16	10.86
13	73.91	10.30	3.15	0.50	12.14	65.95	8.22	8.33	0.74	16.76
14	75.87	9.56	4.84	1.07	8.66	71.37	7.63	8.26	1.27	11.47
15	75.96	9.16	5.25	0.91	8.72	71.96	7.15	8.39	0.97	11.53
16	73.89	10.15	3.69	0.59	11.68	67.33	8.24	8.63	0.82	14.98
19	74.26	10.38	4.17	0.67	10.52	68.09	8.07	8.79	0.78	14.27
Note: Run numbers correspond to those in Table 2.1										

APPENDIX B

Supplementary Information for Chapter III

This appendix contains the light and heavy biocrude yields from fast and isothermal HTL of different microbial biomass (Table B.1), atomic ratios of the light and heavy biocrudes from fast and isothermal HTL of microbial biomass (Figures B.1 to B.4), C and N distribution among the different products of microbial HTL (Figures B.5 and B.6, respectively), and the elemental composition of the light and heavy biocrudes from fast and isothermal HTL of microbial biomass (Tables B.2 to B.6).

Table B.1: Yields of light and heavy biocrude product fractions (wt %, dry basis) for each biomass and fast and isothermal HTL

Organism	HTL	Light Biocrude (wt %)	Heavy Biocrude (wt %)
E. coli TB	Fast	5.9 ± 1.2	19 ± 5
	Isothermal	15 ± 1	9.3 ± 0.6
E. coli MM	Fast	5.8 ± 0.1	22 ± 2
	Isothermal	14 ± 1	16 ± 0
P. putida	Fast	8.5 ± 1.9	32 ± 6
	Isothermal	20 ± 1	11 ± 1
B. subtilis	Fast	0.76 ± 0.22	2.6 ± 0.6
	Isothermal	4.7 ± 1.4	10 ± 1
S. cerevisiae	Fast	19 ± 4	26 ± 3
	Isothermal	16 ± 2	16 ± 2

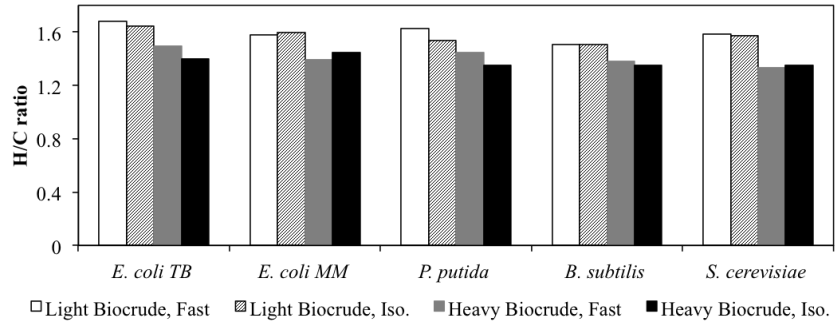

Figure B.1: H/C atomic ratio in the light and heavy biocrudes

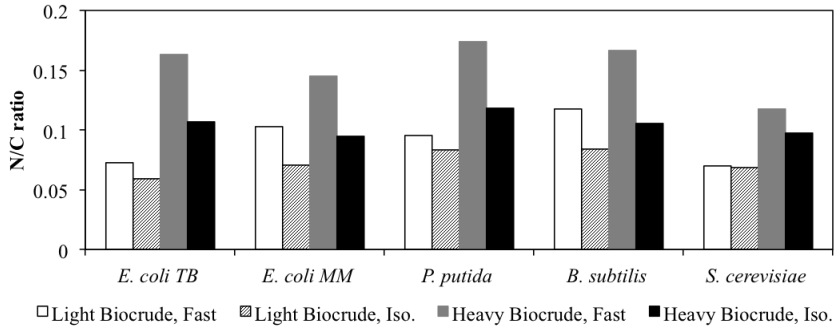

Figure B.2: N/C atomic ratio in the light and heavy biocrudes

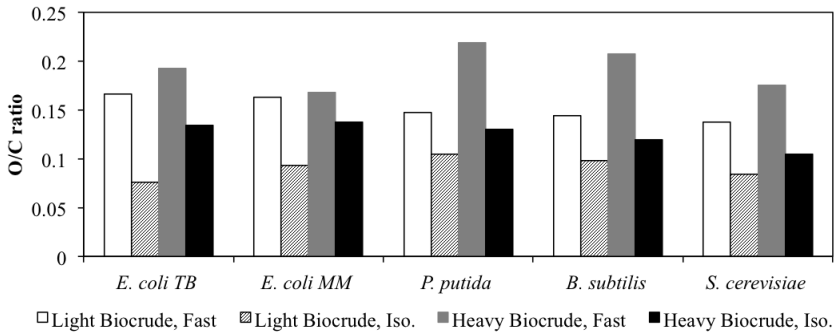

Figure B.3: O/C atomic ratio in the light and heavy biocrudes

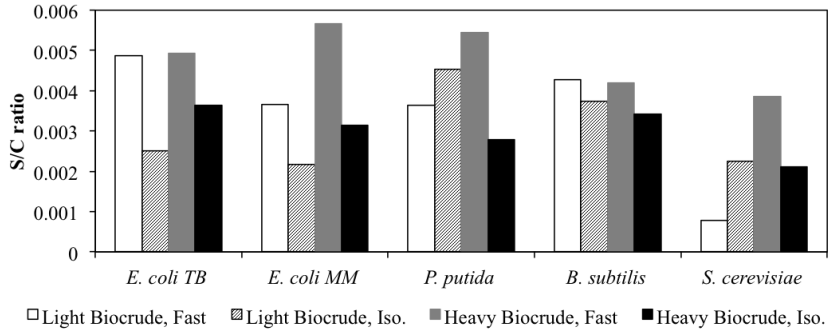

Figure B.4: S/C atomic ratio in the light and heavy biocrudes

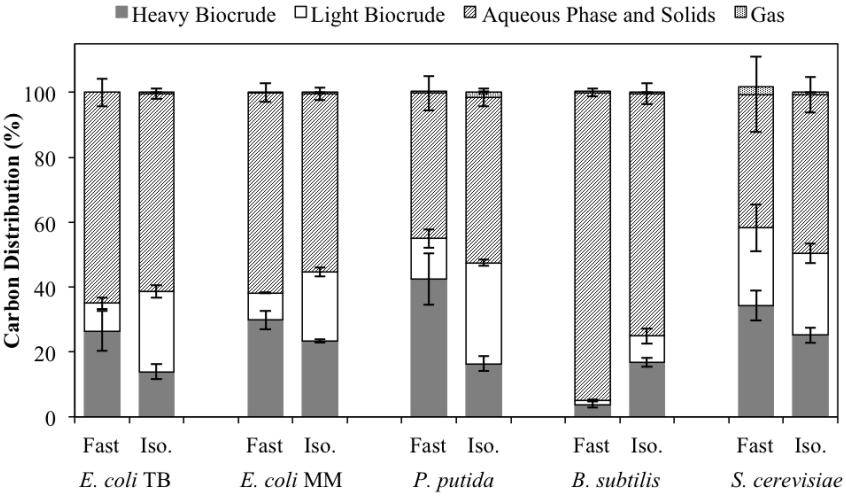

Figure B.5: Carbon distribution among the product fractions

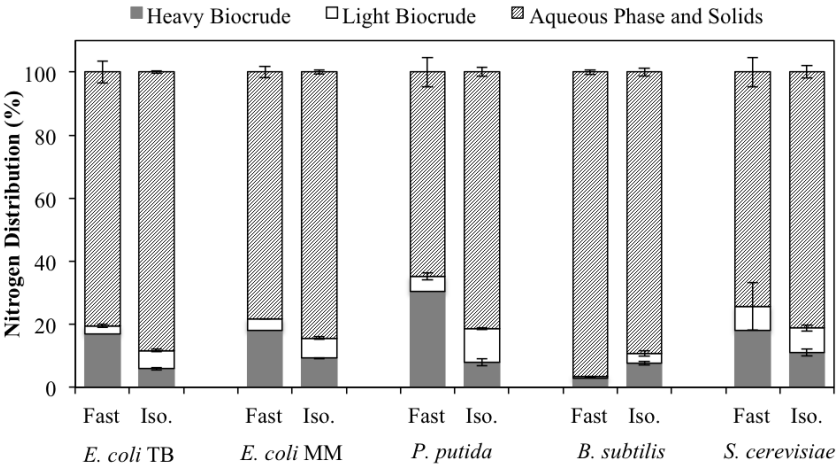

Figure B.6: Nitrogen distribution among the product fractions

Table B.2: Carbon content (wt %) of the light and heavy biocrudes

	Light Biocrude		Heavy Biocrude	
	Fast	Isothermal	Fast	Isothermal
E. coli TB	68.47	76.09	63.09	69.9
E. coli MM	67.64	74.27	65.56	70.28
P. putida	68.76	72.59	61.31	69.81
B. subtillus	68.18	73.28	62.58	71.18
S. cerevisiae	71.43	75.17	67	72.89

Table B.3: Nitrogen content (wt %) of the light and heavy biocrudes

	Light Biocrude		Heavy Biocrude	
	Fast	Isothermal	Fast	Isothermal
E. coli TB	5.82	5.24	11.99	8.7
E. coli MM	8.09	6.09	11.11	7.75
P. putida	7.63	7.07	12.45	9.61
B. subtillus	9.35	7.17	12.17	8.73
S. cerevisiae	5.85	6.01	9.19	8.26

Table B.4: Sulfur content (wt %) of the light and heavy biocrudes

	Light Biocrude		Heavy Biocrude	
	Fast	Isothermal	Fast	Isothermal
E. coli TB	0.89	0.51	0.83	0.68
E. coli MM	0.66	0.43	0.99	0.59
P. putida	0.67	0.88	0.89	0.52
B. subtillus	0.78	0.73	0.7	0.65
S. cerevisiae	0.15	0.45	0.69	0.41

Table B.5: Oxygen content (wt %) of the light and heavy biocrudes

	Light Biocrude		Heavy Biocrude	
	Fast	Isothermal	Fast	Isothermal
E. coli TB	15.15	7.67	16.18	12.53
E. coli MM	14.66	9.26	14.67	12.85
P. putida	13.54	10.09	17.9	12.13
B. subtillus	13.06	9.56	17.29	11.37
S. cerevisiae	13.06	8.46	15.62	10.18

Table B.6: Hydrogen content (wt %) of the light and heavy biocrudes

	Light Biocrude		Heavy Biocrude	
	Fast	Isothermal	Fast	Isothermal
E. coli TB	9.67	10.49	7.91	8.19
E. coli MM	8.95	9.95	7.67	8.53
P. putida	9.4	9.37	7.45	7.93
B. subtillus	8.63	9.26	7.26	8.07
S. cerevisiae	9.51	9.91	7.5	8.26

APPENDIX C

Supplementary Information for Chapter IV

This appendix contains reactor loadings for the experiments investigating the effects of algae species (Table C.1), reaction time (Table C.2), algae loadings at a fixed water loading (Table C.3), slurry loadings at a fixed slurry solids content (Table C.4), and water loadings at a fixed algae loading (Table C.5). The results of the HTL experiments with these reactor loadings were initially discussed in Chapter IV.

Table C.1: Reactor loadings for algae species experiments

		Neochloris	*Chlorella*	*Botryococcus*	*Nannochloropsis*
Fast HTL	Dry Algae (g)	0.0915 ± 0.0004	0.0917 ± 0.0004	0.0923 ± 0.0003	0.0899 ± 0.0001
	Water (g)	0.5031 ± 0.0001	0.5033 ± 0.0001	0.5030 ± 0.0000	0.5048 ± 0.0002
	% Solid in Slurry	15.39 ± 0.05	15.41 ± 0.06	15.5012 ± 0.04	15.11 ± 0.70
	Volume % Water	30.13 ± 0.00	30.14 ± 0.01	30.12 ± 0.00	30.23 ± 1.24
Isothermal HTL	Dry Algae (g)	0.1635 ± 0.0003	0.1645 ± 0.0006	0.1637 ± 0.0003	0.1649
	Water (g)	0.9144 ± 0.0000	0.9144 ± 0.0001	0.9145 ± 0.0000	0.9078
	% Solid in Slurry	15.17 ± 0.02	15.24 ± 0.05	15.18 ± 0.03	15.38
	Volume % Water	54.76 ± 0.00	54.76 ± 0.01	54.76 ± 0.00	54.36

Table C.2: Reactor loadings for reaction time experiments

Reaction Time (min)	Dry Algae (g)	Water (g)	% Solid in Slurry	Volume % Water
0.25	0.0317 ± 0.0007	0.1786 ± 0.0048	15.08 ± 0.09	10.69 ± 0.28
0.50	0.0337 ± 0.0007	0.1885 ± 0.0036	15.17 ± 0.02	11.29 ± 0.22
0.74	0.0348 ± 0.0002	0.1933 ± 0.0003	15.26 ± 0.04	11.57 ± 0.02
1.00	0.0340 ± 0.0003	0.1903 ± 0.0018	15.17 ± 0.04	11.40 ± 0.11
1.25	0.0339 ± 0.0008	0.1882 ± 0.0043	15.25 ± 0.07	11.27 ± 0.26
1.50	0.0336 ± 0.0006	0.1877 ± 0.004	15.19 ± 0.05	11.24 ± 0.24
1.75	0.0354 ± 0.0001	0.1946 ± 0.0002	15.41 ± 0.02	11.65 ± 0.01
2.00	0.0349 ± 0.0002	0.1934 ± 0.0004	15.28 ± 0.04	11.58 ± 0.02

Table C.3: Reactor loadings for fixed water loading experiments

	Low Loading (11.5 volume % water)		High Loading (30.2 volume % water)	
Solids Content (wt %)	Dry Algae (g)	Water (g)	Dry Algae (g)	Water (g)
5	0.0114 ± 0.0002	0.1936 ± 0.0005	0.0284 ± 0.0003	0.5068 ± 0.0006
7.5	0.0158 ± 0.0002	0.1915 ± 0.0004	0.041 ± 0.0004	0.5032 ± 0.0008
10	0.0215 ± 0.0002	0.1914 ± 0.0004	0.057 ± 0.0003	0.5050 ± 0.0006
15	0.0343 ± 0.0003	0.1921 ± 0.0006	0.0899 ± 0.0002	0.5048 ± 0.0004
20	0.048 ± 0.0002	0.1914 ± 0.0004	0.1257 ± 0.0003	0.5026 ± 0.0007
25	0.064 ± 0.0002	0.1915 ± 0.0004	0.1679 ± 0.0003	0.5034 ± 0.0005

Table C.4: Reactor loadings for a fixed slurry solids content and variable vol % water

Total Mass (g)	Dry Algae (g)	Water (g)	% Solid in Slurry	Volume % Water
0.2166	0.0329 ± 0.0004	0.1838 ± 0.0024	15.17 ± 0.03	11.00 ± 0.14
0.4481	0.0681 ± 0.0000	0.3800 ± 0.0016	15.21 ± 0.05	22.75 ± 0.10
0.6974	0.1067 ± 0.0002	0.5907 ± 0.0024	15.30 ± 0.07	35.37 ± 0.15
0.9464	0.1442 ± 0.0001	0.8022 ± 0.0014	15.24 ± 0.01	48.04 ± 0.08
1.1965	0.1822 ± 0.0000	1.0143 ± 0.0001	15.22 ± 0.00	60.74 ± 0.01

Table C.5: Reactor loadings for fixed algae solids loading experiments

Total Mass (g)	Dry Algae (g)	Water (g)	% Solid in Slurry	Volume % Water
0.1531	0.0309 ± 0.0002	0.1223 ± 0.0004	20.15 ± 0.05	7.32 ± 0.03
0.1835	0.0309 ± 0.0003	0.1526 ± 0.0006	16.84 ± 0.08	9.14 ± 0.04
0.2152	0.0326 ± 0.0006	0.1826 ± 0.0031	15.17 ± 0.04	10.93 ± 0.18
0.3349	0.0310 ± 0.0002	0.3039 ± 0.0005	9.25 ± 0.05	18.20 ± 0.03
0.4337	0.031 ± 0.0002	0.4027 ± 0.0016	7.14 ± 0.06	24.11 ± 0.10
0.6328	0.0311 ± 0.0001	0.6017 ± 0.0041	4.92 ± 0.03	36.03 ± 0.25

APPENDIX D

Supplementary Information for Chapter V

This appendix contains the reactor loadings and product yields for Chapter V. Table D.1 contains the loadings of the control experiments, and Tables D.2 and D.3 contain the loadings for HTL experiments with T_{sp} from 200 - 350 ℃ and from 400 - 600 ℃, respectively.

Table D.1: Chapter V control experiment loadings and yields

Set-point Temperature	Quench Time		Quench Temperature	Algae slurry mass	Total mass	Gas Yield	Solid Yield	Biocrude Yield	Dry Aqueous Yield	Wet Recovery
T_{sp} (℃)	t_q (min)	$+t_q$ (s)	T_q (℃)	m_{S0} (g)	m_T (g)	Y_G (wt %)	Y_S (wt %)	Y_B (wt %)	Y_{DA} [wt %]	Y_{WA} [wt %]
25	0	0	25	0.1423	0.3035	0.00%	32.57%	2.84%	5.03%	22.27%
25	0	0	25	0.1426	0.3042	0.00%	84.86%	1.53%	11.78%	44.90%
25	0	0	25	0.5884	1.2489	0.00%	40.76%	0.63%	10.84%	43.31%
25	0	0	25	0.5885	1.2437	0.00%	49.96%	0.32%	12.11%	46.23%

Table D.2: Chapter V experiment loadings for HTL with T_{sp} from 200 - 350 ℃

T_{sp} (℃)	t_q (min)	$+t_q$ (s)	T_q (℃)	Loading	m_{S0} (g)	m_T (g)	Y_G (wt%)	Y_S (wt%)	Y_B (wt%)	Y_{DA} (wt%)	Y_{WA} (wt%)
200	3	0	188	Low	0.1464	0.3128	0.00%	40.89%	7.33%	20.22%	42.10%
200	3	0	188	High	0.5882	1.2561	0.00%	50.22%	7.08%	26.27%	55.51%
200	7	0	200	Low	0.1476	0.3163	2.20%	50.25%	19.18%	27.11%	59.88%
200	7	0	200	High	0.5882	1.2559	1.11%	54.09%	12.11%	30.47%	65.52%
200	15	0	200	Low	0.1479	0.3171	2.20%	33.21%	22.22%	38.27%	72.60%
200	15	0	200	High	0.5884	1.2535	1.66%	37.60%	17.75%	37.32%	73.64%
200	40	0	200	Low	0.1479	0.3176	0.00%	30.57%	25.08%	38.27%	70.78%
200	40	0	200	High	0.5875	1.2547	1.66%	27.74%	23.04%	43.19%	74.17%
250	1	33	175	Low	0.145	0.309	12.87%	46.34%	15.02%	24.89%	63.30%
250	1	33	175	High	0.5878	1.254	3.18%	42.66%	12.12%	24.24%	64.39%
250	2	30	223	Low	0.1498	0.323	10.86%	34.53%	20.20%	33.66%	74.52%
250	2	30	223	High	0.5889	1.2565	0.00%	45.63%	16.74%	35.08%	78.23%
250	5	0	250	Low	0.1567	0.3315	11.91%	26.21%	25.61%	33.55%	74.21%
250	5	0	250	High	0.5885	1.2546	5.29%	24.42%	23.74%	39.38%	80.11%
250	20	0	250	Low	0.1564	0.3381	15.91%	9.55%	41.77%	38.79%	82.25%
250	20	0	250	High	0.5885	1.2517	11.63%	6.82%	33.04%	35.68%	81.60%
250	60	0	250	Low	0.1561	0.3355	20.84%	6.04%	43.77%	30.84%	79.85%
250	60	0	250	High	0.5882	1.2521	22.12%	5.59%	40.87%	34.68%	81.80%
300	0	58	150	Low	0.1426	0.3062	10.91%	30.76%	20.29%	28.14%	69.11%
300	0	58	150	High	0.5878	1.2526	4.23%	41.76%	3.49%	14.55%	39.96%
300	0	58	150	High	0.5882	1.2541	0.00%	46.49%	13.12%	27.03%	66.87%
300	1	27	200	Low	0.1478	0.3185	10.52%	38.73%	19.15%	25.05%	65.65%
300	1	27	200	High	0.5883	1.2516	3.70%	39.77%	18.35%	31.94%	80.85%
300	2	6	250	Low	0.1541	0.3349	8.08%	18.17%	35.53%	33.92%	77.37%
300	2	6	250	High	0.588	1.2559	6.35%	30.05%	26.14%	32.43%	70.79%
300	3	30	289	Low	0.1688	0.363	5.53%	9.58%	39.26%	29.86%	77.25%
300	3	30	289	High	0.5887	1.2528	17.44%	10.15%	39.32%	33.77%	83.82%
300	8	30	300	Low	0.1745	0.3748	26.74%	5.88%	45.10%	30.66%	86.74%
300	8	30	300	High	0.5876	1.2549	11.12%	6.51%	42.36%	32.72%	90.84%
300	15	0	300	Low	0.1755	0.3755	12.41%	10.10%	43.43%	21.45%	72.73%
300	15	0	300	High	0.5884	1.2539	11.10%	5.08%	43.04%	28.18%	89.56%
300	40	0	300	Low	0.1758	0.3704	12.39%	9.20%	45.48%	17.70%	74.35%
300	40	0	300	High	0.5883	1.2609	13.22%	10.68%	37.86%	22.63%	87.59%
350	0	30	100	Low	0.1423	0.3031	9.14%	53.50%	9.83%	21.72%	47.01%
350	0	30	100	High	0.5882	1.2556	1.66%	40.60%	1.83%	11.84%	37.56%
350	0	40	125	Low	0.1428	0.3044	17.43%	27.23%	25.05%	35.29%	77.73%
350	0	40	125	High	0.5888	1.2512	2.64%	35.51%	2.85%	12.94%	46.56%
350	1	11	200	Low	0.1468	0.3164	10.60%	29.03%	29.67%	33.06%	72.12%
350	1	11	200	High	0.5877	1.2534	9.53%	35.94%	26.73%	39.07%	77.50%
350	1	24	225	Low	0.1507	0.3231	4.13%	26.22%	29.31%	36.54%	76.91%
350	1	24	225	High	0.5868	1.2535	5.83%	24.12%	26.99%	39.55%	84.16%
350	2	15	300	Low	0.1758	0.3759	5.31%	4.25%	34.51%	29.02%	78.93%
350	2	15	300	High	0.5886	1.2509	13.21%	9.67%	37.21%	35.31%	81.54%
350	4	30	347	Low	0.2183	0.4683	8.55%	2.99%	47.74%	22.37%	80.20%
350	4	30	347	High	0.5032	1.0744	17.93%	4.45%	41.98%	22.87%	85.68%
350	7	0	350	Low	0.2196	0.4668	17.00%	3.40%	46.18%	18.42%	75.56%
350	7	0	350	High	0.5048	1.0738	6.16%	5.48%	40.00%	17.50%	73.51%
350	9	30	350	Low	0.2153	0.4589	7.22%	4.19%	41.33%	15.46%	71.74%
350	9	30	350	High	0.513	1.0989	7.28%	4.18%	43.48%	18.80%	89.13%
350	25	0	350	Low	0.2199	0.4673	16.98%	3.40%	41.03%	12.59%	77.34%
350	25	0	350	High	0.5042	1.0733	25.91%	3.15%	42.39%	11.54%	73.87%
350	60	0	350	Low	0.2199	0.4673	21.22%	1.41%	41.73%	11.03%	74.06%
350	60	0	350	High	0.5042	1.0774	23.87%	6.77%	38.58%	11.68%	81.30%

Table D.3: Chapter V experiment loadings for HTL with T_{sp} from 400 - 600 ℃

T_{sp} (℃)	t_q (min)	$+t_q$ (s)	T_q (℃)	Loading	m_{S0} (g)	m_T (g)	Y_G (wt%)	Y_S (wt%)	Y_B (wt%)	Y_{DA} (wt%)	Y_{WA} (wt%)
400	0	42	150	Low	0.1454	0.3098	14.98%	23.11%	32.09%	28.24%	68.08%
400	0	42	150	High	0.5881	1.2561	3.70%	28.99%	25.50%	41.42%	88.44%
400	1	20	250	Low	0.1568	0.337	11.90%	4.36%	44.24%	27.78%	78.40%
400	1	20	250	High	0.5881	1.2471	11.11%	10.95%	38.25%	38.30%	87.32%
400	2	23	350	Low	0.2193	0.4659	9.93%	4.68%	45.25%	20.29%	82.42%
400	2	23	350	High	0.5011	1.0715	20.49%	6.70%	39.98%	16.64%	77.11%
400	3	30	384	Low	0.3003	0.639	13.47%	4.97%	44.13%	15.33%	78.47%
400	3	30	384	High	0.502	1.0658	9.92%	3.84%	44.87%	18.28%	91.94%
400	6	0	400	Low	0.3004	0.6394	16.57%	6.32%	42.56%	12.53%	75.49%
400	6	0	400	High	0.4626	0.9845	7.40%	3.36%	39.61%	13.52%	75.76%
400	8	30	400	Low	0.3	0.6371	14.52%	2.70%	43.76%	11.72%	77.74%
400	8	30	400	High	0.4623	0.9841	12.79%	3.77%	42.60%	9.82%	81.15%
400	15	0	400	Low	0.3001	0.6344	18.66%	3.84%	38.98%	11.51%	80.88%
400	15	0	400	High	0.4622	0.9909	12.79%	3.37%	35.61%	8.75%	72.30%
400	40	0	400	Low	0.3	0.6408	16.59%	2.18%	40.65%	10.47%	72.19%
400	40	0	400	High	0.4619	0.984	16.16%	2.56%	33.00%	10.30%	82.51%
450	0	23	100	Low	0.1426	0.3063	15.97%	25.55%	29.89%	36.27%	74.47%
450	0	23	100	High	0.589	1.256	2.21%	38.99%	19.39%	33.69%	74.19%
450	0	30	125	Low	0.1429	0.3081	34.83%	16.33%	29.61%	33.96%	80.23%
450	0	30	125	High	0.5879	1.2549	0.53%	41.96%	20.11%	31.80%	77.65%
450	0	46	175	Low	0.1454	0.3118	13.42%	22.37%	32.67%	35.35%	80.60%
450	0	46	175	High	0.5875	1.2552	42.08%	14.29%	38.10%	35.38%	84.80%
450	0	53	200	Low	0.1478	0.3178	15.41%	2.42%	45.34%	33.02%	83.67%
450	0	53	200	High	0.5881	1.2568	8.85%	15.05%	33.30%	39.11%	81.62%
450	1	28	300	Low	0.1755	0.3769	30.13%	1.77%	38.29%	15.78%	75.70%
450	1	28	300	High	0.5881	1.2513	7.93%	4.81%	38.62%	19.94%	76.45%
450	2	30	400	Low	0.3005	0.64	17.60%	2.48%	40.79%	13.04%	79.69%
450	2	30	400	High	0.4286	0.9152	13.79%	2.54%	40.65%	15.46%	84.52%
500	0	33	150	Low	0.1431	0.3075	22.73%	34.56%	33.42%	32.74%	77.11%
500	0	33	150	High	0.5877	1.2564	17.71%	11.90%	37.20%	34.82%	85.24%
500	0	48	200	Low	0.147	0.3174	26.56%	8.41%	53.34%	21.69%	81.29%
500	0	48	200	High	0.5876	1.2547	9.97%	6.37%	40.69%	29.23%	83.18%
500	1	1	250	Low	0.1561	0.3349	7.97%	24.71%	31.09%	39.06%	76.92%
500	1	1	250	High	0.588	1.255	12.17%	8.84%	39.95%	34.02%	80.75%
500	1	35	350	Low	0.2188	0.4675	18.48%	3.55%	42.23%	16.78%	81.35%
500	1	35	350	High	0.5037	1.0773	16.06%	4.88%	43.73%	12.78%	75.95%
550	0	24	125	Low	0.1424	0.3059	13.71%	9.60%	49.35%	33.13%	82.18%
550	0	24	125	High	0.5876	1.2565	3.32%	36.43%	25.14%	35.05%	75.48%
550	0	37	175	Low	0.1452	0.3111	12.86%	7.07%	45.42%	19.93%	70.78%
550	0	37	175	High	0.587	1.2546	6.89%	8.37%	38.53%	32.12%	82.70%
550	0	42	200	Low	0.1479	0.3178	31.55%	5.89%	49.85%	18.93%	71.08%
550	0	42	200	High	0.5883	1.2529	8.99%	8.62%	34.32%	20.62%	80.87%
550	0	56	250	Low	0.1568	0.3375	22.82%	2.90%	42.33%	18.47%	80.09%
550	0	56	250	High	0.588	1.253	12.70%	8.52%	34.34%	20.26%	72.34%
550	1	9	300	Low	0.1745	0.3724	41.00%	3.57%	37.44%	12.12%	67.21%
550	1	9	300	High	0.5672	1.2005	13.71%	4.22%	39.82%	11.30%	80.81%
550	1	41	400	Low	0.3005	0.6417	37.27%	2.17%	29.61%	12.11%	79.55%
550	1	41	400	High	0.3087	0.6618	17.13%	2.02%	34.36%	11.59%	78.20%
600	0	17	100	Low	0.1429	0.3057	15.94%	38.25%	22.99%	30.05%	69.74%
600	0	17	100	High	0.588	1.2552	4.98%	55.77%	1.66%	15.55%	43.04%
600	0	27	150	Low	0.1431	0.3074	13.04%	11.09%	51.96%	30.87%	76.90%
600	0	27	150	High	0.5879	1.2539	11.64%	19.42%	31.80%	37.94%	81.25%
600	0	45	225	Low	0.1514	0.324	12.89%	7.95%	56.08%	25.36%	81.39%
600	0	45	225	High	0.5881	1.2555	9.40%	6.31%	41.16%	24.17%	78.04%
600	0	50	250	Low	0.1558	0.335	16.70%	2.30%	41.55%	18.58%	74.72%
600	0	50	250	High	0.5887	1.2548	10.50%	4.20%	25.75%	10.22%	54.85%
600	1	15	350	Low	0.2193	0.467	17.02%	1.56%	36.46%	11.63%	71.16%
600	1	15	350	High	0.4207	0.8978	14.05%	1.77%	29.14%	10.13%	81.94%

APPENDIX E

Supplementary Information for Chapter VI

This appendix contains the loadings for the HTL reactions for Chapter VI (Table E.1) and the elemental recoveries to the aqueous-phase and biocrude products (Figures E.1 and E.2). Details about the percentage of assigned peaks in the FT-ICR MS broadband spectra are included here (Table E.2), along with the broadband spectra that were not included in the text of Chapter VI (Figures E.3 to E.5). We also include the relative abundances of compounds over a variety of C numbers (Figures E.6 and E.7) heteroatom densities (Figure E.8 and E.9), and distributions of specific heteroatoms over a range of C numbers or molecular weights (Figures E.10 to E.12).

Table E.1: Reactor loadings for HTL experiments

	Fast, Low Loading	Fast, High Loading	Isothermal
Dried Algae (g)	0.0835 ± 0.0001	0.4997 ± 0.0002	0.4979 ± 0.0001
Total Water (g)	0.4705 ± 0.0003	2.7768 ± 0.0005	2.7732 ± 0.0002

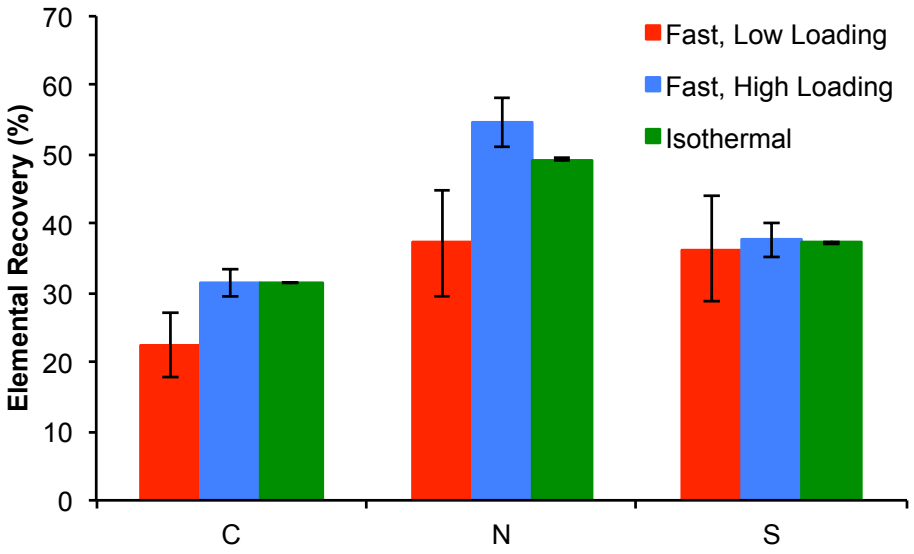

Figure E.1: Recovery of C, N and S in the aqueous phase from HTL at different conditions

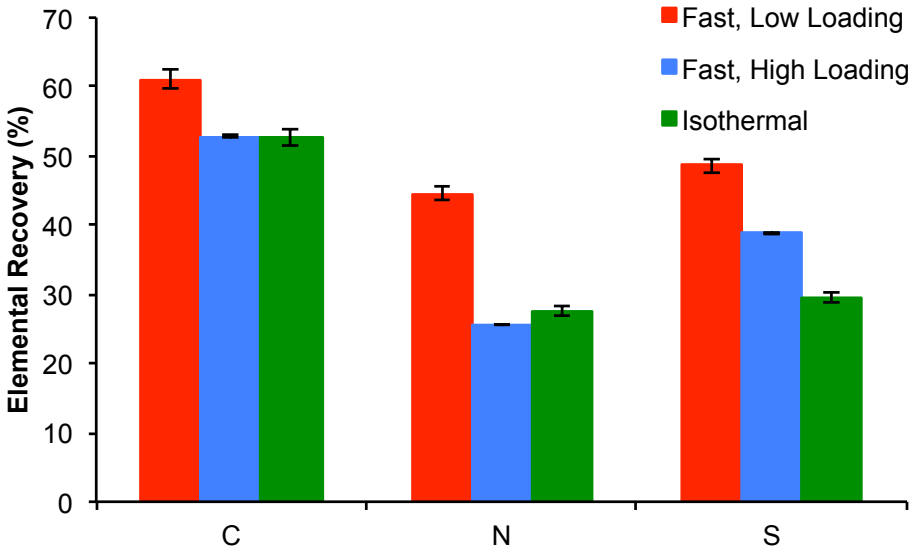

Figure E.2: Recovery of C, N, and S in the biocrude from HTL at different conditions

Table E.2: Percentage of peaks with assigned molecular formulae for each sample using each ionization method

Sample	Positive ESI	Negative ESI
Fast, Low Loading - Aqueous	88.7%	69.5%
Fast, High Loading - Aqueous	79.2%	83.8%
Isothermal - Aqueous	93.3%	60.9%
Fast, Low Loading - Biocrude	88.6%	94.4%
Fast, High Loading - Biocrude	90.2%	90.0%
Isothermal - Biocrude	95.0%	92.1%

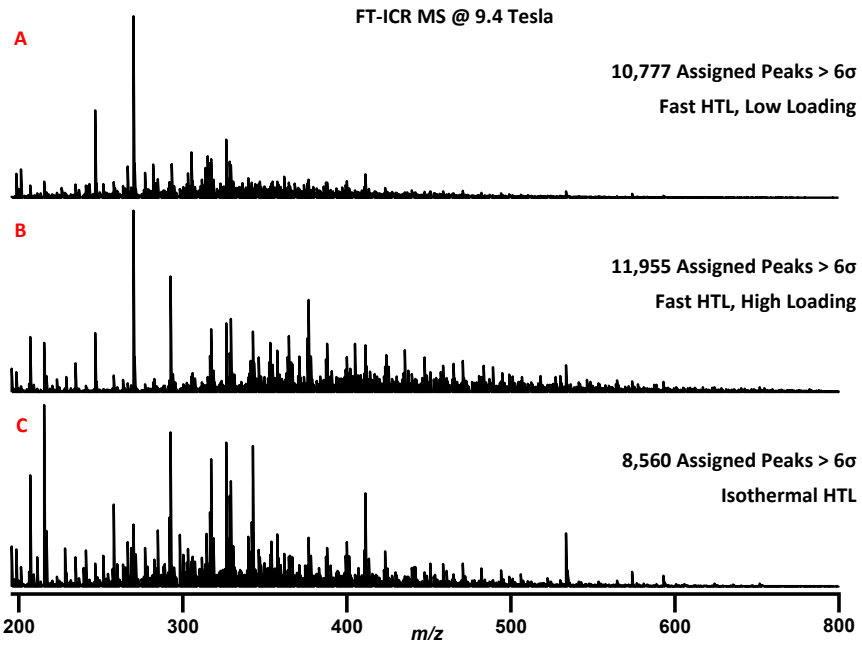

Figure E.3: Negative ESI FT-ICR MS broadband spectra of aqueous-phase samples for HTL at different conditions

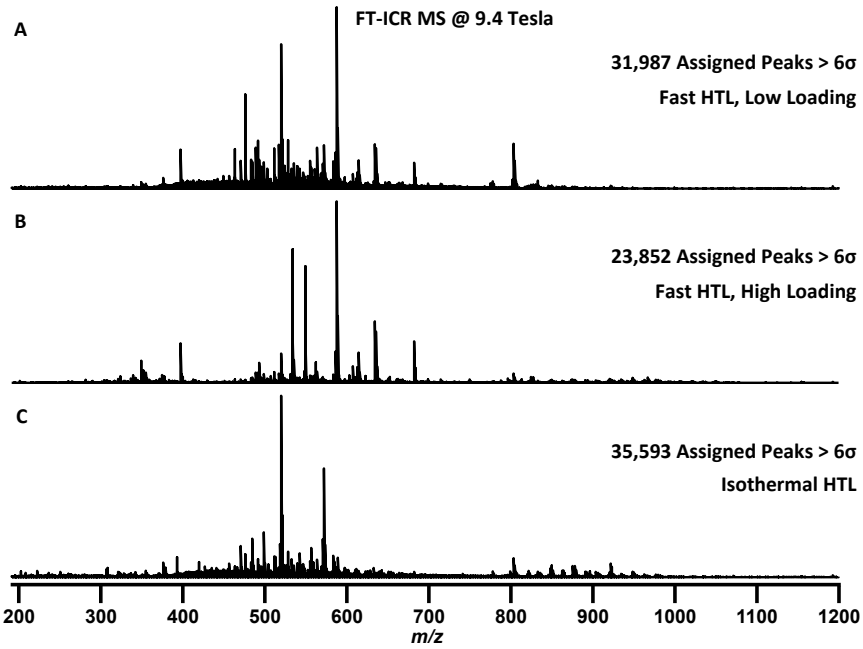

Figure E.4: Positive ESI FT-ICR MS broadband spectra of biocrude samples for HTL at different conditions

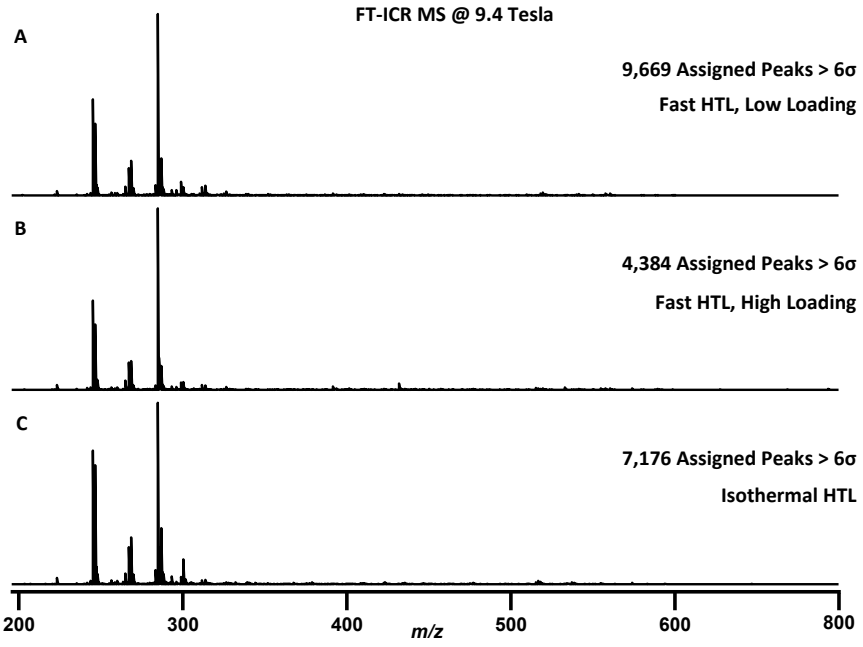

Figure E.5: Negative ESI FT-ICR MS broadband spectra of biocrude samples for HTL at different conditions

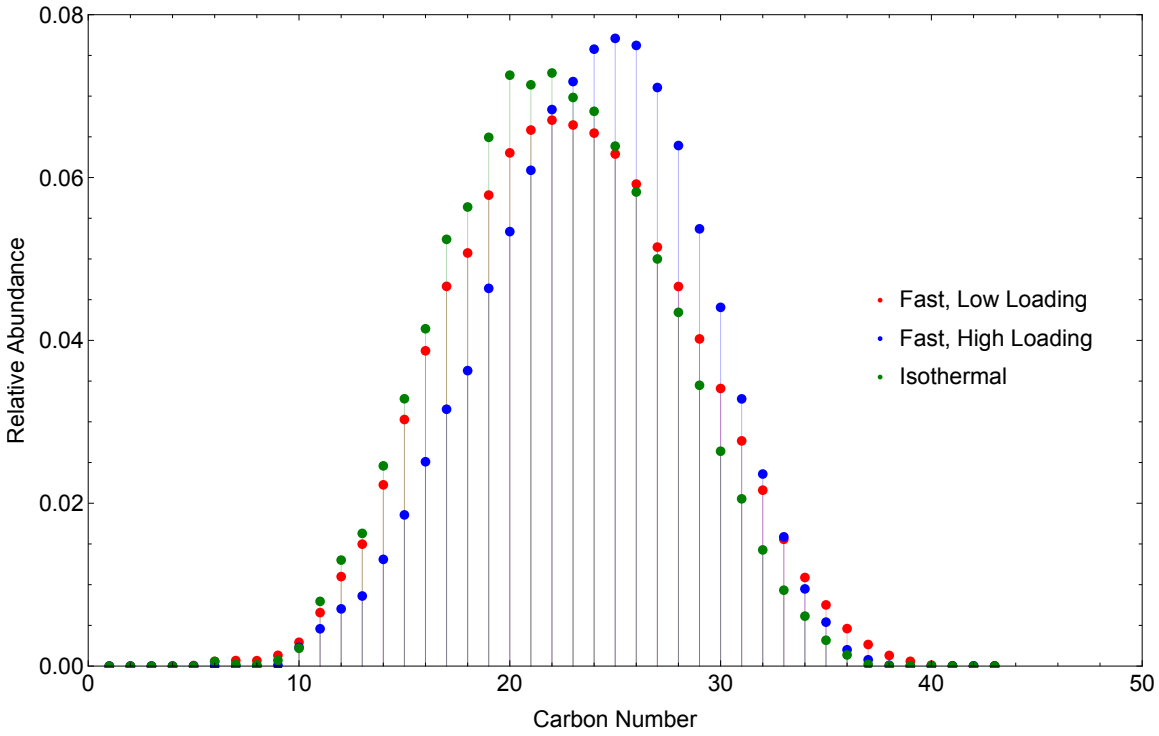

Figure E.6: Carbon number distributions for positive ESI analysis of aqueous-phase samples

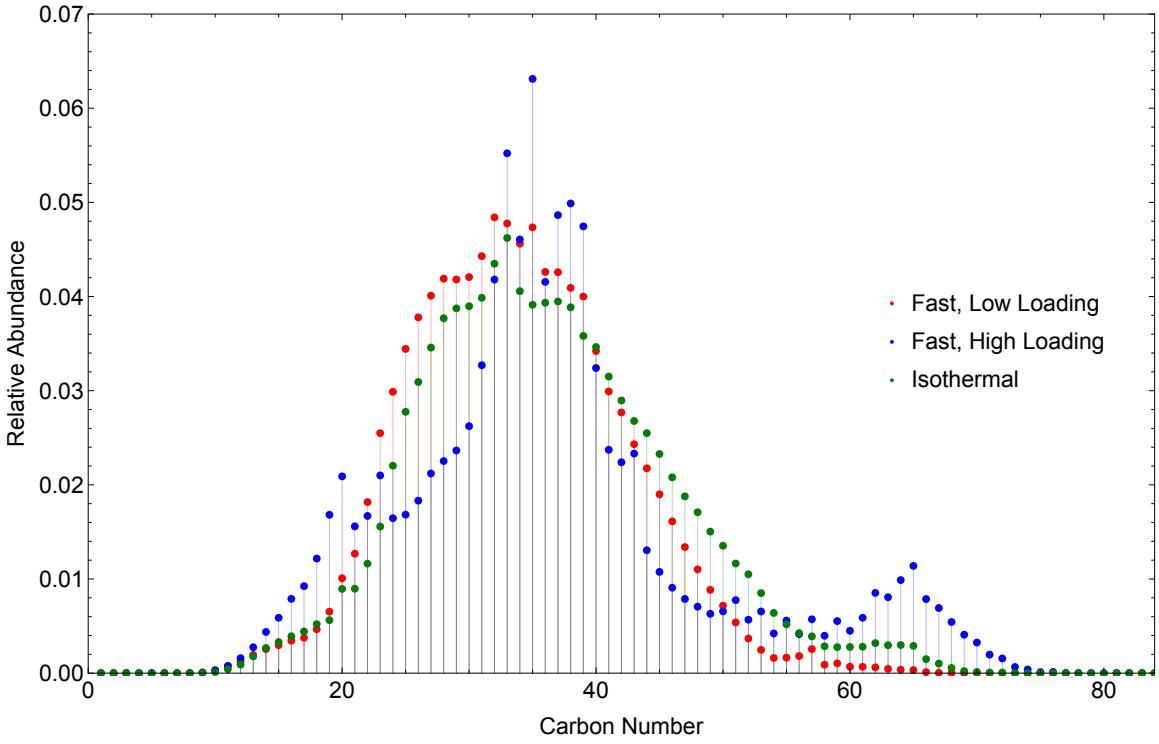

Figure E.7: Carbon number distributions for positive ESI analysis of biocrude samples

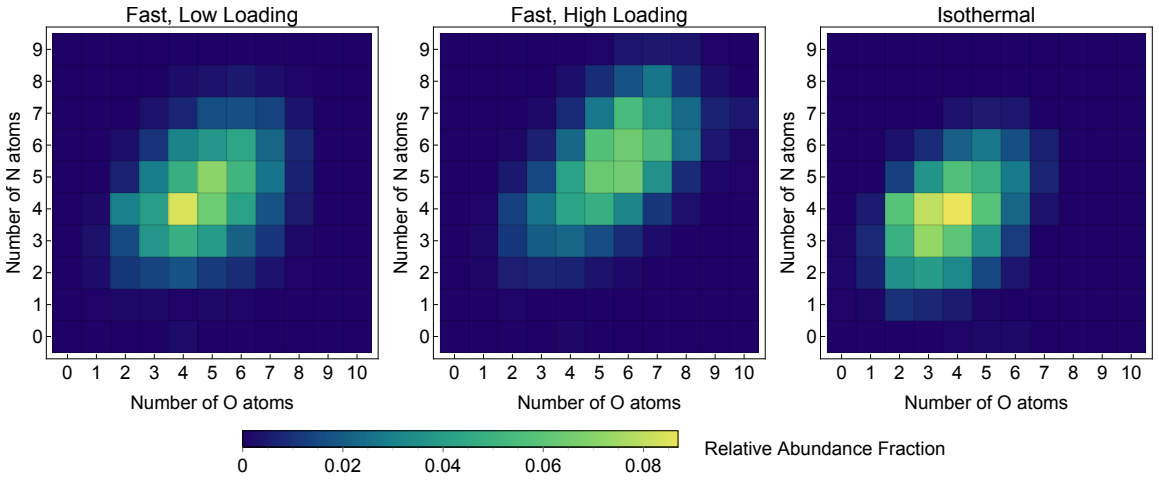

Figure E.8: Heteroatom density graph for positive ESI analysis of aqueous-phase samples

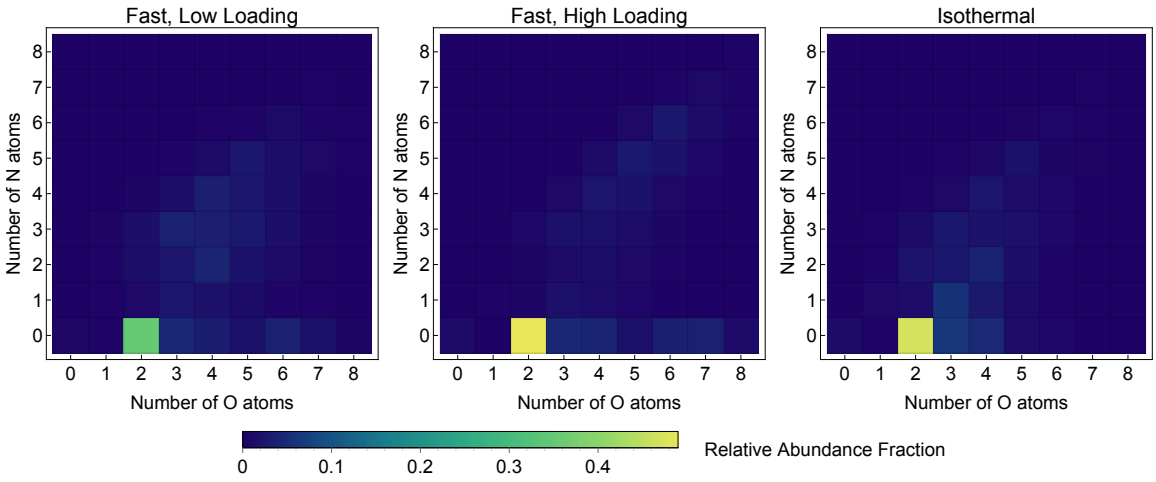

Figure E.9: Heteroatom density graph for negative ESI analysis of biocrude samples

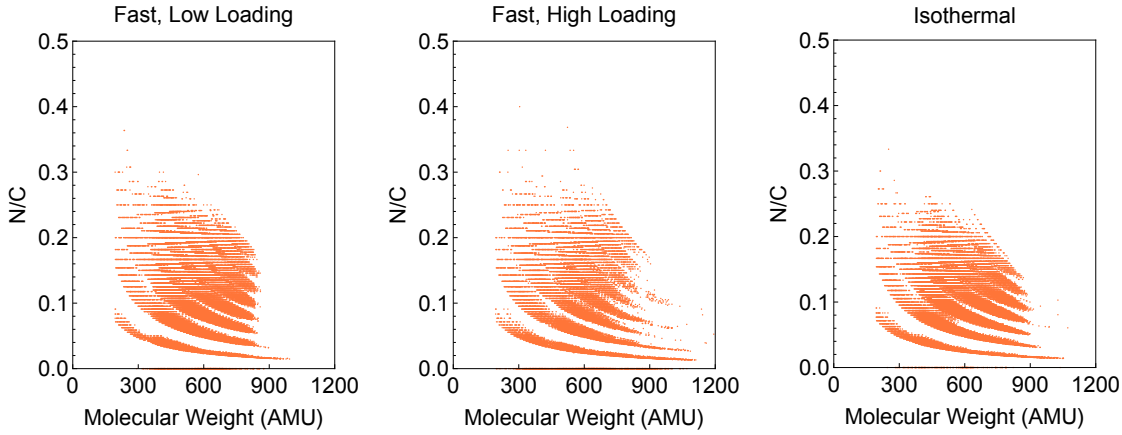

Figure E.10: N/C ratios vs. average molecular weight for positive ESI analysis of biocrude samples

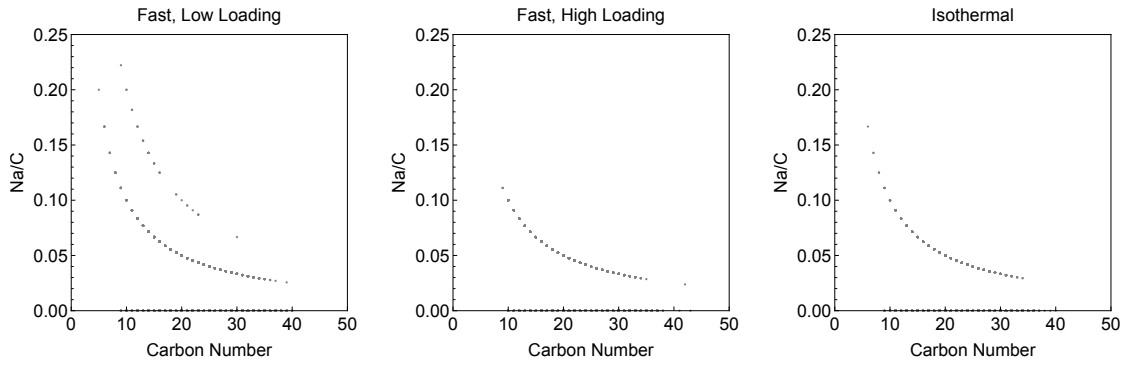

a Aqueous phase (positive ESI)

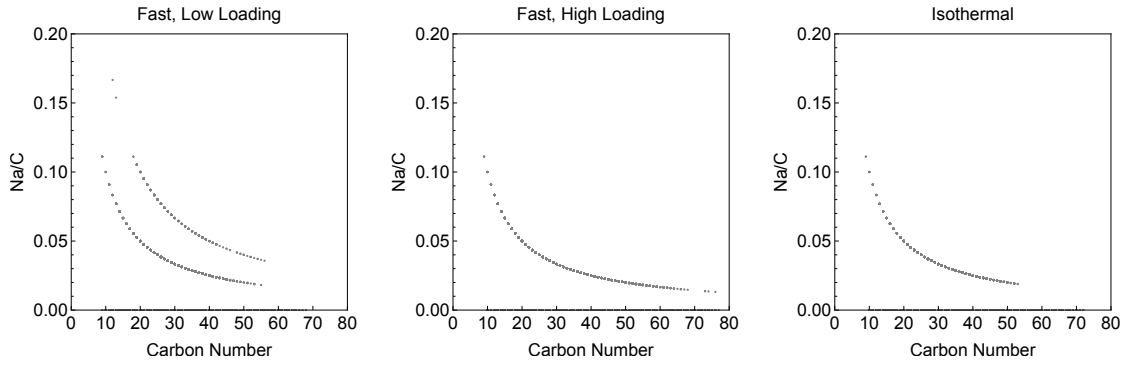

b Biocrude (positive ESI)

Figure E.11: Na/C ratios vs. carbon number for samples analyzed using positive ESI analysis

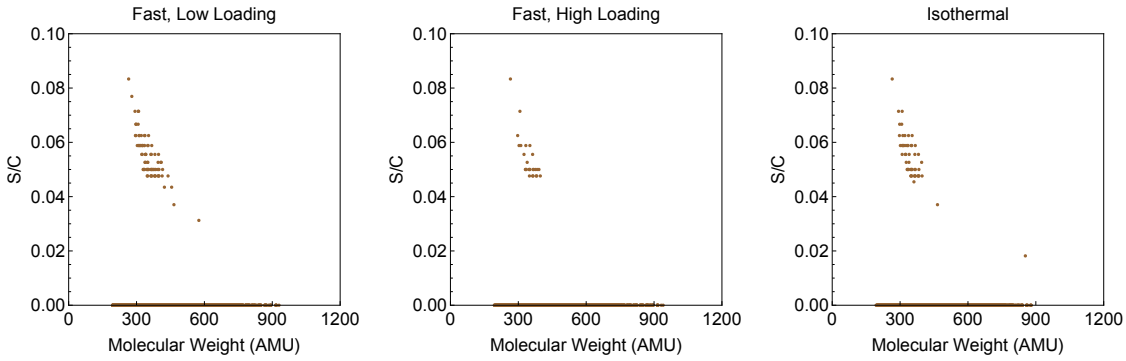

Figure E.12: S/C ratios vs. average molecular weight for biocrude samples (negative ESI)

APPENDIX F

Supplementary Information for Chapter VII

This appendix contains the reactor loadings and original product yields for control experiments (Table F.1) and HTL experiments (Table F.2). Adjusted product yields (calculated using Equations 7.1 - 7.9) for the HTL experiments in Chapter VII are depicted in Table F.3.

Table F.1: Reactor loadings and original product yields from control experiments in Chapter VII

Set-point Temperature	Quench Time		Quench Temperature	Algae slurry	Total mass	Gas Yield	Solid Yield	Biocrude Yield	Dry Aqueous Yield	Wet Recovery
T_{sp} (℃)	t_q (min)	$+t_q$ (s)	T_q (℃)	m_{S0} (g)	m_T (g)	Y_G (wt %)	Y_S (wt %)	Y_B (wt %)	Y_{DA} (wt %)	Y_{WA} (wt %)
25	0	0	25	0.5884	1.2489	0.00%	40.76%	0.63%	10.84%	43.31%
25	0	0	25	0.5885	1.2437	0.00%	49.96%	0.32%	12.11%	46.23%

Table F.2: Reactor loadings and original product yields from HTL experiments in Chapter VII

T_{sp} (℃)	t_q (min)	$+t_q$ (s)	T_q (℃)	m_{S0} (g)	m_T (g)	Y_G (wt%)	Y_S (wt%)	Y_B (wt%)	Y_{DA} (wt%)	Y_{WA} (wt%)
200	3	0	188	0.5882	1.2561	0.00%	50.22%	7.08%	26.27%	55.51%
200	7	0	200	0.5882	1.2559	1.11%	54.09%	12.11%	30.47%	65.52%
200	15	0	200	0.5884	1.2535	1.66%	37.60%	17.75%	37.32%	73.64%
200	40	0	200	0.5875	1.2547	1.66%	27.74%	23.04%	43.19%	74.17%
250	1	33	175	0.5878	1.254	3.18%	42.66%	12.12%	24.24%	64.39%
250	2	30	223	0.5889	1.2565	0.00%	45.63%	16.74%	35.08%	78.23%
250	5	0	250	0.5885	1.2546	5.29%	24.42%	23.74%	39.38%	80.11%
250	20	0	250	0.5885	1.2517	11.63%	6.82%	33.04%	35.68%	81.60%
250	60	0	250	0.5882	1.2521	22.12%	5.59%	40.87%	34.68%	81.80%
300	0	58	150	0.5878	1.2526	4.23%	41.76%	3.49%	14.55%	39.96%
300	0	58	150	0.5882	1.2541	0.00%	46.49%	13.12%	27.03%	66.87%
300	1	27	200	0.5883	1.2516	3.70%	39.77%	18.35%	31.94%	80.85%
300	2	6	250	0.588	1.2559	6.35%	30.05%	26.14%	32.43%	70.79%
300	3	30	289	0.5887	1.2528	17.44%	10.15%	39.32%	33.77%	83.82%
300	8	30	300	0.5876	1.2549	11.12%	6.51%	42.36%	32.72%	90.84%
300	15	0	300	0.5884	1.2539	11.10%	5.08%	43.04%	28.18%	89.56%
300	40	0	300	0.5883	1.2609	13.22%	10.68%	37.86%	22.63%	87.59%
350	0	30	100	0.5882	1.2556	1.66%	40.60%	1.83%	11.84%	37.56%
350	0	40	125	0.5888	1.2512	2.64%	35.51%	2.85%	12.94%	46.56%
350	1	11	200	0.5877	1.2534	9.53%	35.94%	26.73%	39.07%	77.50%
350	1	24	225	0.5868	1.2535	5.83%	24.12%	26.99%	39.55%	84.16%
350	2	15	300	0.5886	1.2509	13.21%	9.67%	37.21%	35.31%	81.54%
350	4	30	347	0.5032	1.0744	17.93%	4.45%	41.98%	22.87%	85.68%
350	7	0	350	0.5048	1.0738	6.16%	5.48%	40.00%	17.50%	73.51%
350	9	30	350	0.513	1.0989	7.28%	4.18%	43.48%	18.80%	89.13%
350	25	0	350	0.5042	1.0733	25.91%	3.15%	42.39%	11.54%	73.87%
350	60	0	350	0.5042	1.0774	23.87%	6.77%	38.58%	11.68%	81.30%
400	0	42	150	0.5881	1.2561	3.70%	28.99%	25.50%	41.42%	88.44%
400	1	20	250	0.5881	1.2471	11.11%	10.95%	38.25%	38.30%	87.32%
400	2	23	350	0.5011	1.0715	20.49%	6.70%	39.98%	16.64%	77.11%
400	3	30	384	0.502	1.0658	9.92%	3.84%	44.87%	18.28%	91.94%
400	6	0	400	0.4626	0.9845	7.40%	3.36%	39.61%	13.52%	75.76%
400	8	30	400	0.4623	0.9841	12.79%	3.77%	42.60%	9.82%	81.15%
400	15	0	400	0.4622	0.9909	12.79%	3.37%	35.61%	8.75%	72.30%
400	40	0	400	0.4619	0.984	16.16%	2.56%	33.00%	10.30%	82.51%
450	0	23	100	0.589	1.256	2.21%	38.99%	19.39%	33.69%	74.19%
450	0	30	125	0.5879	1.2549	0.53%	41.96%	20.11%	31.80%	77.65%
450	0	46	175	0.5875	1.2552	42.08%	14.29%	38.10%	35.38%	84.80%
450	0	53	200	0.5881	1.2568	8.85%	15.05%	33.30%	39.11%	81.62%
450	1	28	300	0.5881	1.2513	7.93%	4.81%	38.62%	19.94%	76.45%
450	2	30	400	0.4286	0.9152	13.79%	2.54%	40.65%	15.46%	84.52%
500	0	33	150	0.5877	1.2564	17.71%	11.90%	37.20%	34.82%	85.24%
500	0	48	200	0.5876	1.2547	9.97%	6.37%	40.69%	29.23%	83.18%
500	1	1	250	0.588	1.255	12.17%	8.84%	39.95%	34.02%	80.75%
500	1	35	350	0.5037	1.0773	16.06%	4.88%	43.73%	12.78%	75.95%
550	0	24	125	0.5876	1.2565	3.32%	36.43%	25.14%	35.05%	75.48%
550	0	37	175	0.587	1.2546	6.89%	8.37%	38.53%	32.12%	82.70%
550	0	42	200	0.5883	1.2529	8.99%	8.62%	34.32%	20.62%	80.87%
550	0	56	250	0.588	1.253	12.70%	8.52%	34.34%	20.26%	72.34%
550	1	9	300	0.5672	1.2005	13.71%	4.22%	39.82%	11.30%	80.81%
550	1	41	400	0.3087	0.6618	17.13%	2.02%	34.36%	11.59%	78.20%
600	0	17	100	0.588	1.2552	4.98%	55.77%	1.66%	15.55%	43.04%
600	0	27	150	0.5879	1.2539	11.64%	19.42%	31.80%	37.94%	81.25%
600	0	45	225	0.5881	1.2555	9.40%	6.31%	41.16%	24.17%	78.04%
600	0	50	250	0.5887	1.2548	10.50%	4.20%	25.75%	10.22%	54.85%
600	1	15	350	0.4207	0.8978	14.05%	1.77%	29.14%	10.13%	81.94%

Table F.3: Reactor loadings and adjusted product yields from HTL experiments in Chapter VII

T_{sp} (℃)	t_q (min)	$+t_q$ (s)	T_q (℃)	m_{S0} (g)	m_T (g)	Y_G (wt%)	Y_S (wt%)	Y_B (wt%)	Y_{DA} (wt%)	Y_{WA} (wt%)
200	3	0	188	0.5882	1.2561	0.00%	61.01%	7.08%	31.91%	0.00%
200	7	0	200	0.5882	1.2559	1.07%	55.53%	12.11%	31.29%	0.00%
200	15	0	200	0.5884	1.2535	1.60%	39.46%	17.75%	39.17%	2.02%
200	40	0	200	0.5875	1.2547	1.60%	28.58%	23.04%	44.49%	2.30%
250	1	33	175	0.5878	1.254	3.20%	52.14%	12.12%	29.63%	2.91%
250	2	30	223	0.5889	1.2565	0.00%	45.63%	16.74%	35.08%	2.55%
250	5	0	250	0.5885	1.2546	5.33%	24.42%	23.74%	39.38%	7.13%
250	20	0	250	0.5885	1.2517	11.72%	6.82%	33.04%	35.68%	12.74%
250	60	0	250	0.5882	1.2521	21.32%	5.59%	40.87%	34.68%	0.00%
300	0	58	150	0.5878	1.2526	4.27%	68.40%	3.49%	23.84%	0.00%
300	0	58	150	0.5882	1.2541	0.00%	54.57%	13.12%	31.72%	0.59%
300	1	27	200	0.5883	1.2516	3.73%	39.77%	18.35%	31.94%	6.21%
300	2	6	250	0.588	1.2559	6.40%	32.45%	26.14%	35.02%	0.00%
300	3	30	289	0.5887	1.2528	17.57%	10.15%	39.32%	33.77%	0.00%
300	8	30	300	0.5876	1.2549	11.20%	6.51%	42.36%	32.72%	7.21%
300	15	0	300	0.5884	1.2539	11.19%	5.08%	43.04%	28.18%	12.52%
300	40	0	300	0.5883	1.2609	13.32%	10.68%	37.86%	22.63%	15.50%
350	0	30	100	0.5882	1.2556	1.60%	74.78%	1.83%	21.80%	0.00%
350	0	40	125	0.5888	1.2512	2.66%	59.73%	2.85%	21.78%	12.98%
350	1	11	200	0.5877	1.2534	9.60%	35.94%	26.73%	39.07%	0.00%
350	1	24	225	0.5868	1.2535	5.88%	24.12%	26.99%	39.55%	3.47%
350	2	15	300	0.5886	1.2509	13.31%	9.67%	37.21%	35.31%	4.50%
350	4	30	347	0.5032	1.0744	18.07%	4.45%	41.98%	22.87%	12.63%
350	7	0	350	0.5048	1.0738	6.21%	5.48%	40.00%	17.50%	30.81%
350	9	30	350	0.513	1.0989	7.33%	4.18%	43.48%	18.80%	26.20%
350	25	0	350	0.5042	1.0733	26.11%	3.15%	42.39%	11.54%	16.81%
350	60	0	350	0.5042	1.0774	23.00%	6.77%	38.58%	11.68%	19.96%
400	0	42	150	0.5881	1.2561	3.73%	28.99%	25.50%	41.42%	0.00%
400	1	20	250	0.5881	1.2471	11.19%	10.95%	38.25%	38.30%	1.31%
400	2	23	350	0.5011	1.0715	10.59%	6.70%	39.98%	16.64%	26.08%
400	3	30	384	0.502	1.0658	9.99%	3.84%	44.87%	18.28%	23.02%
400	6	0	400	0.4626	0.9845	7.45%	3.36%	39.61%	13.52%	36.06%
400	8	30	400	0.4623	0.9841	12.88%	3.77%	42.60%	9.82%	30.93%
400	15	0	400	0.4622	0.9909	12.89%	3.37%	35.61%	8.75%	39.39%
400	40	0	400	0.4619	0.984	16.29%	2.56%	33.00%	10.30%	37.85%
450	0	23	100	0.589	1.256	2.13%	40.85%	19.39%	35.30%	2.34%
450	0	30	125	0.5879	1.2549	0.53%	41.96%	20.11%	31.80%	5.59%
450	0	46	175	0.5875	1.2552	2.40%	14.29%	38.10%	35.38%	9.83%
450	0	53	200	0.5881	1.2568	8.53%	15.05%	33.30%	39.11%	4.01%
450	1	28	300	0.5881	1.2513	8.00%	4.81%	38.62%	19.94%	28.63%
450	2	30	400	0.4286	0.9152	13.90%	2.54%	40.65%	15.46%	27.45%
500	0	33	150	0.5877	1.2564	17.07%	11.90%	37.20%	34.82%	-0.99%
500	0	48	200	0.5876	1.2547	9.60%	6.37%	40.69%	29.23%	14.10%
500	1	1	250	0.588	1.255	12.26%	8.84%	39.95%	34.02%	4.94%
500	1	35	350	0.5037	1.0773	16.18%	4.88%	43.73%	12.78%	22.43%
550	0	24	125	0.5876	1.2565	3.20%	36.53%	25.14%	35.14%	0.00%
550	0	37	175	0.587	1.2546	6.94%	8.37%	38.53%	32.12%	14.04%
550	0	42	200	0.5883	1.2529	9.06%	8.62%	34.32%	20.62%	27.38%
550	0	56	250	0.588	1.253	12.80%	9.05%	34.34%	21.54%	22.28%
550	1	9	300	0.5672	1.2005	13.82%	4.22%	39.82%	11.30%	30.84%
550	1	41	400	0.3087	0.6618	17.26%	2.02%	34.36%	11.59%	34.77%
600	0	17	100	0.588	1.2552	4.80%	73.15%	1.66%	20.39%	0.00%
600	0	27	150	0.5879	1.2539	11.73%	19.42%	31.80%	37.94%	0.00%
600	0	45	225	0.5881	1.2555	9.06%	6.31%	41.16%	24.17%	19.30%
600	0	50	250	0.5887	1.2548	10.12%	5.87%	25.75%	14.29%	43.97%
600	1	15	350	0.4207	0.8978	14.16%	1.77%	29.14%	10.13%	44.80%

BIBLIOGRAPHY

BIBLIOGRAPHY

[1] John Cook, Dana Nuccitelli, Sarah A. Green, Mark Richardson, Bärbel Winkler, Rob Painting, Robert Way, Peter Jacobs, and Andrew Skuce. Quantifying the consensus on anthropogenic global warming in the scientific literature. *Environmental Research Letters*, 8(2):024024, jun 2013.

[2] August 2015 Monthly Energy Review. Technical report, U.S. Energy Information Administration Office of Energy Statistics, Washington, DC, 2015.

[3] Pieter Tans and Ralph Keeling. Trends in Atmospheric Carbon Dioxide, 2015.

[4] Robert E. Blankenship, David M. Tiede, James Barber, Gary W. Brudvig, Graham Fleming, Maria Ghirardi, M. R. Gunner, Wolfgang Junge, David M. Kramer, Anastasios Melis, Thomas A. Moore, Christopher C. Moser, Daniel G. Nocera, Arthur J. Nozik, Donald R. Ort, William W. Parson, Roger C. Prince, and Richard T. Sayre. Comparing photosynthetic and photovoltaic efficiencies and recognizing the potential for improvement. *Science (New York, N.Y.)*, 332(6031):805–809, 2011.

[5] Qiang Hu, Milton Sommerfeld, Eric Jarvis, Maria Ghirardi, Matthew Posewitz, Michael Seibert, and Al Darzins. Microalgal triacylglycerols as feedstocks for biofuel production: perspectives and advances. *The Plant Journal*, 54(4):621–39, may 2008.

[6] Chun Yen Chen, Kuei Ling Yeh, Rifka Aisyah, Duu Jong Lee, and Jo Shu Chang. Cultivation, photobioreactor design and harvesting of microalgae for biodiesel production: A critical review. *Bioresource Technology*, 102(1):71–81, 2011.

[7] Ioannis Dogaris, Michael Welch, Andreas Meiser, Lawrence Walmsley, and George Philippidis. A novel horizontal photobioreactor for high-density cultivation of microalgae. *Bioresource Technology*, 2015.

[8] Andrew A. Peterson, Frédéric Vogel, Russell P. Lachance, Morgan Fröling, Michael J. Antal, Jr., and Jefferson W. Tester. Thermochemical biofuel production in hydrothermal media: A review of sub- and supercritical water technologies. *Energy & Environmental Science*, 1(1):32–65, 2008.

[9] Naoko Akiya and Phillip E. Savage. Roles of water for chemical reactions in high-temperature water. *Chemical Reviews*, 102(8):2725–50, aug 2002.

[10] Yutaka Shin-ya Dote, Shigeki Yokoyama Sawayama, Seiichi Inoue, and Tomoaki Minowa. Recovery of liquid fuel from hydrocarbon-rich microalgae by thermochemical liquefaction. *Fuel*, 73(12):1855–1857, 1994.

[11] Seiichi Inoue, Yutaka Dote, Shigeki Sawayama, Tomoaki Minowa, Tomoko Ogi, and Shin-Ya Yokoyama. Analysis of Oil Derived from Liquefaction of Botryococcus braunii. *Biomass & Bioenergy*, 6(4):269–274, 1994.

[12] S. Sawayama, T. Minowa, and S.-Y. Yokoyama. Possibility of renewable energy production and CO2 mitigation by thermochemical liquefaction of microalgae. *Biomass & Bioenergy*, 17:33–39, 1999.

[13] Christopher Jazrawi, Patrick Biller, Andrew B. Ross, Alejandro Montoya, Thomas Maschmeyer, and Brian S. Haynes. Pilot plant testing of continuous hydrothermal liquefaction of microalgae. *Algal Research*, 2(3):268–277, jul 2013.

[14] Hao Li, Zhidan Liu, Yuanhui Zhang, Baoming Li, Haifeng Lu, Na Duan, Minsheng Liu, Zhangbing Zhu, and Buchun Si. Conversion efficiency and oil quality of low-lipid high-protein and high-lipid low-protein microalgae via hydrothermal liquefaction. *Bioresource Technology*, 154:322–9, feb 2014.

[15] Nilusha Sudasinghe, Harvind Reddy, Nicholas Csakan, Shuguang Deng, Peter Lammers, and Tanner Schaub. Temperature-Dependent Lipid Conversion and Nonlipid Composition of Microalgal Hydrothermal Liquefaction Oils Monitored by Fourier Transform Ion Cyclotron Resonance Mass Spectrometry. *BioEnergy Research*, 2015.

[16] G. Yu, Y. Zhang, L. Schideman, T. L. Funk, and Z. Wang. Hydrothermal Liquefaction of Low Lipid Content Microalgae into Bio-Crude Oil. *Transactions of the ASABE*, 54(1):239–246, 2011.

[17] Peigao Duan, Binbin Jin, Yuping Xu, Yan Yang, Xiujun Bai, Feng Wang, Lei Zhang, and Jun Miao. Thermo-chemical conversion of Chlorella pyrenoidosa to liquid biofuels. *Bioresource Technology*, 133:197–205, apr 2013.

[18] J. Zhang, Z. Luo, and Y. Zhang. Hydrothermal Liquefaction of Chlorella pyrenoidosa in Water and Ethanol. *Transactions of the ASABE*, 56(1):253–259, 2013.

[19] Chao Gai, Yuanhui Zhang, Wan-Ting Chen, Peng Zhang, and Yuping Dong. Energy and nutrient recovery efficiencies in biocrude oil produced via hydrothermal liquefaction of Chlorella pyrenoidosa. *RSC Advances*, 4(33):16958, 2014.

[20] Diego López Barreiro, Carlos Zamalloa, Nico Boon, Wim Vyverman, Frederik Ronsse, Wim Brilman, and Wolter Prins. Influence of strain-specific parameters on hydrothermal liquefaction of microalgae. *Bioresource Technology*, 146:463–71, oct 2013.

[21] P. Biller and A. B. Ross. Potential yields and properties of oil from the hydrothermal liquefaction of microalgae with different biochemical content. *Bioresource Technology*, 102(1):215–225, jan 2011.

[22] Christopher Jazrawi, Patrick Biller, Yaya He, Alejandro Montoya, Andrew B. Ross, Thomas Maschmeyer, and Brian S. Haynes. Two-stage hydrothermal liquefaction of a high-protein microalga. *Algal Research*, 8:15–22, 2015.

[23] Tomoaki Minowa, Shin-ya Yokoyama, and Michimasa Kishimoto. Oil production from algal cells of Dunaliella tertiolecta by direct thermochemical liquefaction. *Fuel*, 74(12):1735–1738, 1995.

[24] Harvind K Reddy, Tapaswy Muppaneni, Jalal Rastegary, Saeid A. Shirazi, and Abbas Ghassemi. ASI: Hydrothermal Extraction and Characterization of Bio-Crude Oils from Wet Chlorella Sorokiniana and Dunaliella Tertiolecta. *Environmental Progress & Sustainable Energy*, 32(4):910–915, 2013.

[25] Saqib S. Toor, Harvind Reddy, Shuguang Deng, Jessica Hoffmann, Dorte Spangsmark, Linda B. Madsen, Jens Bo Holm-Nielsen, and Lasse A. Rosendahl. Hydrothermal Liquefaction of Spirulina and Nannochloropsis salina under Subcritical and Supercritical Water Conditions. *Bioresource Technology*, 131:413–9, mar 2013.

[26] HongYi Li, Jiao Hu, ZhiJian Zhang, Hang Wang, Fan Ping, ChangFeng Zheng, HaiLuo Zhang, and Qiang He. Insight into the effect of hydrogenation on efficiency of hydrothermal liquefaction and physico-chemical properties of biocrude oil. *Bioresource Technology*, 163:143–51, jul 2014.

[27] Tylisha M. Brown, Peigao Duan, and Phillip E. Savage. Hydrothermal Liquefaction and Gasification of Nannochloropsis sp. *Energy & Fuels*, 24(6):3639–3646, jun 2010.

[28] Peigao Duan and Phillip E. Savage. Hydrothermal liquefaction of a microalga with heterogeneous catalysts. *Industrial & Engineering Chemistry Research*, 50:52–61, 2011.

[29] Peter J. Valdez, Jacob G. Dickinson, and Phillip E. Savage. Characterization of Product Fractions from Hydrothermal Liquefaction of Nannochloropsis sp . and the Influence of Solvents. *Energy & Fuels*, 25:3235–3243, 2011.

[30] Stilianos G. Roussis, Richard Cranford, and Naum Sytkovetskiy. Thermal Treatment of Crude Algae Oils Prepared Under Hydrothermal Extraction Conditions. *Energy & Fuels*, 26:5294–5299, jul 2012.

[31] Peter J. Valdez, Michael C. Nelson, Henry Y. Wang, Xiaoxia Nina Lin, and Phillip E. Savage. Hydrothermal liquefaction of Nannochloropsis sp.: Systematic study of process variables and analysis of the product fractions. *Biomass & Bioenergy*, 46:317–331, 2012.

[32] Douglas C. Elliott, Todd R. Hart, Andrew J. Schmidt, Gary G. Neuenschwander, Leslie J. Rotness, Mariefel V. Olarte, Alan H. Zacher, Karl O. Albrecht, Richard T. Hallen, and Johnathan E. Holladay. Process development for hydrothermal liquefaction of algae feedstocks in a continuous-flow reactor. *Algal Research*, 2(4):445–454, oct 2013.

[33] Julia L. Faeth, Peter J. Valdez, and Phillip E. Savage. Fast Hydrothermal Liquefaction of Nannochloropsis sp. To Produce Biocrude. *Energy & Fuels*, 27(3):1391–1398, mar 2013.

[34] Bhavish Patel and Klaus Hellgardt. Hydrothermal Upgrading of Algae Paste: Application of 31 P-NMR. *Environmental Progress & Sustainable Energy*, 00(00), 2013.

[35] Peter J. Valdez and Phillip E. Savage. A reaction network for the hydrothermal liquefaction of Nannochloropsis sp. *Algal Research*, 2(4):416–425, oct 2013.

[36] Peter J. Valdez, Vincent J. Tocco, and Phillip E. Savage. A general kinetic model for the hydrothermal liquefaction of microalgae. *Bioresource Technology*, 163:123–127, 2014.

[37] Per Sigaard Christensen and Gae Peng. Hydrothermal Liquefaction of the Microalgae Phaeodactylum tricornutum: Impact of Reaction Conditions on Product and Elemental Distribution. *Energy & Fuels*, 28:5792–5803, 2014.

[38] Derek R. Vardon, Brajendra K. Sharma, Grant V. Blazina, Kishore Rajagopalan, and Timothy J. Strathmann. Thermochemical conversion of raw and defatted algal biomass via hydrothermal liquefaction and slow pyrolysis. *Bioresource Technology*, 109:178–87, apr 2012.

[39] Taka-o Matsui, Akihiro Nishihara, Chiyo Ueda, and Munetaka Ohtsuki. Liquefaction of micro-algae with iron catalyst. *Fuel*, 76(11):1043–1048, 1997.

[40] Derek R. Vardon, B. K. Sharma, John Scott, Guo Yu, Zhichao Wang, Lance Schideman, Yuanhui Zhang, and Timothy J. Strathmann. Chemical properties of biocrude oil from the hydrothermal liquefaction of Spirulina algae, swine manure, and digested anaerobic sludge. *Bioresource Technology*, 102(17):8295–8303, jul 2011.

[41] Hua-jun Huang, Xing-zhong Yuan, Hui-na Zhu, Hui Li, Yan Liu, Xue-li Wang, and Guang-ming Zeng. Comparative studies of thermochemical liquefaction characteristics of microalgae, lignocellulosic biomass and sewage sludge. *Energy*, 56:52–60, jul 2013.

[42] Umakanta Jena, K. C. Das, and J. R. Kastner. Effect of operating conditions of thermochemical liquefaction on biocrude production from Spirulina platensis. *Bioresource Technology*, 102(10):6221–6229, may 2011.

[43] Umakanta Jena and K. C. Das. Comparative Evaluation of Thermochemical Liquefaction and Pyrolysis for Bio-Oil Production from Microalgae. *Energy & Fuels*, 25:5472 – 5482, nov 2011.

[44] Binbin Jin, Peigao Duan, Yuping Xu, Feng Wang, and Yunchang Fan. Co-liquefaction of micro- and macroalgae in subcritical water. *Bioresource Technology*, 149:103–10, dec 2013.

[45] Griffin W. Roberts, Marie-Odile P. Fortier, Belinda S. M. Sturm, and Susan M. Stagg-Williams. Promising Pathway for Algal Biofuels through Wastewater Cultivation and Hydrothermal Conversion. *Energy & Fuels*, 27:857867, 2013.

[46] Yang Guo, Wenhan Song, Jiaming Lu, Qiran Ma, Donghai Xu, and Shuzhong Wang. Hydrothermal liquefaction of Cyanophyta: Evaluation of potential biocrude oil production and component analysis. *Algal Research*, 11:242–247, 2015.

[47] Laura Garcia Alba, Cristian Torri, Chiara Samorì, Jaapjan Van Der Spek, Daniele Fabbri, Sascha R. A. Kersten, and Derk W. F. Wim Brilman. Hydrothermal Treatment (HTT) of Microalgae: Evaluation of the Process As Conversion Method in an Algae Biorefinery Concept. *Energy & Fuels*, 26:642–657, 2012.

[48] Michael C. Johnson and Jefferson W. Tester. Lipid Transformation in Hydrothermal Processing of Whole Algal Cells. *Industrial & Engineering Chemistry Research*, 52:1098810995, 2013.

[49] B. E. Eboibi, D. M. Lewis, P. J. Ashman, and S. Chinnasamy. Effect of operating conditions on yield and quality of biocrude during hydrothermal liquefaction of halophytic microalga Tetraselmis sp. *Bioresource Technology*, 170:20–29, jul 2014.

[50] Jinhua Li, Guoming Wang, Zonghua Wang, Lixin Zhang, Chao Wang, and Zhengyu Yang. Conversion of Enteromorpha prolifera to high-quality liquid oil via deoxy-liquefaction. *Journal of Analytical and Applied Pyrolysis*, 104:494–501, nov 2013.

[51] K. Anastasakis and A. B. Ross. Hydrothermal liquefaction of the brown macroalga Laminaria saccharina: effect of reaction conditions on product distribution and composition. *Bioresource Technology*, 102(7):4876–83, apr 2011.

[52] Quang-Vu Bach, Miguel Valcuende Sillero, Khanh-Quang Tran, and Jorunn Skjermo. Fast hydrothermal liquefaction of a Norwegian macro-alga: Screening tests. *Algal Research*, 6:271–276, jun 2014.

[53] Demao Li, Limei Chen, Dong Xu, Xiaowen Zhang, Naihao Ye, Fangjian Chen, and Shulin Chen. Preparation and characteristics of bio-oil from the marine brown alga Sargassum patens C. Agardh. *Bioresource Technology*, 104:737–42, jan 2012.

[54] Douglas C. Elliott, Todd R. Hart, Gary G. Neuenschwander, Leslie J. Rotness, Guri Roesijadi, Alan H. Zacher, and Jon K. Magnuson. Hydrothermal Processing of Macroalgal Feedstocks in Continuous-Flow Reactors. *ACS Sustainable Chemistry & Engineering*, 2:207215, 2014.

[55] Jinhua Li, Guoming Wang, Ming Chen, Jiedong Li, Yaoyao Yang, Qiuyan Zhu, Xiaohuan Jiang, Zonghua Wang, and Haichao Liu. Deoxy-liquefaction of three different species of macroalgae to high-quality liquid oil. *Bioresource Technology*, 169:110–118, jul 2014.

[56] N. Neveux, A. K. L. Yuen, C. Jazrawi, M. Magnusson, B. S. Haynes, A. F. Masters, A. Montoya, N. A. Paul, T. Maschmeyer, and R. de Nys. Biocrude yield and productivity from the hydrothermal liquefaction of marine and freshwater green macroalgae. *Bioresource Technology*, 155:334–41, mar 2014.

[57] Rawel Singh, Thallada Bhaskar, and Bhavya Balagurumurthy. Effect of solvent on the hydrothermal liquefaction of macro algae Ulva fasciata. *Process Safety and Environmental Protection*, 93:154–160, mar 2015.

[58] P. Biller, R. Riley, and A. B. Ross. Catalytic hydrothermal processing of microalgae: decomposition and upgrading of lipids. *Bioresource Technology*, 102(7):4841–8, apr 2011.

[59] P. Biller, A .B. Ross, S. C. Skill, A. Lea-Langton, B. Balasundaram, C. Hall, R. Riley, and C. A. Llewellyn. Nutrient recycling of aqueous phase for microalgae cultivation from the hydrothermal liquefaction process. *Algal Research*, 1:70–76, may 2012.

[60] Umakanta Jena, Nisha Vaidyanathan, Senthil Chinnasamy, and K. C. Das. Evaluation of microalgae cultivation using recovered aqueous co-product from thermochemical liquefaction of algal biomass. *Bioresource Technology*, 102(3):3380–3387, feb 2011.

[61] Arno Barnard. *Extraction of oil from algae for biofuel production by thermochemical liquefaction.* Master of engineering, North-West University, Potchefstroom Campus, 2009.

[62] Y. F. Yang, C. P. Feng, Y. Inamori, and T. Maekawa. Analysis of energy conversion characteristics in liquefaction of algae. *Resources, Conservation and Recycling*, 43(1):21–33, dec 2004.

[63] Guo Yu, Yuanhui Zhang, Lance Schideman, Ted Funk, and Zhichao Wang. Distributions of carbon and nitrogen in the products from hydrothermal liquefaction of low-lipid microalgae. *Energy & Environmental Science*, 4(11):4587, 2011.

[64] Shuping Zou, Yulong Wu, Mingde Yang, Chun Li, and Junmao Tong. Bio-oil production from sub- and supercritical water liquefaction of microalgae

Dunaliella tertiolecta and related properties. *Energy & Environmental Science*, 3(8):1073, 2010.

[65] A. V. Bridgwater, D. Meier, and D. Radlein. An overview of fast pyrolysis of biomass. *Organic Geochemistry*, 30:1479–1493, 1999.

[66] Peter J. Valdez, Michael C. Nelson, Julia L. Faeth, Henry Y. Wang, Xiaoxia Nina Lin, and Phillip E. Savage. Hydrothermal Liquefaction of Bacteria and Yeast Monocultures. *Energy & Fuels*, 28:67–75, 2014.

[67] Julia L. Faeth and Phillip E. Savage. Effects of Processing Conditions on Biocrude Yields from Fast Hydrothermal Liquefaction of Microalgae. In preparation.

[68] Julia L. Faeth, David C. Hietala, and Phillip E. Savage. Modeling the effects of heating rate, temperature, and time on the hydrothermal liquefaction of Nannochloropsis sp. In preparation.

[69] Julia L. Faeth, Jacqueline M. Jarvis, Amy M. McKenna, and Phillip E. Savage. Characterization of Products from Fast and Isothermal Hydrothermal Liquefaction of Microalgae. *AIChE Journal*, 2015. Submitted.

[70] Shujauddin Changi, Adam J. Matzger, and Phillip E. Savage. Kinetics and pathways for an algal phospholipid (1,2-dioleoyl-sn-glycero-3-phosphocholine) in high-temperature (175350 C) water. *Green Chemistry*, 14:2856–2867, 2012.

[71] Dragan Knezevic, Wim van Swaaij, and Sascha Kersten. Hydrothermal Conversion Of Biomass. II. Conversion Of Wood, Pyrolysis Oil, And Glucose In Hot Compressed Water. *Industrial & Engineering Chemistry Research*, 49(1):104–112, jan 2010.

[72] J. Rhett Mayor and Alexander Williams. Residence Time Influence on the Fast Pyrolysis of Loblolly Pine Biomass. *Journal of Energy Resources Technology*, 132(4):041801–1 – 041801–6, 2010.

[73] Xiaoling Miao and Qingyu Wu. High yield bio-oil production from fast pyrolysis by metabolic controlling of Chlorella protothecoides. *Journal of Biotechnology*, 110(1):85–93, may 2004.

[74] K. Annamalai, J. M. Sweeten, and S. C. Ramalingam. Estimation of Gross Heating Values of Biomass Fuels. *Transaction of the ASAE*, 30(4):1205–1208, 1987.

[75] J. M. Vargas-Moreno, A. J. Callejón-Ferre, J. Pérez-Alonso, and B. Velázquez-Martí. A review of the mathematical models for predicting the heating value of biomass materials. *Renewable and Sustainable Energy Reviews*, 16(5):3065–3083, jun 2012.

[76] R. P. Overend, E. Chornet, and J. A. Gascoigne. Fractionation of lignocellulosics by steam-aqueous pretreatments [and Discussion]. *Philisophical Transaction of the Royal Society of London Series A: Mathematical and Physical Sciences*, 321(1561):523–526, 1987.

[77] Tim Rogalinski, Thomas Ingram, and Gerd Brunner. Hydrolysis of lignocellulosic biomass in water under elevated temperatures and pressures. *The Journal of Supercritical Fluids*, 47(1):54–63, nov 2008.

[78] D. J. Brasch and K. W. Free. Prehydrolysis-Kraft Pulping of Pinus radiata Grown in New Zealand. *Tappi*, 48(4):245–248, 1965.

[79] K. E. Vroom. The H Factor: A Means of Expressing Cooking Times and Temperatures as a Single Variable. *Pulp and Paper Research Institute of Canada*, 38(2):228–231, 1957.

[80] James G. Speight. *The Chemistry and Technology of Petroleum*. CRC Press (Taylor and Francis Group), Boca Raton, FL, 4th editio edition, 2007.

[81] Maria Gavrilescu and Yusuf Chisti. Biotechnology - A sustainable alternative for chemical industry. *Biotechnology Advances*, 23(7-8):471–499, 2005.

[82] Frédéric Leroy and Luc De Vuyst. Lactic acid bacteria as functional starter cultures for the food fermentation industry. *Trends in Food Science and Technology*, 15(2):67–78, 2004.

[83] C. Angerbauer, M. Siebenhofer, M. Mittelbach, and G. M. Guebitz. Conversion of sewage sludge into lipids by Lipomyces starkeyi for biodiesel production. *Bioresource Technology*, 99(8):3051–3056, 2008.

[84] Sarah Huffer, Christine M. Roche, Harvey W. Blanch, and Douglas S. Clark. Escherichia coli for biofuel production: Bridging the gap from promise to practice. *Trends in Biotechnology*, 30(10):538–545, 2012.

[85] Colin Ratledge and Zvi Cohen. Microbial and algal oils: Do they have a future for biodiesel or as commodity oils? *Lipid Technology*, 20(7):155–160, 2008.

[86] Bradley D. Wahlen, Michael R. Morgan, Alex T. McCurdy, Robert M. Willis, Michael D. Morgan, Daniel J. Dye, Bruce Bugbee, Byard D. Wood, and Lance C. Seefeldt. Biodiesel from microalgae, yeast, and bacteria: Engine performance and exhaust emissions. *Energy and Fuels*, 27(1):220–228, 2013.

[87] N. J. Horan. *Biological Wastewater Treatment Systems: Theory and Operation*. Wiley, Chichester, U.K., 1990.

[88] Masanori Murakami, Shin-ya Yokoyama, Tomoko Ogi, and Katsuya Koguchi. Direct liquefaction of activated sludge from aerobic treatment of effluents from the cornstarch industry. *Biomass*, 23(3):215–228, 1990.

[89] Chunbao Xu and Jody Lancaster. Conversion of secondary pulp/paper sludge powder to liquid oil products for energy recovery by direct liquefaction in hot-compressed water. *Water Research*, 42(6-7):1571–1582, 2008.

[90] W. J. Catallo and J. L. Comeaux. Reductive hydrothermal treatment of sewage sludge. *Waste Management*, 28(11):2213–2219, 2008.

[91] Laura Garcia Alba, Cristian Torri, Daniele Fabbri, Sascha R. A. Kersten, and Derk W. F. Wim Brilman. Microalgae growth on the aqueous phase from Hydrothermal Liquefaction of the same microalgae. *Chemical Engineering Journal*, 228:214–223, 2013.

[92] Mai Pham, Lance Schideman, John Scott, Nandakishore Rajagopalan, and Michael J. Plewa. Chemical and biological characterization of wastewater generated from hydrothermal liquefaction of Spirulina. *Environmental Science & Technology*, 47(4):2131–2138, feb 2013.

[93] Michael Nelson, Lian Zhu, Anne Thiel, Yan Wu, Mary Guan, Jeremy Minty, Henry Y. Wang, and Xiaoxia Nina Lin. Microbial utilization of aqueous co-products from hydrothermal liquefaction of microalgae Nannochloropsis oculata. *Bioresource Technology*, 136:522–528, may 2013.

[94] Simoncyril U. Nwachukwu. Bioremediation of sterile agricultural soils polluted with crude petroleum by application of the soil bacterium, Pseudomonas putida, with inorganic nutrient supplementations. *Current Microbiology*, 42(4):231–236, 2001.

[95] Luisa S. Gronenberg, Ryan J. Marcheschi, and James C. Liao. Next generation biofuel engineering in prokaryotes. *Current Opinion in Chemical Biology*, 17(3):462–471, 2013.

[96] Robert B. Levine, Alexandra A. Bollas, Matthew D. Durham, and Phillip E. Savage. Triflate-catalyzed (trans)esterification of lipids within carbonized algal biomass. *Bioresource Technology*, 111:222–229, may 2012.

[97] Tom Lewis, Peter D. Nichols, and Tom A. McMeekin. Evaluation of extraction methods for recovery of fatty acids from lipid-producing microheterotrophs. *Journal of Microbiological Methods*, 43:107–116, 2000.

[98] Margret Piorreck, Klaus-Hinnerk Baasch, and Peter Pohl. Biomass production, total protein, chlorophylls, lipids and fatty acids of freshwater green and blue-green algae under different nitrogen regimes. *Phytochemistry*, 23(2):207–216, 1984.

[99] Arthur. M. A. Pistorius, Willem J. DeGrip, and Tatjana A. Egorova-Zachernyuk. Monitoring of biomass composition from microbiological sources by means of FT-IR spectroscopy. *Biotechnology and Bioengineering*, 103(1):123–129, 2009.

[100] Kjell Magne Fagerbakke, Mikal Heldal, and Svein Norland. Content of carbon, nitrogen, oxygen, sulfur and phosphorus in native aquatic and cultured bacteria. *Aquatic Microbial Ecology*, 10(1):15–27, 1996.

[101] H. C. Lange and J. J. Heijnen. Statistical reconciliation of the elemental and molecular biomass composition of Saccharomyces cerevisiae. *Biotechnology and Bioengineering*, 75(3):334–344, 2001.

[102] Yusuf Chisti. Constraints to commercialization of algal fuels. *Journal of Biotechnology*, 167(3):201–214, oct 2013.

[103] E. W. Becker. Micro-algae as a source of protein. *Biotechnology Advances*, 25(2):207–210, 2007.

[104] A. B. Ross, P. Biller, M. L. Kubacki, H. Li, A. Lea-Langton, and J. M. Jones. Hydrothermal processing of microalgae using alkali and organic acids. *Fuel*, 89(9):2234–2243, sep 2010.

[105] Cristian Torri, Laura Garcia Alba, Chiara Samorì, Daniele Fabbri, and Derk W. F. Wim Brilman. Hydrothermal Treatment (HTT) of Microalgae: Detailed Molecular Characterization of HTT Oil in View of HTT Mechanism Elucidation. *Energy & Fuels*, 26:658–671, 2012.

[106] H. Tao, C. Bausch, C. Richmond, F. R. Blattner, and T. Conway. Functional genomics: expression analysis of Escherichia coli growing on minimal and rich media. *Journal of Bacteriology*, 181(20):6425–6440, 1999.

[107] Nobuaki Sato, Armando T. Quitain, Kilyoon Kang, and Hiroyuki Daimon. Reaction Kinetics of Amino Acid Decomposition in High-Temperature and High-Pressure Water. *Industrial & Engineering Chemistry Research*, 43:3217–3222, 2004.

[108] J. G. Speight. *The Chemistry and Technology of Petroleum*. Marcel Dekker, Inc., New York, 3rd edition, 1999.

[109] K. Sasaki, M. Watanabe, T. Tanaka, and T. Tanaka. Biosynthesis, biotechnological production and applications of 5-aminolevulinic acid. *Applied Microbiology and Biotechnology*, 58(1):23–29, 2002.

[110] Varoujan A. Yaylayan and Alexis Huyghues-Despointes. Identification of per-O-(trimethylsilyl) derivatives of aldoses generated from thermal decomposition of N-(1-deoxy-D-fructopyranos-1-y1)proline: Reversibility of the Amadori rearrangement. *Carbohydrate Research*, 286:179–187, 1996.

[111] Nolan D. Orfield, Andrew J. Fang, Peter J. Valdez, Michael C. Nelson, Phillip E. Savage, Xiaoxia Nina Lin, and Gregory A. Keoleian. Life Cycle Design of an Algal Biorefinery Featuring Hydrothermal Liquefaction: Effect of Reaction Conditions and an Alternative Pathway Including Microbial Regrowth. *ACS Sustainable Chemistry & Engineering*, 2:867874, 2014.

[112] Lester Haar, John S. Gallagher, and George S. Kell. *NBS/NRC Steam Tables*. Hemisphere Publishing Corporation, Washington, DC, 1984.

[113] Bo Zhang, Marc von Keitz, and Kenneth Valentas. Thermal effects on hydrothermal biomass liquefaction. *Applied biochemistry and biotechnology*, 147(1-3):143–50, mar 2008.

[114] Steffen Brand, Flabianus Hardi, Jaehoon Kim, and Dong Jin Suh. Effect of heating rate on biomass liquefaction: Differences between subcritical water and supercritical ethanol. *Energy*, 68:420–427, 2014.

[115] Patrick Biller, Brajendra K. Sharma, Bidhya Kunwar, and Andrew B. Ross. Hydroprocessing of bio-crude from continuous hydrothermal liquefaction of microalgae. *Fuel*, 159:197–205, 2015.

[116] S. V. Smith. Physical, chemical and biological characteristics of CO2 gas flux across the air-water interface. *Plant, Cell and Environment*, 8:387–398, 1985.

[117] Bhavish Patel and Klaus Hellgardt. Hydrothermal Upgrading of Algae Paste in a Continuous Flow Reactor. *Bioresource Technology*, (April), 2015.

[118] Patrick Biller and Andrew B. Ross. Hydrothermal processing of algal biomass for the production of biofuels and chemicals. *Biofuels*, 3(5):603–623, sep 2012.

[119] F. B. Jr. Metting. Biodiversity and application of microalgae. *Journal of Industrial Microbiology*, 17(March):477–489, 1996.

[120] Alan G. Marshall, C. L. Hendrickson, and G. S. Jackson. Fourier transform ion cyclotron resonance mass spectrometry: a primer. *Mass Spectrometry Reviews*, 17(1):1–35, 1998.

[121] Alan G. Marshall and Ryan P. Rodgers. Petroleomics: The Next Grand Challenge for Chemical Analysis Petroleum and Mass Spectrometry: Divergent. *Accounts of Chemical Research*, 37:53–59, 2004.

[122] Alan G. Marshall and Ryan P. Rodgers. Petroleomics: chemistry of the underworld. *Proceedings of the National Academy of Sciences of the United States of America*, 105(47):18090–18095, nov 2008.

[123] Andras Gaspar, Elio Zellermann, Sami Lababidi, Jennifer Reece, and Wolfgang Schrader. Impact of different ionization methods on the molecular assignments of asphaltenes by FT-ICR mass spectrometry. *Analytical Chemistry*, 84(12):5257–5267, jun 2012.

[124] Yinhua Pan. Acidic and Neutral Polar NSO Compounds in Heavily Biodegraded Oils Characterized by Negative-Ion ESI FT-ICR MS. *Energy & Fuels*, 27(6):2960–2973, jun 2013.

[125] Stefanie Poetz, Brian Hors, and Heinz Wilkes. Maturity-Driven Generation and Transformation of Acidic Compounds in the Organic-Rich Posidonia Shale as Revealed by Electrospray Ionization Fourier Transform Ion Cyclotron Resonance Mass Spectrometry. *Energy & Fuels*, 28:4877–4888, 2014.

[126] Brian M. Ruddy, Markus Huettel, Joel E. Kostka, Vladislav V. Lobodin, Benjamin J. Bythell, Amy M. Mckenna, Christoph Aeppli, Christopher M. Reddy, Robert K. Nelson, Alan G. Marshall, and Ryan P. Rodgers. Targeted Petroleomics: Analytical Investigation of Macondo Well Oil Oxidation Products from Pensacola Beach. *Energy & Fuels*, 28:4043–4050, 2014.

[127] Robert B. Levine, Christian O. Sambolin Sierra, Ryan Hockstad, Wassim Obeid, Patrick G. Hatcher, and Phillip E. Savage. The Use of Hydrothermal Carbonization to Recycle Nutrients in Algal Biofuel Production. *Environmental Progress & Sustainable Energy*, 32(4):962–975, 2013.

[128] Nilusha Sudasinghe, Barry Dungan, Peter Lammers, Karl Albrecht, Doug Elliott, Rich Hallen, and Tanner Schaub. High resolution FT-ICR mass spectral analysis of bio-oil and residual water soluble organics produced by hydrothermal liquefaction of the marine microalga Nannochloropsis salina. *Fuel*, 119:47–56, mar 2014.

[129] Michael Mario Sanguineti, Nadim Hourani, Matthias Witt, S. Mani Sarathy, Laurenz Thomsen, and Nikolai Kuhnert. Analysis of impact of temperature and saltwater on Nannochloropsis salina bio-oil production by ultra high resolution APCI FT-ICR MS. *Algal Research*, 9:227–235, 2015.

[130] Jacqueline M. Jarvis, Amy M. McKenna, Roger N. Hilten, K. C. Das, Ryan P. Rodgers, and Alan G. Marshall. Characterization of Pine Pellet and Peanut Hull Pyrolysis Bio-oils by Negative-Ion Electrospray Ionization Fourier Transform Ion Cyclotron Resonance Mass Spectrometry. *Energy & Fuels*, 26(6):3810–3815, jun 2012.

[131] Yantao Bi, Gang Wang, Quan Shi, Chunming Xu, and Jinsen Gao. Compositional Changes during Hydrodeoxygenation of Biomass Pyrolysis Oil. *Energy & Fuels*, 28:2571–2580, 2014.

[132] Stefano Chiaberge, Irene Leonardis, Tiziana Fiorani, Pietro Cesti, Samantha Reale, and Francesco De Angelis. Bio-Oil from Waste: A Comprehensive Analytical Study by Soft-Ionization FTICR Mass Spectrometry. *Energy & Fuels*, 28:2019–2026, 2014.

[133] F. Omar Holguin and Tanner Schaub. Characterization of microalgal lipid feedstock by direct-infusion FT-ICR mass spectrometry. *Algal Research*, 2(1):43–50, jan 2013.

[134] Timo Kekäläinen, Tapani Venäläinen, and Janne Jänis. Characterization of Birch Wood Pyrolysis Oils by Ultrahigh- Resolution Fourier Transform Ion

Cyclotron Resonance Mass Spectrometry: Insights into Thermochemical Conversion. *Energy & Fuels*, 28(7):4596–4602, jul 2014.

[135] Sandeep Kumar, Elodie Hablot, Jose Luis Garcia Moscoso, Wassim Obeid, Patrick G. Hatcher, Brandon Michael DuQuette, Daniel Graiver, Ramani Narayan, and Venkatesh Balan. Polyurethanes preparation using proteins obtained from microalgae. *Journal of Materials Science*, 49(22):7824–7833, aug 2014.

[136] Irene Leonardis, Stefano Chiaberge, Tiziana Fiorani, Silvia Spera, Ezio Battistel, Aldo Bosetti, Pietro Cesti, Samantha Reale, and Francesco De Angelis. Characterization of bio-oil from hydrothermal liquefaction of organic waste by NMR spectroscopy and FTICR mass spectrometry. *ChemSusChem*, 6(1):160–167, jan 2013.

[137] Nathalia S. Tessarolo, Renzo C. Silva, Gabriela Vanini, Andrea Pinho, Wanderson Romão, Eustáquio V. R. de Castro, and Débora A. Azevedo. Assessing the chemical composition of bio-oils using FT-ICR mass spectrometry and comprehensive two-dimensional gas chromatography with time-of-flight mass spectrometry. *Microchemical Journal*, 117:68–76, nov 2014.

[138] Adrien Nyakas, Jun Han, John V. Headley, and Christoph H. Borchers. Comprehensive Analysis of Oil Sands Processed Water by Direct-Infusion Fourier-Transform Ion Cyclotron Resonance Mass Spectrometry with and without Offline UHPLC Sample Prefractionation. *Environmental Science & Technology*, 47:4471–4479, 2013.

[139] Nathan K. Kaiser, Joshua J. Savory, Amy M. McKenna, John P. Quinn, Christopher L. Hendrickson, and Alan G. Marshall. Electrically compensated Fourier transform ion cyclotron resonance cell for complex mixture mass analysis. *Analytical Chemistry*, 83(17):6907–6910, sep 2011.

[140] Greg T. Blakney, Christopher L. Hendrickson, and Alan G. Marshall. Predator data station: A fast data acquisition system for advanced FT-ICR MS experiments. *International Journal of Mass Spectrometry*, 306(2-3):246–252, sep 2011.

[141] Feng Xian, Christopher L. Hendrickson, Greg T. Blakney, Steven C. Beu, and Alan G. Marshall. Automated broadband phase correction of Fourier transform ion cyclotron resonance mass spectra. *Analytical Chemistry*, 82(21):8807–8812, nov 2010.

[142] Feng Xian, Yuri E. Corilo, Christopher L. Hendrickson, and Alan G. Marshall. Baseline correction of absorption-mode Fourier transform ion cyclotron resonance mass spectra. *International Journal of Mass Spectrometry*, 325-327:67–72, jul 2012.

[143] E. B. Ledford, D. L. Rempel, and M. L. Gross. Space charge effects in Fourier transform mass spectrometry. Mass calibration. *Analytical Chemistry*, 56(14):2744–2748, dec 1984.

[144] Joshua J. Savory, Nathan K. Kaiser, Amy M. Mckenna, Feng Xian, Greg T. Blakney, Ryan P. Rodgers, Christopher L. Hendrickson, and Alan G. Marshall. Measurement Accuracy with a Walking Calibration Equation. *Analytical Chemistry*, 83:1732–1736, 2011.

[145] Edward Kendrick. A Mass Scale Based on CH2 = 14.0000 for High Resolution Mass Spectrometry of Organic Compounds. *Analytical Chemistry*, 35(13):2146–2154, 1963.

[146] Yuri E. Corilo. PetroOrg Software; Florida State University; All Rights Reserved.

[147] Udo Armbruster, Andreas Martin, and André Krepel. Partial oxidation of propane in sub- and supercritical water. *The Journal of Supercritical Fluids*, 21:233–243, 2001.

[148] Jose L. Garcia-Moscoso, Ali Teymouri, and Sandeep Kumar. Kinetics of Peptides and Arginine Production from Microalgae (Scenedesmus sp.) by Flash Hydrolysis. *Industrial & Engineering Chemistry Research*, 54:2048–2058, 2015.

[149] Venn Diagram Plotter — Pan-Omics Research.

[150] Christine A. Hughey, Ryan P. Rodgers, Alan G. Marshall, Kuangnan Qian, and Winston K. Robbins. Identification of NSO Compounds in Crude Oils of Different Geochemical Origins by Negative Ion Electrospray Fourier Transform Ion Cyclotron Resonance Mass Spectrometry. *Organic Geochemistry*, 33:743–759, 2002.

[151] Yingda Lu, Robert B. Levine, and Phillip E. Savage. Fatty Acids for Nutraceuticals and Biofuels from Hydrothermal Carbonization of Microalgae. *Industrial & Engineering Chemistry Research*, 54:4066–4071, 2015.

[152] D. W. van Krevelen. Graphical-statistical method for the study of structure and reaction processes of coal. *Fuel*, 1950.

[153] Sunghwan Kim, Robert W. Kramer, and Patrick G. Hatcher. Graphical method for analysis of ultrahigh-resolution broadband mass spectra of natural organic matter, the van Krevelen diagram. *Analytical Chemistry*, 75(20):5336–5344, oct 2003.

[154] Jim Barker, Stephen Cook, and Paul Richards. Sodium Contamination of Diesel Fuel, its Interaction with Fuel Additives and the Resultant Effects on Filter Plugging and Injector Fouling. *SAE International Journal of Fuels and Lubricants*, 6(3):826–838, 2013.

[155] Tim Rogalinski, Kaiyue Liu, Tobias Albrecht, and Gerd Brunner. Hydrolysis kinetics of biopolymers in subcritical water. *The Journal of Supercritical Fluids*, 46(3):335–341, oct 2008.

[156] Mitsuru Sasaki, Bernard Kabyemela, Roberto Malaluan, Satoshi Hirose, Naoko Takeda, Tadafumi Adschiri, and Kunio Arai. Cellulose hydrolysis in subcritical and supercritical water. *Journal of Supercritical Fluids*, 13:261–268, 1998.

[157] Mitsuru Sasaki, Zhen Fang, Yoshiko Fukushima, Tadafumi Adschiri, and Kunio Arai. Dissolution and hydrolysis of cellulose in subcritical and supercritical water. *Industrial & Engineering Chemistry Research*, 39(2331):2883–2890, 2000.

[158] Shujauddin M. Changi, Julia L. Faeth, Na Mo, and Phillip E. Savage. Hydrothermal Reactions of Biomolecules Relevant for Algae Liquefaction. *Industrial & Engineering Chemistry Research*, 2015. Accepted.

[159] H. C. Greenwell, L. M. L. Laurens, R. J. Shields, R. W. Lovitt, and K. J. Flynn. Placing microalgae on the biofuels priority list: a review of the technological challenges. *Journal of the Royal Society, Interface / the Royal Society*, 7(46):703–26, may 2010.

[160] Jennie C. Hunter-Cevera, Sammy Boussiba, Joel L. Cuello, Clifford S. Duke, Rebecca A. Efroymson, Susan S. Golden, Jennifer Holmgren, Donald L. Johnson, Mark E. Jones, Val H. Smith, Cai Steger, Gregory N. Stephanopoulos, Larry P. Walker, Eric Williams, and Paul V. Zimba. Sustainable Development of Algal Biofuels in the United States Committee on the Sustainable Development of Algal Biofuels. Technical report, National Research Council of the National Academies, 2012.

[161] Marie-Odile P. Fortier, Griffin W. Roberts, Susan M. Stagg-Williams, and Belinda S. M. Sturm. Life cycle assessment of bio-jet fuel from hydrothermal liquefaction of microalgae. *Applied Energy*, 122(July 2011):73–82, jun 2014.

[162] Daniel J. Conley, Hans W. Paerl, Robert W. Howarth, Donald F. Boesch, Sybil P. Seitzinger, Karl E. Havens, Christiane Lancelot, and Gene E. Likens. Controlling eutrophication: Nitrogen and Phosphorus. *Science (New York, N.Y.)*, 323(5917):1014–1015, 2009.

[163] T. R. Hopkins. Physical and Chemical Cell Disruption for the Recovery of Intracellular Proteins. In Ramnath Seetharam and Satish K. Sharma, editors, *Purification and Analysis of Recombinant Proteins*, chapter 3, pages 57–83. Marcel Dekker, Inc., New York, 1991.

[164] Anton P. J. Middelberg. PROCESS-SCALE DISRUPTION OF MICROORGANISMS. *Biotechnology Advances*, 13(3):491–551, 1995.